

# Metallurgical Characteristics of High Strength Structural Materials

[Tenth Quarterly Report]

R. J. GOODE, R. W. HUBER, R. W. JUDY, JR., D. G. HOWE,  
P. P. PUZAK, K. B. LLOYD, T. W. CROOKER,  
R. E. MOREY, E. A. LANGE, AND C. N. FREED

*Metallurgy Division*

April 1966



**NAVAL RESEARCH LABORATORY**  
**Washington, D.C.**

DISTRIBUTION OF THIS DOCUMENT IS UNLIMITED

## PREVIOUS REPORTS IN THIS SERIES

First Quarterly Report - "Metallurgical Characteristics of High Strength Structural Materials," P.P. Puzak, K.B. Lloyd, E.A. Lange, R.J. Goode, R.W. Hubert, E.P. Dahlberg and C.D. Beachem, NRL Memo. Rept. 1438, June 30, 1963

Second Quarterly Report - "Metallurgical Characteristics of high Strength Structural Materials," P.P. Puzak, K.B. Lloyd, E.A. Lange, R.J. Goode, and R.W. Huber, NRL Memo. Rept. 1461, Sept. 1963

Third Quarterly Report - "Metallurgical Characteristics of High Strength Structural Materials," P.P. Puzak, K.B. Lloyd, R.J. Goode, R.W. Huber, D.G. Howe, T.W. Crooker, E.A. Lange, and W.S. Pellini, NRL Report 6086, Jan. 1964

Fourth Quarterly Report - "Metallurgical Characteristics of High Strength Structural Materials," R.J. Goode, R.W. Huber, D.G. Howe, R.W. Judy, Jr., T.W. Crooker, R.E. Morey, E.A. Lange, P.P. Puzak, and K.B. Lloyd, NRL Report 6137, June 1964

Fifth Quarterly Report - "Metallurgical Characteristics of High Strength Structural Materials," T.W. Crooker, R.E. Morey, E.A. Lange, R.W. Judy, Jr., C.N. Freed, R.J. Goode, P.P. Puzak, K.B. Lloyd, R.W. Huber, D.G. Howe, and W.S. Pellini, NRL Report 6196, Sept. 1964

Sixth Quarterly Report - "Metallurgical Characteristics of High Strength Structural Materials," W.S. Pellini, R.J. Goode, R.W. Huber, D.G. Howe, R.W. Judy, Jr., P.P. Puzak, K.B. Lloyd, E.A. Lange, E.A. DeFelice, T.W. Crooker, R.E. Morey E.J. Chapin, and L.J. McGeady, NRL Report 6258, Dec. 1964

Seventh Quarterly Report - "Metallurgical Characteristics of High Strength Structural Materials," R.J. Goode, D.G. Howe, R.W. Huber, P.P. Puzak, K.B. Lloyd, T.W. Crooker, R.E. Morey, E.A. Lange, R.W. Judy, Jr., and C.N. Freed, NRL Report 6327, May 1965

Eighth Quarterly Report - "Metallurgical Characteristics of High Strength Structural Materials," P.P. Puzak, K.B. Lloyd, R.J. Goode, R.W. Huber, D.G. Howe, R.W. Judy, Jr., T.W. Crooker, R.E. Morey, E.A. Lange, and C.N. Freed, NRL Report 6364, Aug. 1965

Ninth Quarterly Report - "Metallurgical Characteristics of High Strength Structural Materials," R.J. Goode, R.W. Huber D.G. Howe, R.W. Judy, Jr., P.P. Puzak, K.B. Lloyd, T.W. Crooker, R.E. Morey, E.A. Lange, and C.N. Freed, NRL Report 6405, Nov. 1965

## CONTENTS

Abstract. . . . .	iii
Problem Status. . . . .	iii
Authorization . . . . .	iii
INTRODUCTION. . . . .	1
TITANIUM ALLOYS . . . . .	4
Tensile and Fracture Toughness Data for Titanium Alloy Plates T-88 Through T-95 . . . . .	4
Comparison of $K_{Ic}$ and DWTT Fracture Toughness Data for 1-in. Thick Titanium Alloy Plate. . . . .	6
Fracture Toughness Index Diagram for Titanium . . . . .	12
Stress Corrosion Cracking of Some Titanium Alloys . . . . .	15
The Effects of Heat Treatment on the Stress-Corrosion- Cracking Resistance of Several Ti-Al-Mo-V Alloys. . . . .	28
HIGH STRENGTH STEELS. . . . .	36
Fracture Toughness Index Diagram for Steels . . . . .	37
Fracture Toughness Characterization of Special Melt Practice 180-ksi Yield-Strength Steels. . . . .	37
Fracture Toughness Evaluation and Control of High Strength Steel Weld Metals. . . . .	53
LOW CYCLE FATIGUE CRACK PROPAGATION IN 12%-Ni MARAGING STEELS. . . . .	64
Test Materials. . . . .	64
Results and Discussion. . . . .	65
Comparison with Other Steels. . . . .	67
Summary . . . . .	70
ALUMINUM ALLOYS . . . . .	70
Explosion Tear Test Results . . . . .	71

CONTENTS (contd)

Fracture Toughness Index Diagram. . . . .	71
Tests of Six-Inch-Thick 7039-T6X31. . . . .	75
Stress-Corrosion-Cracking Tests . . . . .	75
COMPARISON OF LOW CYCLE FATIGUE TEST RESULTS-- INITIATION VERSUS PROPAGATION FAILURE CRITERIA. . . . .	81
Index of Structural Fatigue Life. . . . .	81
Discussion. . . . .	83
Conclusions . . . . .	88
PLANE STRAIN FRACTURE TOUGHNESS OF HIGH AND ULTRAHIGH STRENGTH MATERIALS. . . . .	88
$K_{Ic}$ Results for Three Aluminum Alloys . . . . .	89
$K_{Ic}$ Data for an 18%-Ni Maraging Steel . . . . .	93
$K_{Ic}$ Data for Two Titanium Alloys. . . . .	95
Correlation of $K_{Ic}$ with DWTT. . . . .	95
REFERENCES. . . . .	100

## ABSTRACT

A progress report covering the research studies in high strength structural metals conducted in the period December 1965 through March 1966 is presented. The report includes fracture toughness studies on expected normal production 12%-Ni maraging and 9Ni-4Co-0.25C steels, a variety of circular rolled and conventionally rolled titanium alloys, and aluminum alloys using standard engineering, newly developed, and linear elastic fracture mechanics type fracture toughness tests. Preliminary correlations of  $K_{Ic}$  with drop-weight tear test energy for a variety of titanium alloys are presented. Low cycle fatigue crack propagation in 12%-Ni maraging steels in air and salt water is described and compared to the behavior of other steels. Also, crack initiation versus propagation failure criteria for low cycle fatigue in air and in aqueous environments is presented for HY-80 and 5Ni-Cr-Mo-V steels and 12%-Ni maraging steels. The stress-corrosion-cracking resistance of a variety of titanium alloys and several aluminum alloys has been determined using a cantilever-bend test; comparison of results obtained in the laboratory and in natural seawater at Key West are presented for a Ti-7Al-2Cb-1Ta alloy.

## PROBLEM STATUS

This is a progress report; work is continuing.

## AUTHORIZATION

NRL Problem F01-17; Project SP-01426.  
NRL Problem M01-05; Projects RR-007-01-46-5405,  
SF-020-01-01-0724, and SP-01426.  
NRL Problem M01-18; Projects RR-007-01-46-5420,  
SF-020-01-05-0731, SP-01426,  
and MIPR-ENG-NAV-66-2.  
NRL Problem M03-01; Projects RR-007-01-46-5414,  
SF-020-01-01-0850, and SP-01426.

Manuscript Submitted June 28, 1966.

METALLURGICAL CHARACTERISTICS  
OF HIGH STRENGTH STRUCTURAL MATERIALS

[Tenth Quarterly Report]

INTRODUCTION

This report is the tenth in the series of status reports covering the U.S. Naval Research Laboratory Metallurgy Division's long-range Advanced High Strength Structural Metals Program. This program is concerned with determining the performance characteristics of high strength metals and is directed at developing the necessary information to provide "guide line" principles for the metallurgical optimization of alloys, for processing and fabrication techniques, and for the reliable failure-safe utilization of these materials in large, complex welded structures. Fracture toughness aspects of the failure-safe design problem are being studied with newly developed test methods as well as with conventional, established engineering methods. The subcritical crack growth characteristics of the high strength metals are being determined for low cycle fatigue. Environmental effects on subcritical crack growth and the application of fracture mechanics techniques for the spectrum of materials under investigation are also being studied.

The Charpy V-notch (for steels), drop-weight tear, and explosion tear tests have been used to determine the fracture toughness characteristics of steels, titanium, and aluminum over wide ranges of yield strengths and have made possible the development of preliminary fracture toughness index diagrams for these materials. The diagrams provide "guide line" information for purposes of design, alloy development, specification, and quality control. The latest versions of these diagrams are presented in this report.

Preliminary data concerning the as-received and heat-treated fracture toughness (drop-weight tear test and Charpy V) and tensile properties are presented for five circular rolled titanium alloy plates and weldments. The plane-strain fracture toughness ( $K_{Ic}$ ) data for these same alloys in the as-received condition are also presented. A comparison of the fracture toughness data for these alloys provides an amazing correlation between drop-weight tear test energy and the bend-bar  $K_{Ic}$  fracture toughness over a wide range of toughness.

The stress-corrosion-cracking resistance was determined for a large number of titanium alloys in a 3.5-percent-salt-water solution. The data is presented in the form of stress intensity-time curves showing the rapid fall-off of stress intensity ( $K_I$ ) with time once the threshold value ( $K_{Isc}$ ) for stress-corrosion-cracking is exceeded. Also, data is presented showing the similarity of stress-corrosion-cracking results obtained with a 3.5 percent-salt-water solution and natural seawater for a Ti-7Al-2Cb-1Ta alloy. Test results are described which show the beneficial effects of vacuum heat treatments compared to inert gas heat treatments on the stress-corrosion-cracking resistance of several titanium alloys.

The fracture toughness characterization of 180-ksi yield-strength 12Ni-5Cr-3Mo maraging and 9Ni-4Co-0.25C quenched-and-tempered (Q&T) steels representative of expected "normal" production materials is described. The 9Ni-4Co-0.25C steel was received at a yield strength lower than the 180-ksi yield strength specified. Data obtained for NRL full cycle Q&T heat-treated material showed that at the 180-ksi-yield-strength level the fracture toughness values were considerably below previously tested 9Ni-4Co-0.25C steel. The 12%-Ni maraging steel exhibited strength and toughness values far below those expected. The results of a program to determine possible mill deviation from specified heat-treatment conditions and to establish specific heat-treatment conditions to improve the strength and toughness properties are described. It is shown that with proper selections of heat-treating conditions near optimum properties were obtained for the 12%-Ni maraging steel.

Preliminary data on the fracture toughness characteristics of TIG weldments in 12Ni-5Cr-3Mo maraging steel furnished NRL are presented for a matching weld wire composition and a 17Ni-2Co-3Mo composition. Generally, the results indicate the weldments equaled or exceeded the toughness values of other previously studied experimental TIG welds of equivalent strength level. A preliminary study with manual TIG weldments made at NRL using 12Ni-5Cr-3Mo and 17Ni-2Co-3Mo filler metal (stranded weld wire) in 12Ni-5Cr-3Mo maraging steel produced weldments of lower strength and toughness.

Low cycle fatigue studies on the 12Ni-5Cr-3Mo maraging steel in air and in 3.5-percent-salt-water solution indicate good crack propagation characteristics for this material; it compares favorably with HY-80 and HY-140 steels.

Initiation versus propagation failure criteria for low cycle fatigue is presented for HY-80 and 5Ni-Cr-Mo-V Q&T steels and 12Ni-5Cr-3Mo maraging steels. The air data indicate that crack initiation generally tends to be more conservative but a back-up of equal life for the crack propagation stage is not always present. In salt water, fatigue crack propagation is the more critical phase; at elastic strain levels, life based on crack propagation is approximately one-half the life based on crack initiation.

Explosion tear test results are presented for the aluminum alloys 7005-T63, 7106-T63, 5083-0, and 5086-H112. Based upon the results obtained with the first two alloys, modifications to the aluminum Fracture Toughness Index Diagram have been made. Tensile and fracture toughness-through-thickness properties were determined for a 6-in.-thick 7039-T6X31 alloy plate. No variations in properties associated with thickness effects were clearly evident. Preliminary stress-corrosion-cracking studies were conducted on the alloys 2219-T87, 7079-T6, 7075-T7351, and 7106-T63. Cracks parallel to the rolling plane developed in the 7079-T6 and 7106-T63 alloys. No evidence of stress-corrosion-cracking or axial cracking for the other two alloys was noticed.

Plane strain fracture toughness ( $K_{Ic}$ ) determinations have been made for the aluminum alloys 7075-T7351, 2219-T851, 2024-T4, an 18% Ni maraging steel, and two titanium alloys (Ti-6Al-4Zr-2Sn-0.5Mo-0.5V and Ti-6Al-4Zr-2Mo) using varying depths of side grooving on single-edge-notched tensile type plate specimens. The data indicate that excessive side groove depths can result in a lowering of the measured  $K_{Ic}$  plane strain fracture toughness. The degree of validity of the data is indicated. A preliminary correlation of  $K_{Ic}$  with drop-weight tear test energy is presented for titanium alloys studied with the single-edge-notched specimen.

## TITANIUM ALLOYS

(R. J. Goode, R.W. Huber, R.W. Judy, Jr., and D.G. Howe)

Preliminary weldment and heat-treatment data have been obtained for five titanium alloys: 5Al-2Mo-2V-2Sn (T-90), 6Al-4V (T-91), 6Al-6V-2Sn-1Cu-0.5Fe (T-92), 6Al-3V-1Mo (T-93), and 7Al-2.5Mo (T-94). These alloys were furnished as  $\alpha + \beta$  circular rolled plates in nominally 1-in., 2-in., and 3-in. thicknesses. The tensile and drop-weight tear test (DWTT) data obtained for the 1-in.-thick, as-received material were reported in the last Quarterly Progress Report (1). In addition, similar data have been obtained for the titanium alloys 7Al-1Mo-1V (T-88) and 7Al-2Cb-1Ta (T-89) which were conventionally processed. All of these alloys had low interstitial contents with the weight-percent oxygen below 0.08. A commercially designated extra low interstitial (ELI) grade 6Al-4V with 0.12 wt-% oxygen was also studied. All welding was done with the metal inert gas (MIG) process and all heat treatments, both for plates and weldments, were conducted in a cold wall vacuum annealing furnace followed by helium cooling.

### TENSILE AND FRACTURE TOUGHNESS DATA FOR TITANIUM ALLOY PLATES T-88 THROUGH T-95

The yield strength (YS) and DWTT data obtained to date for the as-received plate, heat-treated plate, and as-welded and heat-treated weldments are presented in Table 1. Also included for comparison are stress-corrosion-cracking data and plane strain fracture toughness data obtained for some of these materials; these data are discussed in following sections of this report.

Alloys T-90 through T-94 were produced by rolling an upset-forged, pancake-shaped billet into a large disc-shaped plate by rotating the plate between rolling passes. This was done in an effort to minimize directionality effects on the mechanical properties. The final rolling reductions of the plates were conducted about midway in the  $\alpha + \beta$  phase region. After the last rolling pass, the plates were spray quenched. This rolling procedure would not result in the delineation of a "principal rolling direction" in the normal sense; therefore, for purposes of designating specimen orientation (tensile) and fracture direction (DWTT) with respect to the plate, the reference directions A and B are used, with B  $90^\circ$  to the A direction.

Table 1  
Properties of Some 1-inch-Thick Titanium Alloy Plates and Weldments

Alloy No.	Nominal Composition 0.08% Max. Unless Indicated	Specimen Orientation	Average 0.2% YS (ksi)	DWTT (ft-lb)	K <sub>Ic</sub> ksi√in. ("Kies")	SCC	
						K <sub>Ix</sub>	K <sub>Isc</sub>
T-88	7Al-1Mo-1V As-received  Vac. Ann. 1800° F/1 hr/He cool MIG Weld as-deposited MIG Weld Ht 1800° F/1hr	T	126	1326		90	78
		L	122	1540			
		T		2000			
		L		2100			
				1900			
				1000			
T-89	7Al-2Cb-1Ta As-received Ht 1900° F/1 hr/He cool	T	110.6	1905		122	45
		L	112.8	2146			
				2000			
T-90	5Al-2Mo-2V-2Sn  Ht 1660° F/1 hr/He cool Ht 1850° F/1 hr/He cool MIG Weld as-deposited MIG Weld Ht 1850° F MIG Weld Ht 1660° F	A	116.3	1418	128	108	100
		B	112.7	1723			
		A		1723			
		A		1356			
				811			
				1133			
				870			
T-91	6Al-4V As-received Ht 1800° F/1 hr/He cool Ht 1850° F	A	109.0	870	110	118	90
		B	104.9	1228			
		B		1173			
		B		1540			
T-92	6Al-6V-2Sn-1Cu-0.5 Fe As-received Ht 1660° F/1 hr/He cool MIG Weld as-deposited MIG Weld Ht 1660° F	A	122.0	681	98	111	96
		B	123.8	681			
		A		811			
				455			
				514			
T-93	6Al-3V-1Mo As-received Ht 1675° F/WQ 1300° F/2hr Ht 1800° F/1 hr/He cool Ht 1850° F/1 hr/He cool MIG Weld as-deposited MIG Weld Ht 1850° F/1 hr/ He cool	A	116.5	1173	118	116	110
		B	109.8	1540			
		A		1300			
		A		1662			
				1850			
				1228			
				1723			
T-94	7Al-2.5Mo(1.25 in. thick) As-received (1.13 in.) (1.0 in.) Ht 1800° F/1 hr/He cool (1.25 in.) Ht 1800° F/1 hr/He cool (1.00 in.) MIG Weld as-deposited NOTE: T-71 7Al-2.5Mo MIG Weld MIG Weld Ht 1800° F	A	119.0	1540		101	80
		B	120.5	1662			
		A		1540			
		A		1228			
		A		4380			
		A		2756			
				1540			
				1844			
				1480			
				2200			
T-95	6Al-4V ELI Grade 1200 PPM O <sub>2</sub> (1.19 in.) (1.10 in.) (1.0 in.) Ht 1800° F/1 hr/He cool 1850° F/1 hr/He cool NOTE: T-5 6Al-4V as-received T-27 6Al-4V as-received	T		811			
		L		991			
		L		931			
		L		811			
		L		1228			
				1296			
		T		2200			
		T		1200			

The DWTT energies of the T-90 through T-94 plates were generally lower than those that had been obtained in the past with similar alloy compositions that had been conventionally cross-rolled and air cooled. Vacuum annealing at temperatures below the  $\beta$  transus generally resulted in a marked increase in fracture toughness for all the alloys. The largest increase was shown by the Ti-7Al-2.5Mo alloy (T-94) which increased from an as-received value of 1540 ft-lb to 2756 ft-lb DWTT energy with a single 1-hour 1800°F solution anneal. A comparison of the DWTT data for as-deposited weldments and heat-treated weldments shows an improvement in the fracture toughness of the welds by heat treatment. However, the heat-treatment schedules employed for both the plates and weldments are not to be considered optimum;  $\beta$  transus determinations must be made for each of these alloys before optimum heat treatments can be applied.

The alloys 7Al-1Mo-1V (T-88) and 6Al-4V (T-95) showed the same general response to heat treatments as described above for the circular rolled plates. The overall lower fracture toughness for T-95 is associated with its high oxygen content.

The Charpy V ( $C_V$ ) notch fracture toughness energy was determined for the 1-in.-thick circular-rolled plate material as well as for the alloy T-89. The results are shown in Figs. 1-6 for the A and B orientations.

#### COMPARISON OF $K_{Ic}$ AND DWTT FRACTURE TOUGHNESS DATA FOR 1-IN.-THICK TITANIUM ALLOY PLATE

The failure-safe use of thick section, low-fracture toughness (fracture occurs at elastic stress levels) high and ultra-high strength metals requires knowledge of the critical flaw size-stress level for fracture for the particular material of interest. At the present time, linear elastic fracture mechanics methods best provide this necessary information for these materials. The information that is necessary for the failure-safe use of high toughness (fracture occurs at plastic stress levels) high strength metals has been established through correlations of the DWTT with the explosion tear test (ETT), a structural prototype element test. This correlation establishes the significance of the DWTT in terms of the plastic strain capability of the material in the ETT,

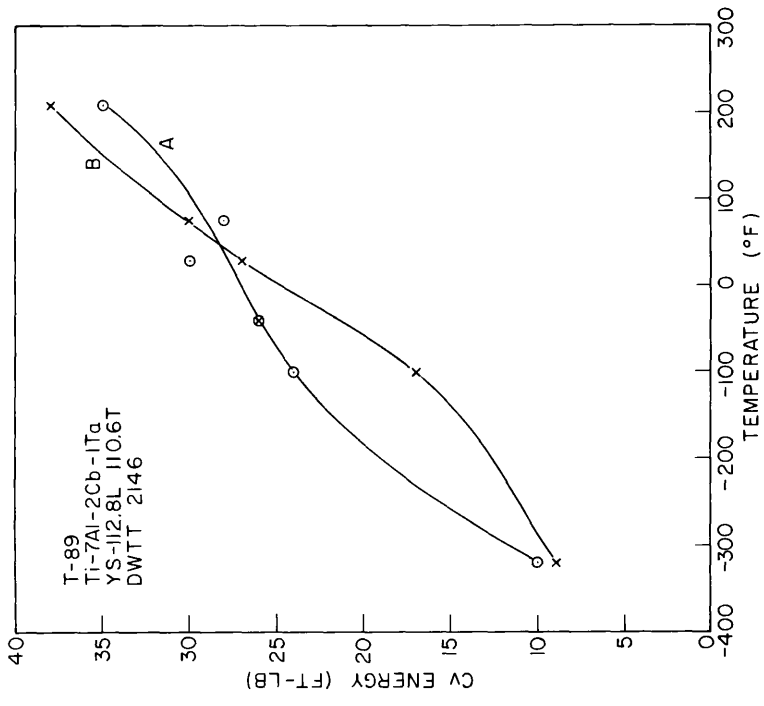


Fig. 1 - Charpy V-notch energy measurements for Ti-7Al-2Cb-1Ta (T-89) 1-inch-thick plate.

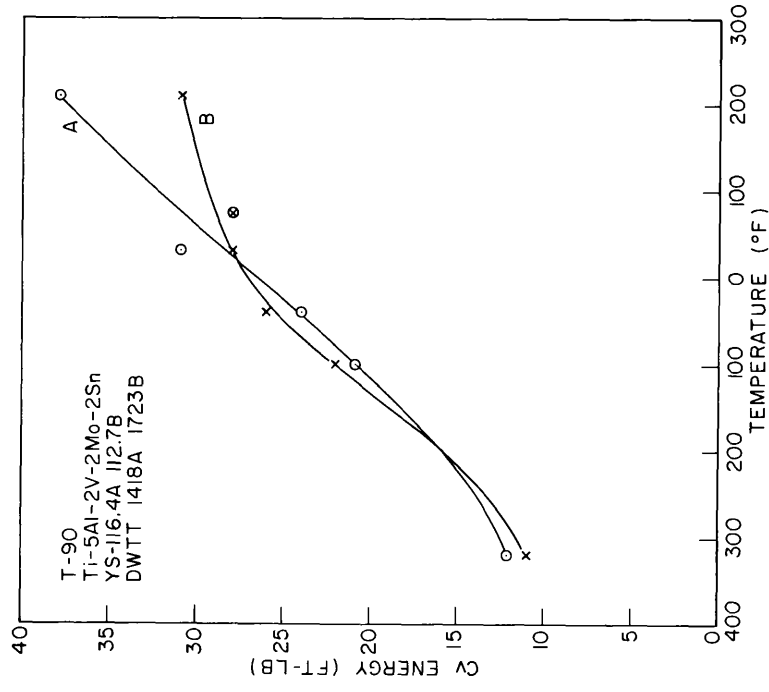


Fig. 2 - Charpy V-notch energy measurements for Ti-5Al-2V-2Mo-2Sn (T-90) circular-rolled 1-inch-thick plate.

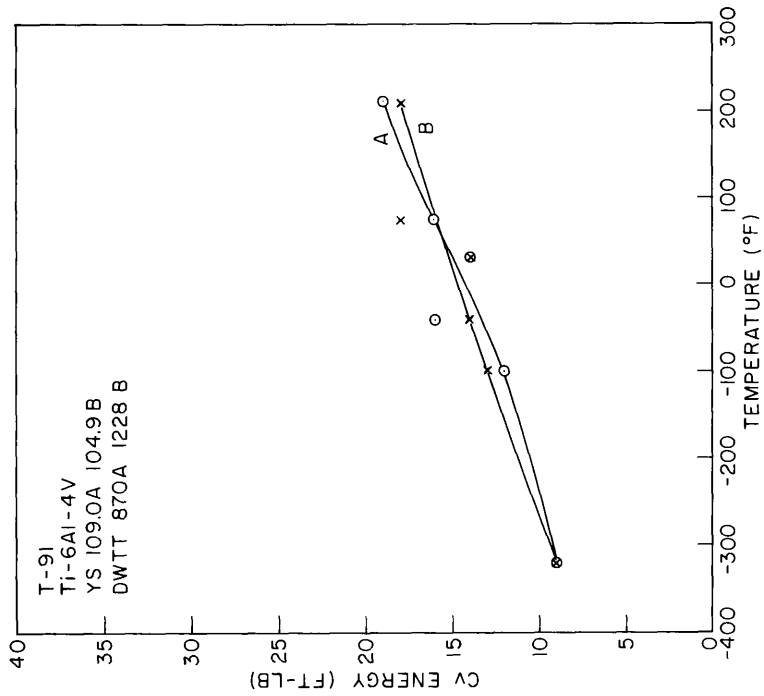


Fig. 3 - Charpy V-notch energy measurements for Ti-6Al-4V (T-91) circular-rolled 1-inch-thick plate

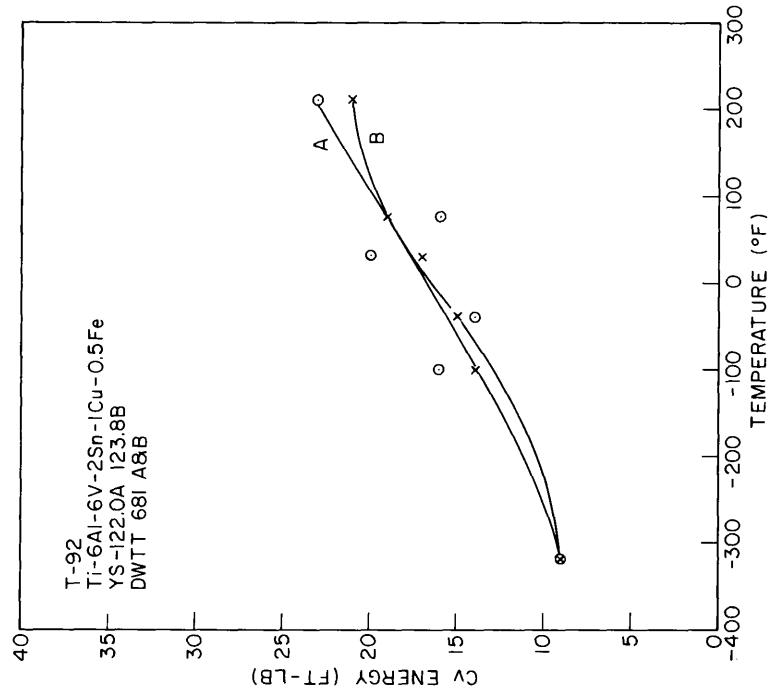


Fig. 4 - Charpy V-notch energy measurements for Ti-6Al-6V-2Sn-1Cu-0.5Fe (T-92) circular-rolled 1-inch-thick plate

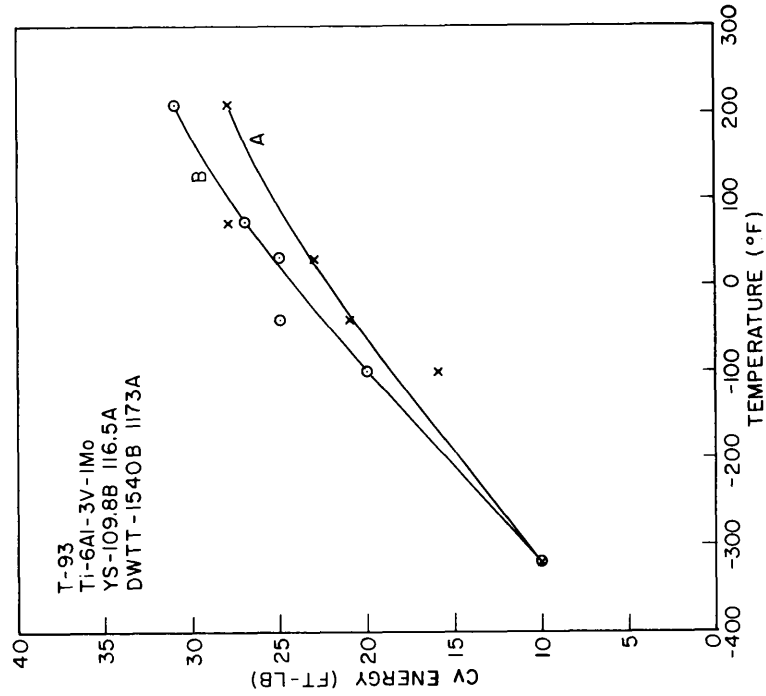


Fig. 5 - Charpy V-notch energy measurements for Ti-6Al-3V-1Mo (T-93) circular-rolled 1-inch-thick plate.

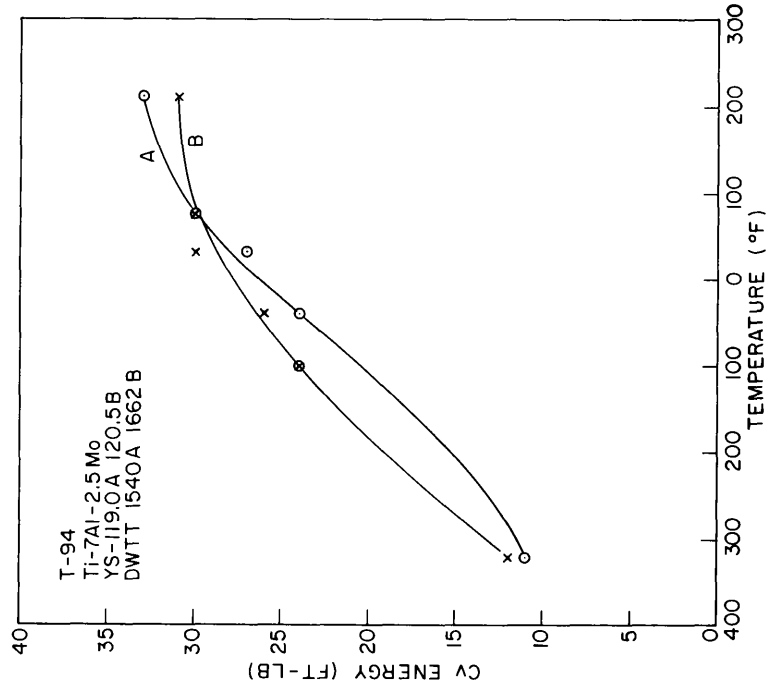


Fig. 6 - Charpy V-notch energy measurements for Ti-7Al-2.5Mo (T-94) circular-rolled 1.25-inch-thick plate.

and it has been presented in the form of fracture toughness index diagrams for steels and titanium and aluminum alloys over a wide yield strength range.

Accurate measurements of the energy required for fracture of low toughness materials can also be made in the DWTT; however, the significance of the energy values has not been established in terms of critical flaw size-stress level for fracture. One approach to establish this significance would be to carefully strain gage the ETT plate and, using different size flaws, establish the amounts of elastic strain required to cause fracturing. The ETT indexing of the DWTT would then incorporate the same strain rate differences for the two tests that are already inherent in the correlation for the tough materials. However, the ETT would now become time-consuming and expensive due to the instrumentation required, placement of strain gages, etc. The advantage of the "Mark I" eyeball evaluation and grid-marking measurement technique, which is rapid and accurate enough for plastic strain for fracture determinations of the tough materials, would now be lost. Also, the attainment of the degree of accuracy required for meaningful measurements of the elastic stresses in the critical specimen locations would require considerable effort before exact critical flaw size-stress level correlations with DWTT could be established.

Since plane strain fracture mechanics tests are presently being conducted on a variety of high strength steels and titanium and aluminum alloys, it was decided that, as a first approach to establishing the significance of the DWTT energy values with respect to critical flaw size-stress level for fracture, a comparison of DWTT energy with  $K_{Ic}$  (plane strain fracture toughness) measurements be made. Bend-bar specimens, 1x1x10 in. (from 1-in. thick plate) and 2x2x20 in. (from 2-in.-thick plate) had been furnished to J. Kies of the Mechanics Division of the U.S. Naval Research Laboratory for  $K_{Ic}$  determinations. The specimens, five for each alloy and thickness, were side-grooved 5% of the specimen width and contained a fatigue crack at the root of the notch. They were tested in three point bending and the measured  $K_{Ic}$  values were corrected for  $r_y$  (plastic zone size).

The results of the bend-bar  $K_{Ic}$  test for the titanium alloys are shown in Table 2. The yield strength values\* used in

\* The 134.0-ksi YS for T-92 indicated in Ref. 1 has subsequently been found to be ~ 123 ksi YS (see Table 1); however, this difference would not significantly change the K value.

Table 2  
 Summary of Titanium Bend-Bar  $K_{Ic}$  Data

Material No.	Material	$\sigma_y$ (ksi)	Plate Thickness (in.)	Notch Location	$K_{Ic}$ (ksi $\sqrt{\text{in.}}$ )	
					Uncorrected	Corrected
T 90	5Al-2V-2Mo-2.5Sn	113.0	1	Base plate	109	128
		106.3	2	Base plate	124	140
T 91	6Al-4V	105.0	1	Base plate	94	110
		98.6	2	Base plate	129	151
T 92	6Al-6V-2.5Sn-1Cu-0.5Fe	134.0	1	Base plate	90	98
		118.8	2	Base plate	112	121
T 93	6Al-3V-1Mo	117.0	1	Base plate	104	118
		102.5	2	Base plate	138	165
T 94	7Al-2.5Mo	121.0	1	Base plate	133	160
		106.5	2	Base plate	144	170

the calculations of  $K_{IC}$  are indicated along with the uncorrected and corrected  $K_{IC}$  fracture toughness values.

A plot of the corrected bend-bar  $K_{IC}$  data with DWTT energy is shown for the 1-in.-thick plate material in Fig. 7. The limits for each point indicate the spread in values obtained for one orientation (testing through thickness of A-oriented specimen) in the  $K_{IC}$  test and the values for the A and B orientations in the DWTT. The degree of agreement between the two tests is amazing and, at this very preliminary stage, indicates that reasonable predictions of  $K_{IC}$ , thus, critical flaw size-stress level for fracture, should be possible from DWTT results.

#### FRACTURE TOUGHNESS INDEX DIAGRAM FOR TITANIUM

The fracture toughness characterization of titanium alloys in thick sections is based upon the correlation of laboratory DWTT results with performance in the ETT, a structural prototype element test. The preliminary Fracture Toughness Index Diagram (FTID) evolved in these studies indicates the fracture toughness characteristics for a wide range of yield strengths and indexes the DWTT in terms of ETT performance of the material. An optimum material trend line (OMTL) has been established which depicts the highest level of toughness that has been seen for any given level of yield strength for present commercially produced material.

The FTID for 1-in.-thick titanium alloy plate is shown in Fig. 8. The variety of alloys that have been investigated in this study is indicated. The significance and interpretation of the features of this diagram have been described in the previous Quarterly Reports, therefore, this will not be repeated in detail. Briefly, the FTID indicates that below 1500 ft-lb DWTT energy the material will act brittle, propagating fractures through elastic stress regions. With increasing DWTT energy above 1500 ft-lb, higher levels of plastic strain are required before fractures will propagate in the ETT. All titanium alloys above about 140 ksi YS would be expected to propagate fractures at elastic stress levels, whereas below 140 ksi YS many of the alloys should be capable of withstanding some amount of plastic strain before fracture--the amount depending upon yield strength level, chemistry, impurities, and processing procedures.

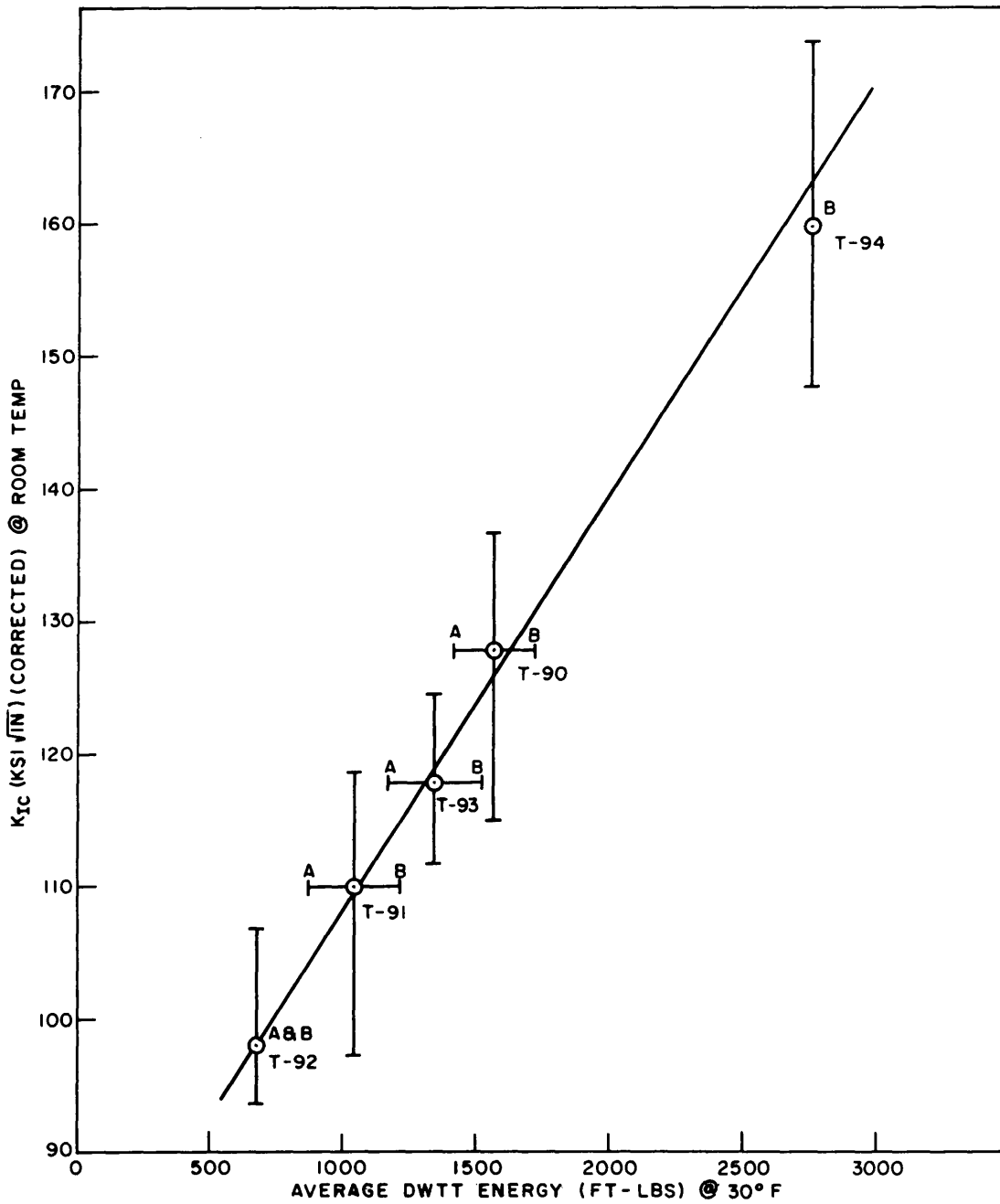


Fig. 7 - Comparison of bend-bar  $K_{Ic}$  data (J. Kies) with drop-weight tear test energy for the 1-inch-thick circular-rolled titanium alloy plates T-90 through T-94

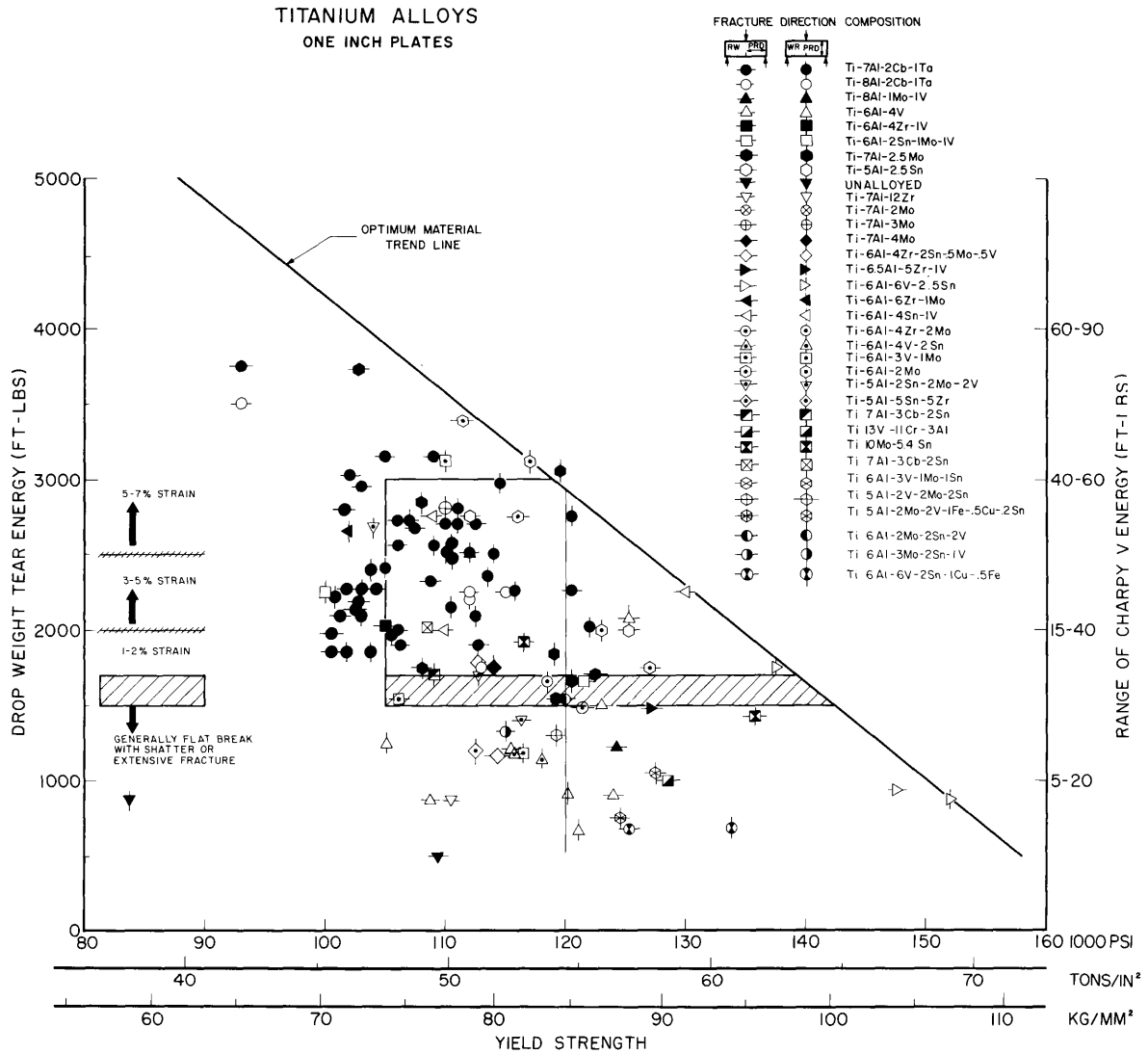


Fig. 8 - Fracture Toughness Index Diagram for titanium alloys. DWTT energy is correlated to ETT performance for 1-inch-thick plate material covering a yield strength spectrum. The optimum material trend line (OMTL) represents an estimate of the presently highest attainable levels of fracture toughness for any given level of yield strength.

## STRESS CORROSION CRACKING OF SOME TITANIUM ALLOYS

Stress-corrosion-cracking (SCC) studies have been conducted on a wide variety of commercial and experimental titanium alloy plates. The tests were conducted by the cantilever method introduced by B. F. Brown (2).

The SCC resistance of a metal can be determined only when certain conditions are met simultaneously; these conditions are a sufficient stress level and flaw size together with an active environment. For a number of titanium alloys, an aqueous (salt water, distilled water, etc.) environment is sufficiently active. The stress level and flaw size necessary to cause SCC to occur are very conveniently combined and expressed in terms of the stress intensity factor  $K_I$ . A threshold level of stress intensity above which SCC will definitely occur has been shown to exist for a number of titanium alloys (3). This stress intensity level is denoted by  $K_{I_{SCC}}$ . Comparison of  $K_{I_{SCC}}$  with  $K_{I_X}$ , the stress intensity required for fracture in air (designated "dry"), gives an indication of the relative resistance of an alloy to environmental cracking. The formula used to calculate K values was the cantilever equation:

$$K_I = \frac{4.12M \sqrt{\frac{1}{\alpha^3} - \alpha^3}}{BD^{3/2}}$$

where

M	=	moment at test section
B	=	specimen width
D	=	specimen thickness
$\alpha$	=	$1 - a/D$
a	=	depth of flaw (notch and fatigue crack).

The specimens tested were 1/2 x 1 x 7 in. long with a machined notch and fatigue crack flaw located at its center in the WR or LT fracture direction (4). The specimens had shallow side grooves to insure plane strain conditions. A 3.5-wt-%-salt-water solution was used as the aqueous environment.

## Results

Environmental cracking data, along with some mechanical properties of the alloys, are shown in Table 3 and Figs. 9 through 28. Except as noted, all the specimens were taken from one-inch plate in the as-received (mill annealed) condition. The Ti-6Al-4V (T-32) alloy was a standard commercial purity grade (high interstitial); all the others had low interstitial contents (below 0.08% O<sub>2</sub>).

The six Ti-7Al-2Cb-1Ta alloys tested in different conditions, the two Ti-5Al-2.5Sn alloys, and the two alloys containing zirconium (Ti-6.5Al-5Zr-1V and Ti-7Al-12Zr) were the most sensitive to environmental cracking. The other alloys were relatively immune to the aqueous environment. Of particular interest in this study are the last five alloys listed in Table 3 (coded T-90 through T-94). These five alloys were the circular rolled plates described earlier in this report. In the as-received condition, they all appear to have a high resistance to stress-corrosion-cracking.

From the beginning of the SCC studies at NRL on titanium alloys, it has always been assumed that the laboratory 3.5-percent-salt-water-solution test results would not be significantly different than those one might obtain using fresh seawater. This assumption was based upon the observation that at a  $K_I$  level only slightly above  $K_{I_{SCC}}$  the subcritical crack growth was relatively rapid and complete fracturing of the specimen would occur in only a few minutes. To test this assumption, a large number of additional specimens of the Ti-7Al-2Cb-1Ta (T-89) alloy were shipped to the NRL corrosion facilities at Key West where they were tested in continuously replenished fresh seawater. The test equipment and procedures are the same as those used at NRL except that the T-89 specimens tested in the laboratory and reported in Table 3 were side-grooved, while the specimens tested at Key West were left ungrooved. Previous tests in the laboratory indicated that similar results could be expected with both types of specimens for titanium alloys of low SCC resistance.

The results of the Key West study on the T-89 alloy are shown in Fig. 23 along with the 3.5-percent-salt-water-solution test results. The  $K_{I_{SCC}}$  value was essentially the same for both tests. Also, the subcritical crack growth portion of

Table 3  
Stress-Corrosion-Cracking Data on Some Titanium Alloys

Composition	Code	YS (ksi)	DWTT (ft-lb)	$K_{I\alpha}$ ksi $\sqrt{in.}$	$K_{I\text{sec}}$ ksi $\sqrt{in.}$	Remarks
Ti-5Al-2-1/2Sn	T3A	112	2750	130	50	
Ti-2Al-2-1/2Sn	T18		1750	112	50	
Ti-6Al-2Sn-1Mo-1V	T25	100	2250	109	70	
Ti-6Al-4V	T32	121	660	101	80	High interstitial
Ti-6-1/2Al-5Zr-1V	T36	127	1480	99	49	
Ti-7Al-12Zr	T62	110.5	870	108	42	Laminated structure
Ti-7Al-2Cb-1Ta	T72	102.8	2174	129	45	2200° F-large red.-AC
Ti-7Al-2Cb-1Ta	T73A	103	2206	129	56	1650° F/1 hr/AC
Ti-7Al-2Cb-1Ta	T74B		2206	122	50	Planetary roll 2010° F
Ti-7Al-2Cb-1Ta	T75			118	43	
Ti-7Al-3Cb-2Sn	T76	108.5	2026	145	75	
Ti-6Al-2Mo-2V-2Sn	T80	120	1540	99	96	
Ti-7Al-1Mo-1V	T88A		2000	94	90	1/2-in. plate 1750° F/1 hr/ vacuum cool
Ti-7Al-1Mo-1V	T88B	126	1326	90	78	1/2-in. plate
Ti-7Al-2Cb-1Ta	T89	110.6	2146	124	45	
Ti-5Al-2V-2Mo-2Sn	T90	112.7	1723	108	100	
Ti-6Al-4V	T91	104.9	1228	118	90	
Ti-6Al-6V-2Sn-1Cu-1/2Fe	T92	133.7	681	111	96	
Ti-6Al-3V-1Mo	T93	116.5	1173	116	110	
Ti-7Al-2-1/2Mo	T94	119	1540	101	80	

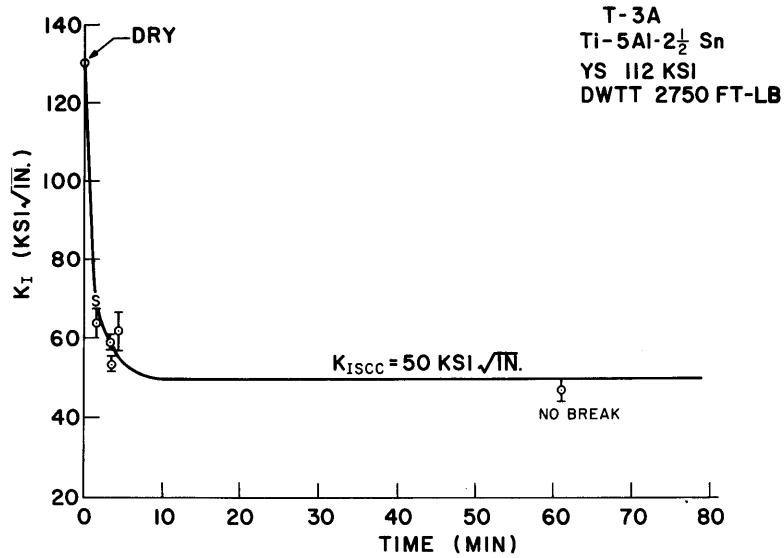


Fig. 9 - Stress-corrosion-cracking characteristics of mill annealed 1-inch-thick Ti-5Al-2.5Sn alloy (T-3A) plate

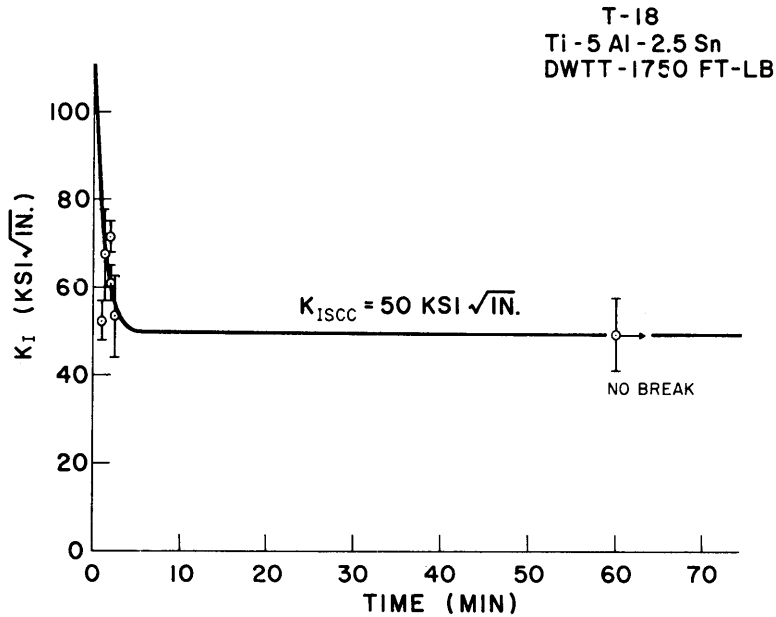


Fig. 10 - Stress-corrosion-cracking characteristics of mill annealed 1-inch-thick Ti-5Al-2.5Sn alloy (T-18) plate

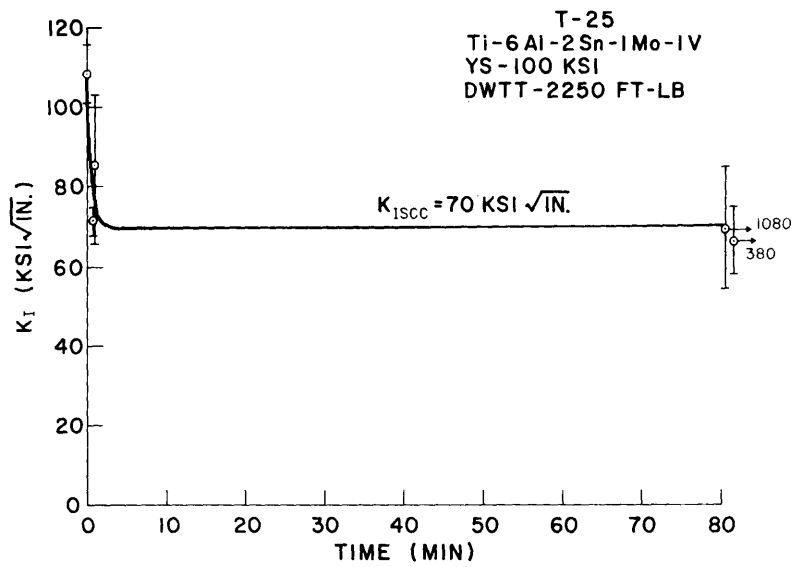


Fig. 11 - Stress-corrosion-cracking characteristics of mill annealed 1-inch-thick Ti-6Al-2Sn-1Mo-1V alloy (T-25) plate

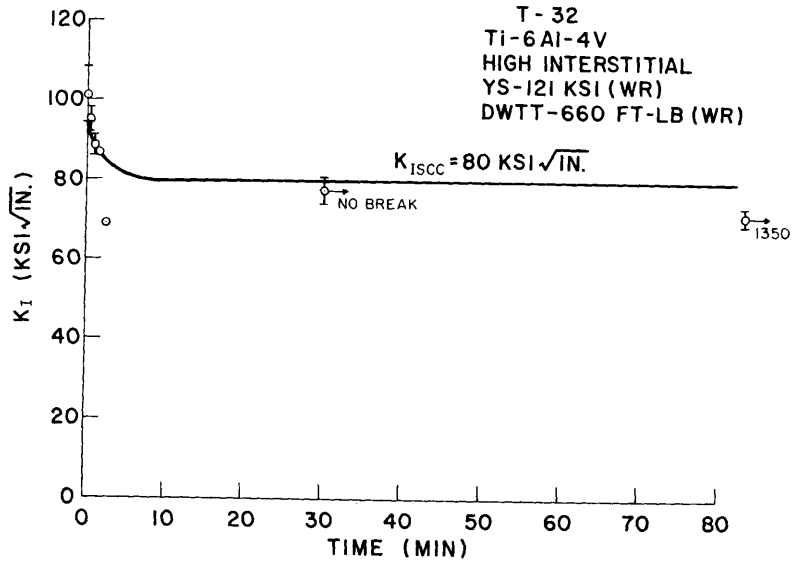


Fig. 12 - Stress-corrosion-cracking characteristics of mill annealed high interstitial 1-inch-thick Ti-6Al-4V alloy (T-32) plate

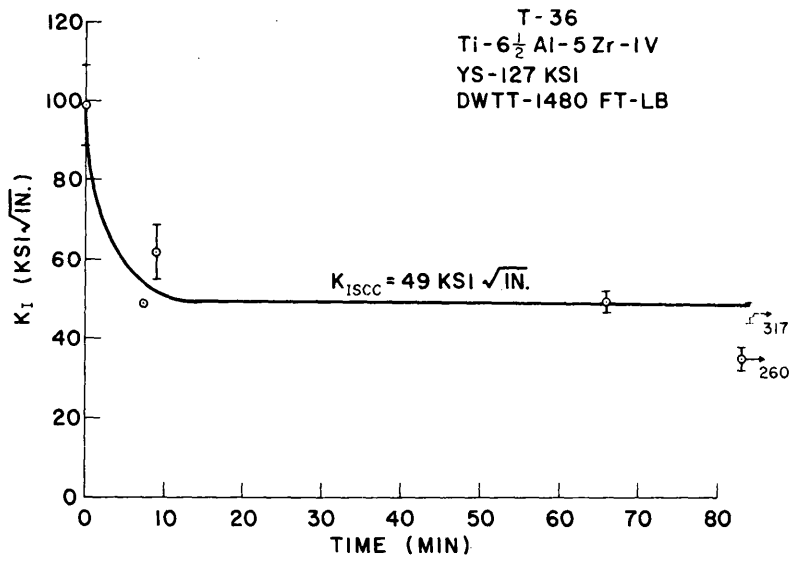


Fig. 13 - Stress-corrosion-cracking characteristics of mill annealed 1-inch-thick Ti-6.5Al-5Zr-1V alloy (T-36) plate

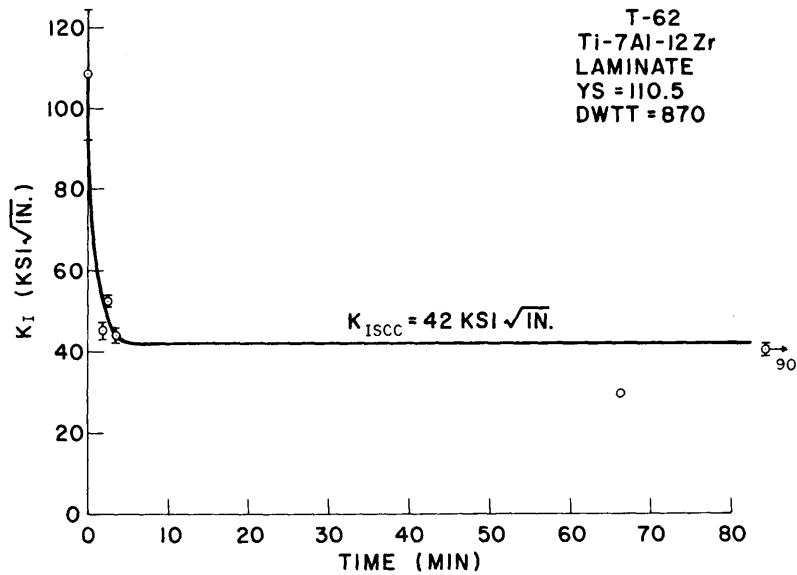


Fig. 14 - Stress-corrosion-cracking characteristics of mill annealed 1-inch-thick laminated (diffusion bonded) Ti-7Al-12Zr alloy (T-62) plate

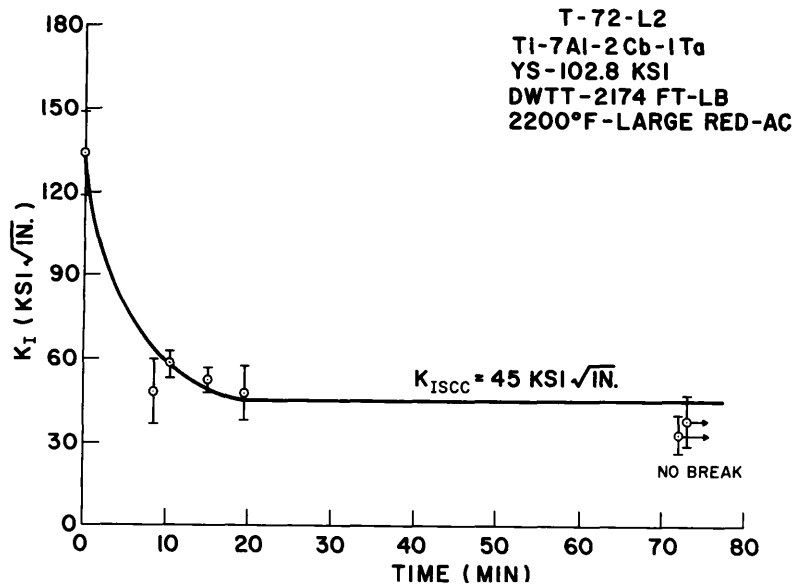


Fig. 15 - Stress - corrosion - cracking characteristics of 1-inch - thick Ti-7Al-2Cb-1Ta alloy (T-72-L2) plate heated to 2200° F, given a large reduction in rolling, and air cooled

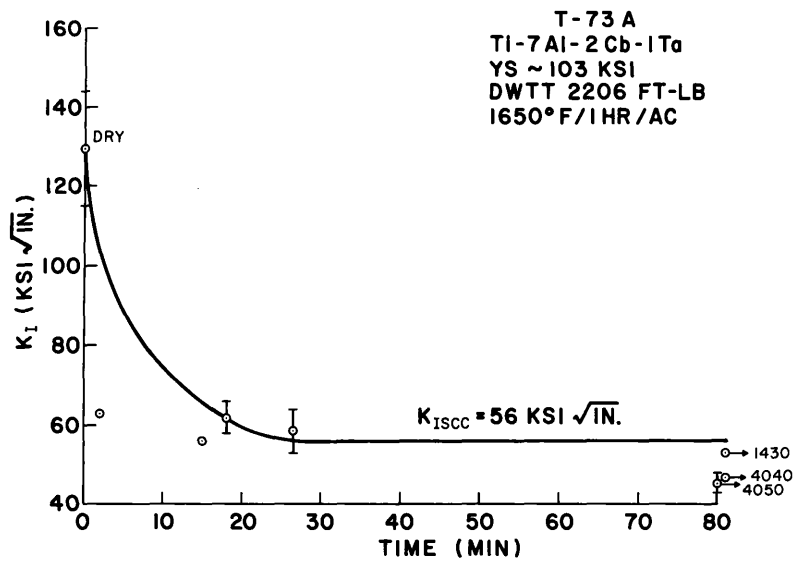


Fig. 16 - Stress-corrosion-cracking characteristics of 1-inch-thick Ti-7Al-2Cb-1Ta alloy (T-73A) plate heated at 1650° F for 1 hour and air cooled

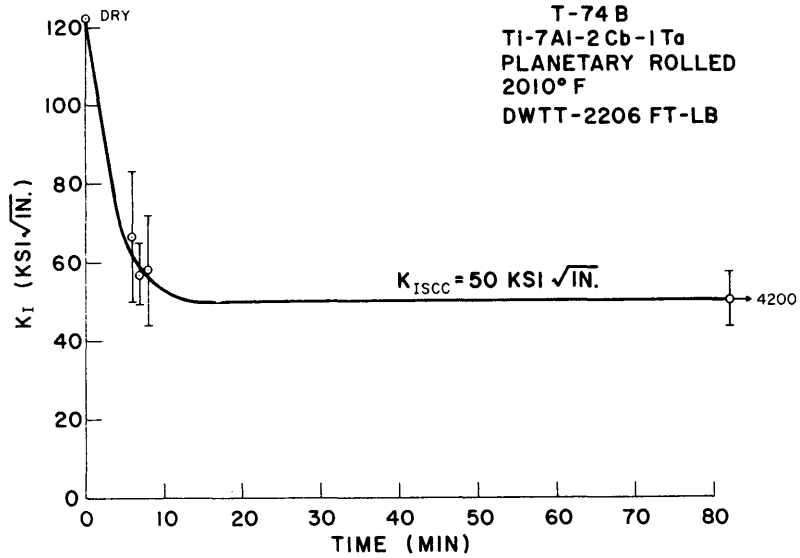


Fig. 17 - Stress-corrosion-cracking characteristics of 1-inch-thick planetary rolled (2010° F) Ti- 7Al - 2Cb - 1Ta alloy (T-74B) plate

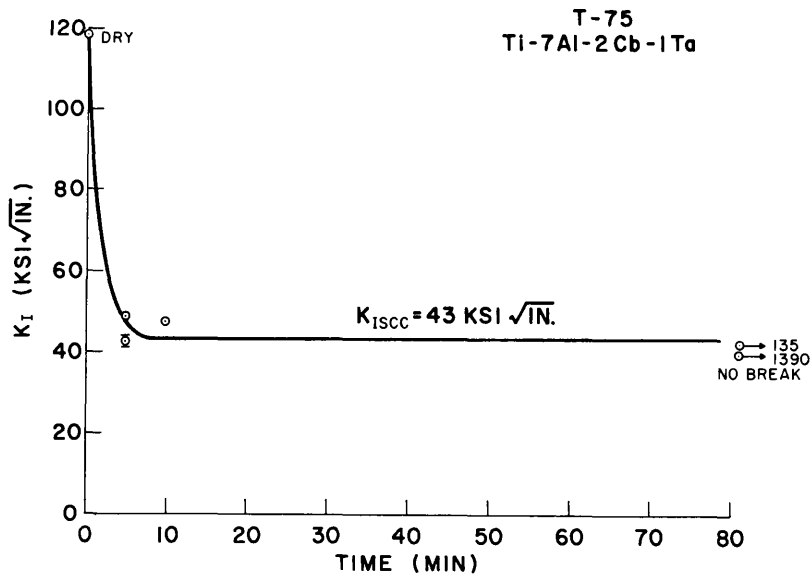


Fig. 18 - Stress-corrosion-cracking characteristics of mill annealed 1-inch-thick Ti-7Al-2Cb-1Ta alloy (T-75) plate

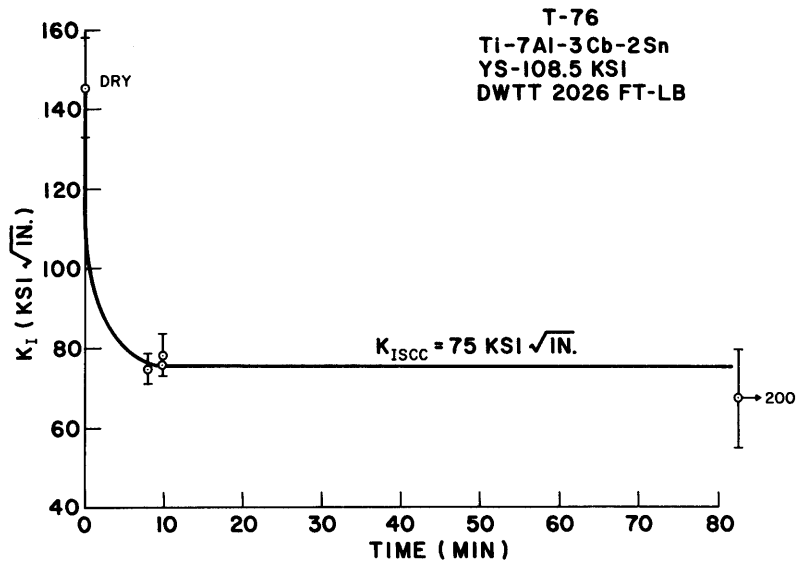


Fig. 19 - Stress-corrosion-cracking characteristics of mill annealed 1-inch-thick Ti-7Al-3Cb-2Sn alloy (T-76) plate

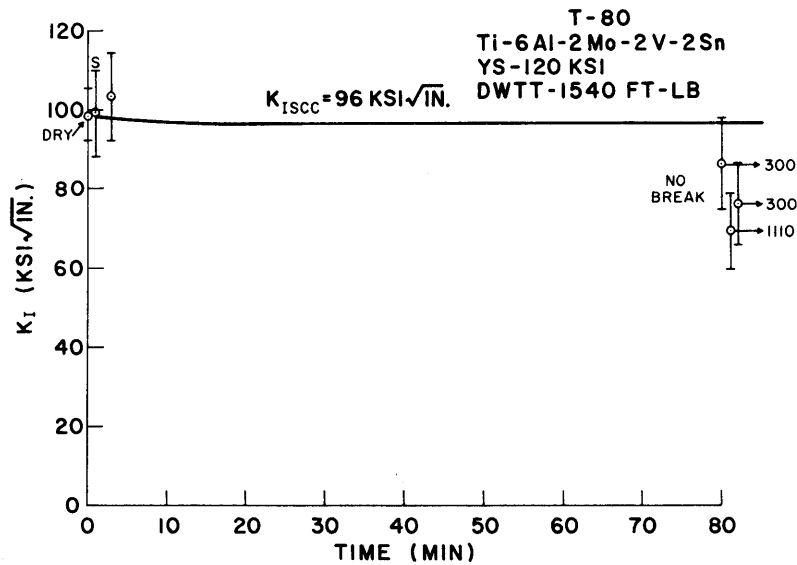


Fig. 20 - Stress-corrosion-cracking characteristics of mill annealed 1-inch-thick Ti-6Al-2Mo-2V-2Sn alloy (T-80) plate

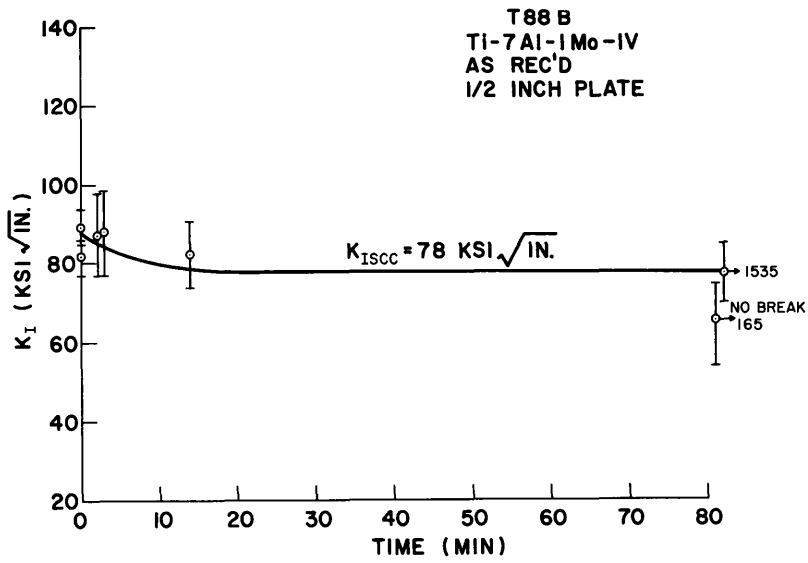


Fig. 21 - Stress-corrosion-cracking characteristics of mill annealed 0.5-inch-thick Ti-7Al-1Mo-1V alloy (T-88B) plate

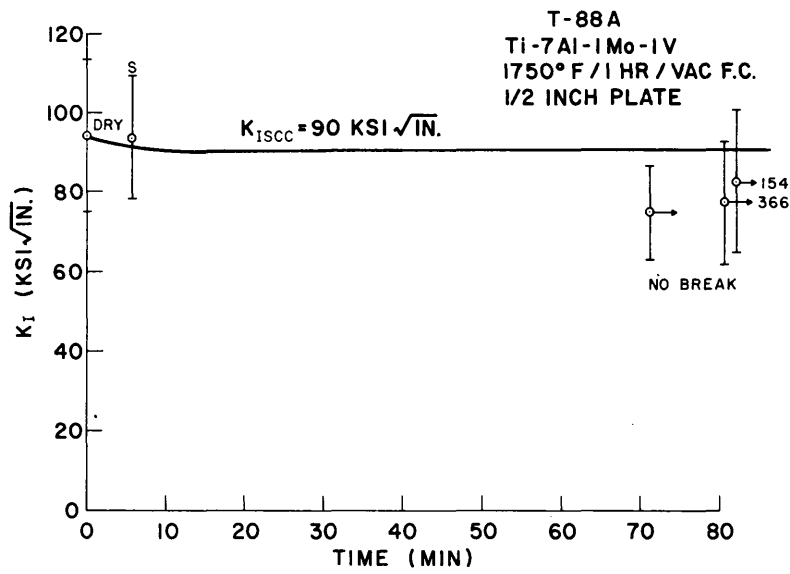


Fig. 22 - Stress-corrosion-cracking characteristics of 0.5-inch-thick Ti-7Al-1Mo-1V alloy (T-88A) plate heat treated at 1750° F for 1 hour and vacuum cooled

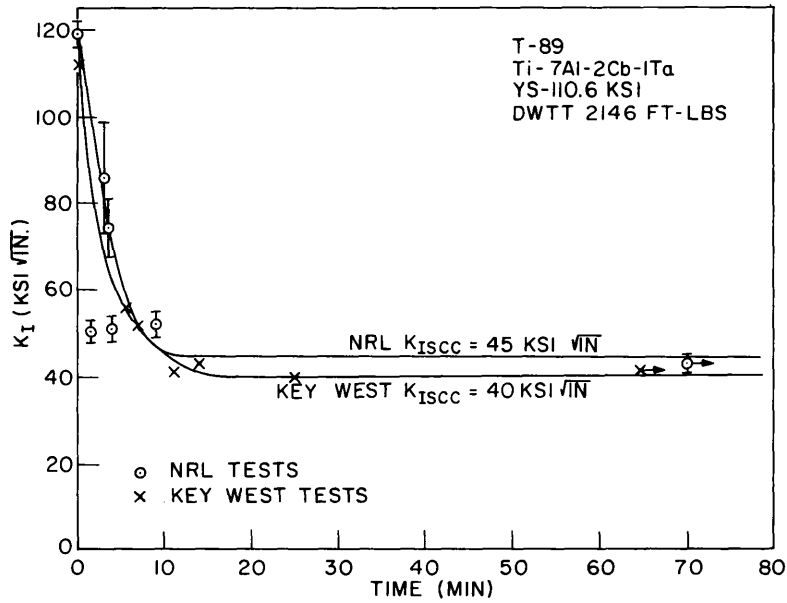


Fig. 23 - Stress-corrosion-cracking characteristics of mill annealed 1-inch-thick Ti-7Al-2Cb-1Ta alloy (T-89) plate

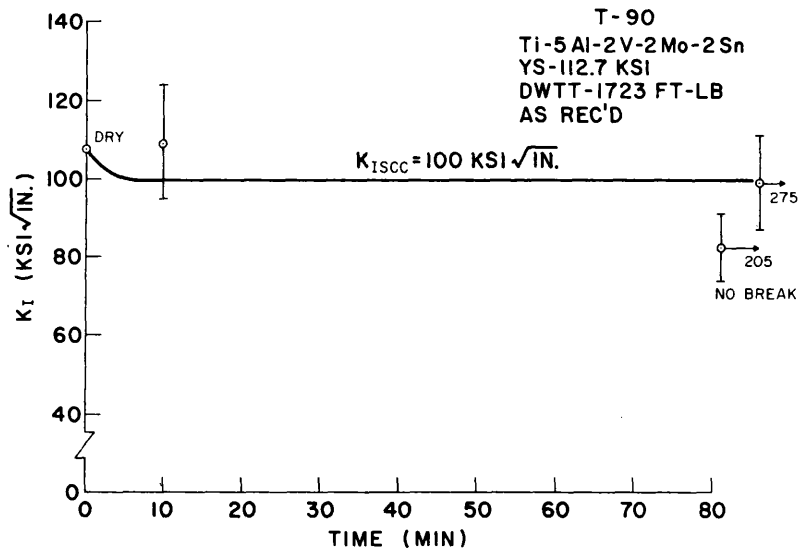


Fig. 24 - Stress-corrosion-cracking characteristics of  $\alpha + \beta$  circular-rolled 1-inch-thick Ti-5Al-2V-2Mo-2Sn alloy (T-90) plate

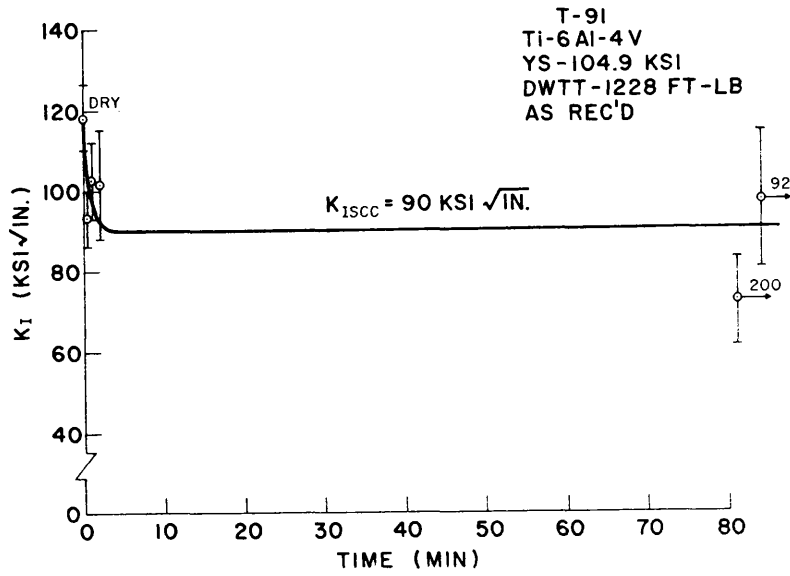


Fig. 25 - Stress-corrosion-cracking characteristics of  $\alpha + \beta$  circular-rolled 1-inch-thick Ti-6Al-4V alloy (T-91) plate

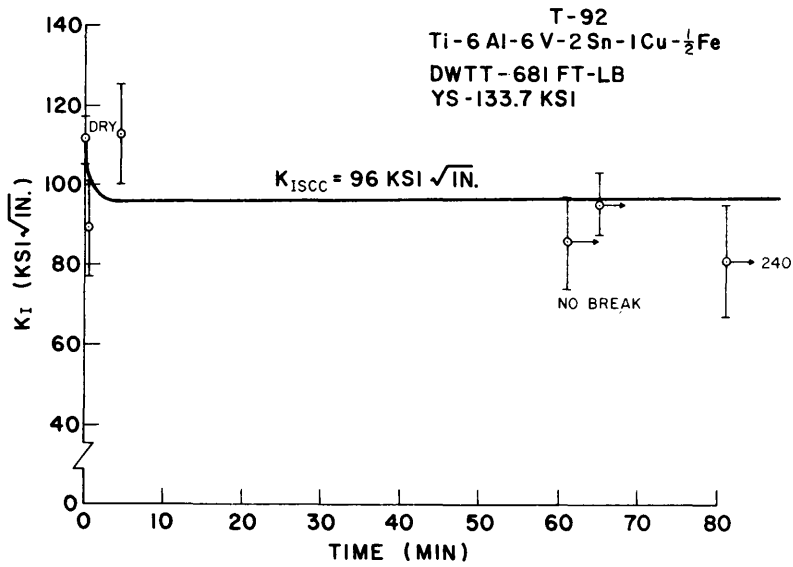


Fig. 26 - Stress-corrosion-cracking characteristics of  $\alpha + \beta$  circular-rolled 1-inch-thick Ti-6Al-6V-2Sn-1Cu-0.5Fe alloy (T-92) plate

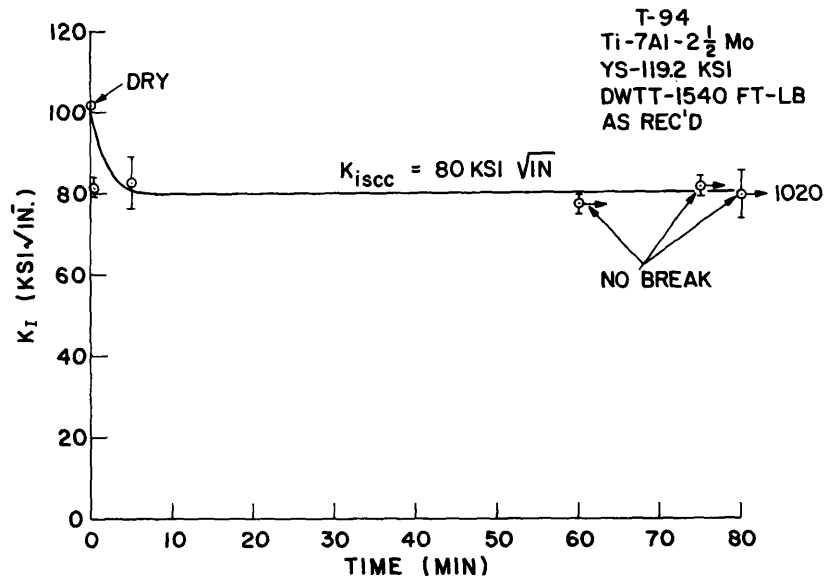


Fig. 27 - Stress-corrosion-cracking characteristics of  $\alpha + \beta$  circular-rolled 1-inch-thick Ti-6Al-3V-1Mo alloy (T-93) plate

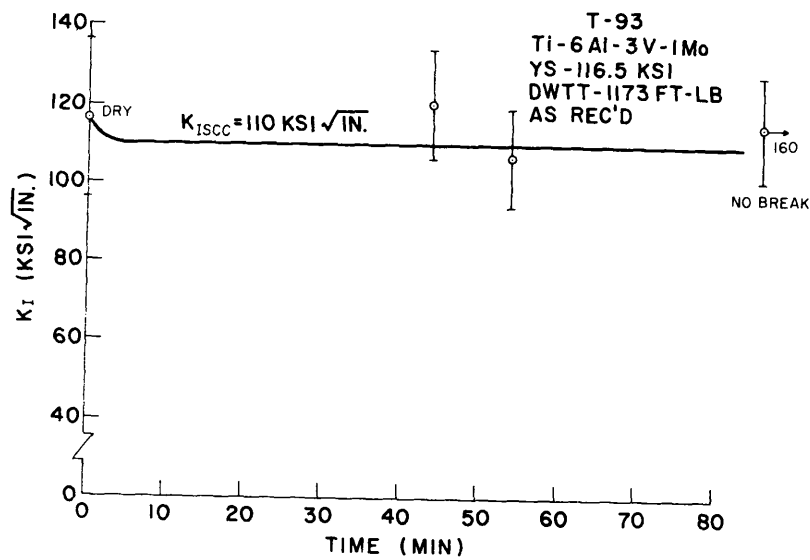


Fig. 28 - Stress-corrosion-cracking characteristics of  $\alpha + \beta$  circular-rolled 1.25-inch-thick Ti-7Al-2.5Mo alloy (T-94) plate

the curves (drop-off time from the "dry"  $K_I$  value to the "threshold" value) are essentially the same. Thus, the original assumption concerning the expected similarity of SCC results for titanium alloys in both types of aqueous environments seems to be borne out. For further confirmation, similar studies will be made on several other titanium alloys.

#### THE EFFECTS OF HEAT TREATMENT ON THE STRESS-CORROSION-CRACKING RESISTANCE OF SEVERAL Ti-Al-Mo-V ALLOYS

The alloys studied in this investigation were the low interstitial alloy Ti-8Al-1Mo-1V (T-19), the extra low interstitial alloy Ti-8Al-1Mo-1V (T-28), and the low interstitial alloy Ti-7Al-1Mo-1V (T-88). Chemical analyses of these alloys are presented in Table 4. The heat-treating data on the T-19 alloy has been presented in an earlier report (1).

Two types of full plate thickness specimens were obtained from 1-in.-thick material. The specimen configurations employed were similar to those used by Brown, et al. (3). Type A specimens were 3/8 in. wide, 1 in. high, and 5 in. long, side-notched to a depth of 1/16 in. The type B specimens were 1/2 in. wide, 1 in. high, and 5 in. long with a side-notch depth of 1/32 in.

The heat treatments shown in Tables 5 and 6 were conducted in a water-jacketed vacuum chamber, designated as the "cold-wall" vacuum furnace, or in an Inconel muffle with an argon gas atmosphere. The specimens were pre-machined, fatigued, and side-notched before heat treatment.

The test apparatus and procedures used for determining the degree of stress-corrosion-cracking resistance for the heat-treated specimens are those described in Refs. 1 and 5. A brief description of the test procedure is given in the preceding section of this report (Stress Corrosion Cracking of Some Titanium Alloys).

The results of stress-corrosion-cracking tests in an aqueous 3.5-percent-NaCl solution are shown in Tables 5 and 6. The corresponding tensile and fracture toughness data for the heat-treated conditions will be reported at a later date. Table 5 shows the effect of annealing above and below the

Table 4  
Chemical Analysis of Alloys (as-received)

Alloy No.	Nominal Composition	Noninterstitials (wt-%)					Interstitials (wt-%)				
		Al	Mo	V	Fe	Sn	O <sub>2</sub>	N <sub>2</sub>	C	H <sub>2</sub>	Total
T-19	Ti-8Al-1Mo-1V; low interstitial*	7.96	0.90	1.0	0.12	0.15	0.07	0.013	0.049	0.006	0.138
T-28	Ti-8Al-1Mo-1V; extra-low interstitial†	7.8	0.92	1.1	0.02	—	0.054	0.003	0.009	0.013	0.079
T-88	Ti-7Al-1Mo-1V low interstitial†	6.9	1.0	0.9	0.04	—	0.07	0.010	0.022	0.006	0.108

\*Coarse-grained structure in the as-received plate.

†Fine-grained structure in the as-received plate.

Table 5  
 Effect of Vacuum and Inert Gas Heat Treatment on Aqueous Stress-Corrosion  
 Cracking Resistance of the Alloy Ti-8Al-1Mo-1V (T-28) in a 3.5% NaCl Solution\*

Specimen Type	Heat Treatment	$K_I$ (ksi√in.) No Break	Time (min)	$K_{I,sec}$ (ksi√in.)	Time to Break (min)	$K_{I,Δ}$ (ksi√in.) Dry Break	Hydrogen Content (ppm)	Remarks
B	1950° F/vacuum 2 hr/ helium cool in a "cold wall" furnace -- No age --	118.2	10	121.2	5	121.2	17 Avg.	Nonsusceptible to stress corrosion cracking
		110.1	450	117.4	2	117.4		
B	1700° F/argon atm. 1 hr/air cool 1200° F/argon atm. 2 hr/water quench	94.6	10	96.3	2		20	Slight susceptibility to stress corrosion cracking
B	1950° F/argon atm. 1 hr/air cool 1200° F/argon atm. 2 hr/water quench	40.3	10	43.7	5		52	VERY susceptible to stress corrosion cracking

\*All specimens are in the longitudinal direction (RW).  
 Beta transus for this material is 1885° F ± 15° F.

Table 6  
Effects of Several Heat Treatments and Cooling Rates on the Resistance of  
Ti-7Al-IMo-1V (T-88)\* to Stress Corrosion Cracking in a 3.5-percent-NaCl Solution†

Specimen Type	Solution Heat Treatment	Aging Heat Treatment	$K_I$ (ksi/in.) No Break	Time (min)	$K_{Isc}$ (ksi/in.)	Time to Break (min)	$K_{ID}$ (ksi) Calcul. Dry Break Load
A	1950° F/Vacuum/1 hr/HeC	1200° F/Vacuum/2 hr/HeC	104.9	5	115.1	1/2	115.1
A	1950° F/Vacuum/1 hr/HeC	1200° F/Argon/2 hr/AC	104.1	10	108.9	1/2	108.9
B	1950° F/Vacuum/1 hr/HeC	1200° F/Argon/2 hr/AC	99.9-110.0	5	104.4-114.9	1/2	109.4
A	1950° F/Vacuum/1 hr/HeC	1200° F/Argon/2 hr/WQ	104.7‡	5	109.4‡	1/2	118.5
B	1950° F/Vacuum/1 hr/HeC	1200° F/Argon/2 hr/WQ	102.5-118.3 113.4‡	5	107.1-123.5 118.5‡	2	105.4
A	1700° F/Vacuum/1 hr/HeC	1200° F/Vacuum/2 hr/HeC	111.5	15	116.9	1/4	116.9
B	1700° F/Vacuum/1 hr/HeC	1200° F/Vacuum/2 hr/HeC	106.9-113.5 110.1‡	5	109.2-115.9 112.4‡	1/2	112.4
A	1700° F/Vacuum/1 hr/HeC	1200° F/Argon/2 hr/AC	94.7	5	101.2	1-1/2	101.2
B	1700° F/Vacuum/1 hr/HeC	1200° F/Argon/2 hr/AC	89.8-112.7	5	94.4-118.5	4	109.4
A	1700° F/Vacuum/1 hr/HeC	1200° F/Argon/2 hr/WQ	104.0‡	5	109.4‡	1/4	117.9
B	1700° F/Vacuum/1 hr/HeC	1200° F/Argon/2 hr/WQ	105.8-122.3 116.2‡	5	107.4-124.1 117.9‡	1/2	113.6
A	1700° F/Argon/1 hr/AC	1200° F/Vacuum/2 hr/HeC	64.6	5	68.5	1	128.3
A	1700° F/Argon/1 hr/AC	1200° F/Argon/2 hr/AC	60.3	5	64.4	1/2	116.6
B	1700° F/Argon/1 hr/AC	1200° F/Argon/2 hr/AC	84.5--91.8	5	89.2--96.8	3	126.9
A	1700° F/Argon/1 hr/AC	1200° F/Argon/2 hr/WQ	61.9	5	66.1	1-1/2	122.9
B	1700° F/Argon/1 hr/AC	1200° F/Argon/2 hr/WQ	72.1--93.1	5	77.1--99.6	3-1/2	106.1

\*Actual dry break load for specimen in as-received condition was 117.3-ksi.

†All specimens tested in the transverse (WR) direction.

‡Observed average.

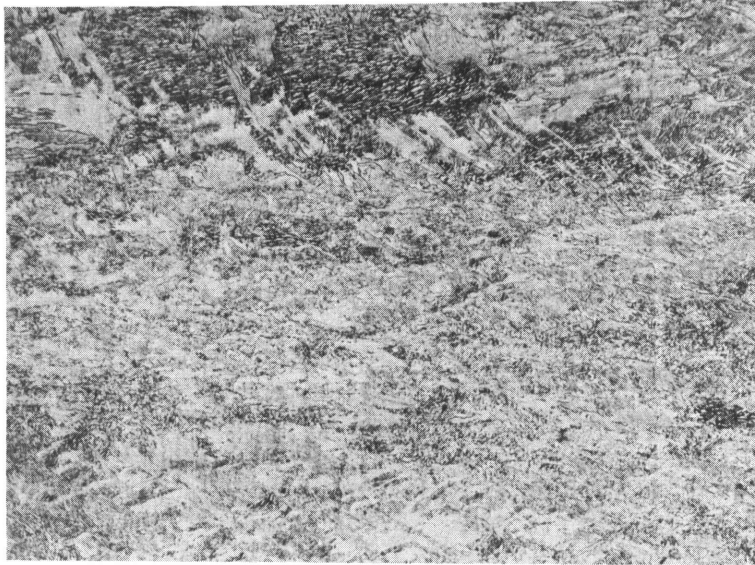
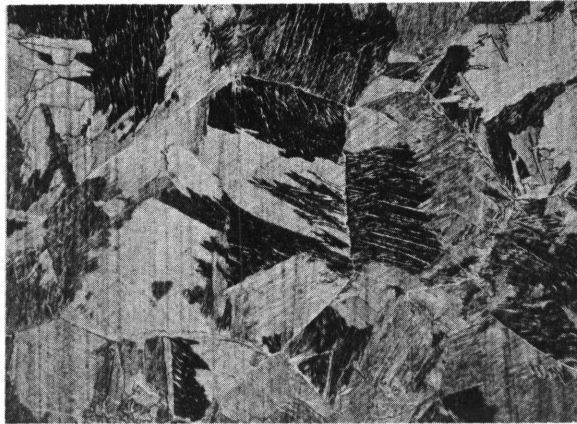
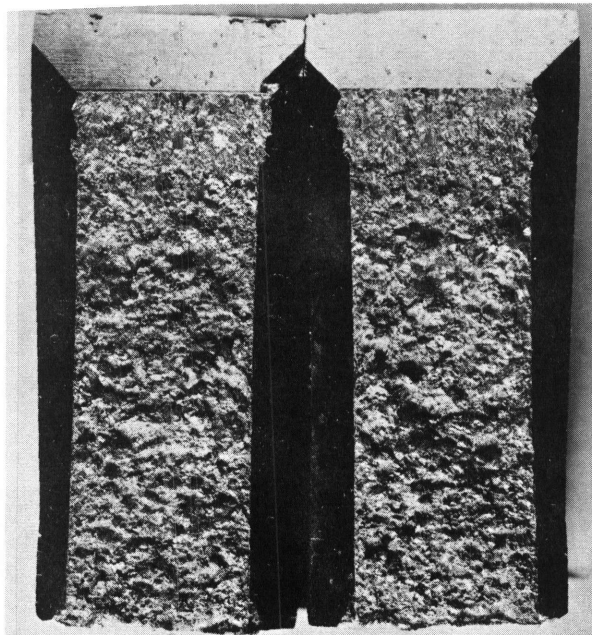


Fig. 29 - Extra low interstitial alloy  
Ti-8Al-1Mo-1V (T-28) in the as-  
received condition. Mag. 50X

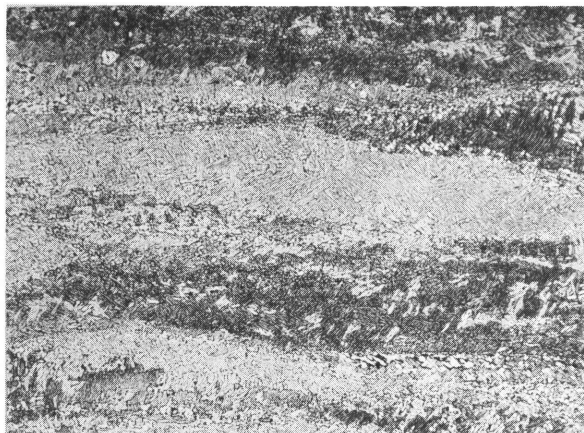


(a)

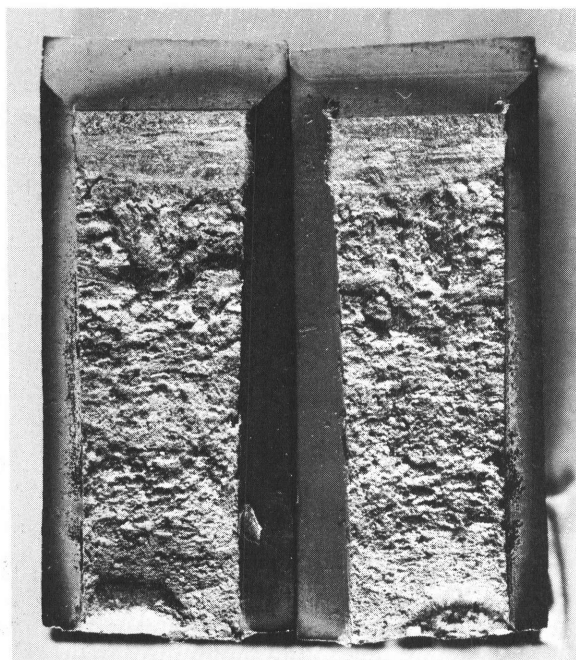


(b)

Fig. 30 - (a) Extra low interstitial alloy  $\text{Al-8Al-1Mo-1V}$  (T - 28) after heat treatment at  $1950^{\circ}\text{F}$  for 2 hours in a "cold wall" vacuum furnace followed by helium cooling. Mag. 50X. (b) Typical fracture appearance of (a) after stress-corrosion-cracking test using a fatigue-cracked cantilever-beam type specimen. Mag. 4X.

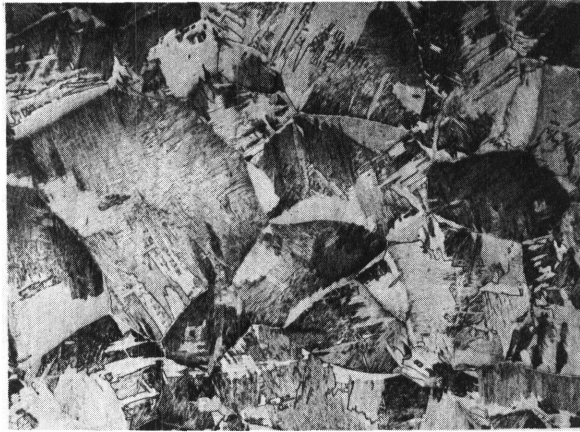


(a)

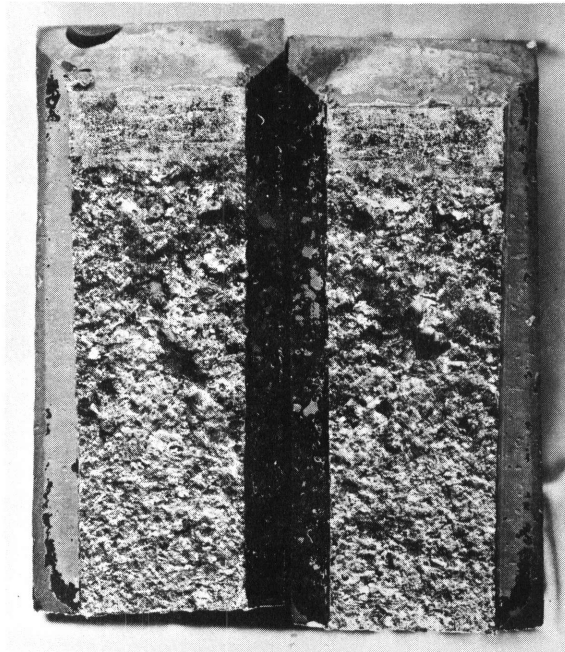


(b)

Fig. 31 - (a) Extra low interstitial alloy Ti-8Al-1Mo-1V (T - 28) after heat treatment at 1700° F for 1 hour in an argon atmosphere followed by air cooling and an age of 1200° F for 2 hours in argon followed by water quenching. Mag. 50X. (b) Typical fracture appearance of (a) after stress-corrosion-cracking test using a fatigue - cracked cantilever - beam type specimen. Mag. 4X.



(a)



(b)

Fig. 32 - (a) Extra low interstitial alloy Ti-8Al-1Mo-1V (T-28) after heat treatment at 1950 F for 1 hour in an argon atmosphere followed by 2 hours in argon followed by water quenching. Mag. 50X. (b) Typical fracture appearance of (a) after stress-corrosion-cracking test using a fatigue-cracked cantilever-beam type specimen. Mag. 4X.

$\beta$  transus on the aqueous stress-corrosion-cracking resistance of the Ti-8Al-1Mo-1V (T-28) alloy. The microstructures for this alloy in the as-received and heat-treated conditions are shown in Figs. 29 through 32. Included in the figures are macrographs of the corresponding fracture surfaces of the broken SCC specimens.

Table 6 shows the effects of comparable vacuum and inert gas treatments above and below the  $\beta$  transus on the SCC resistance of the low interstitial Ti-7Al-1Mo-1V (T-88) alloy.

The preliminary data obtained to date in this study clearly indicate by the data presented here on the Ti-8Al-1Mo-1V (T-28) and Ti-7Al-1Mo-1V (T-88), as well as by the data in Table 4 of the Ninth Quarterly Report (1) on the Ti-8Al-1Mo-1V (T-19) alloy, that the SCC resistance of the Ti-8Al-1Mo-1V and Ti-7Al-1Mo-1V alloys can be significantly improved if a fine grain structure is maintained through processing and the material is given a solution annealing treatment below the  $\beta$  transus in vacuum. The effects of aging in vacuum in preference to aging in argon, as well as variations in the rate of cooling (helium cool, water quench, or air cool) after aging, seem to be of smaller importance.

#### HIGH STRENGTH STEELS

(P.P. Puzak and K.B. Lloyd)

Work completed during this reporting period has primarily been concerned with fracture toughness evaluations of the steels and welds characterized by strengths ranging from approximately 170 to 190 ksi yield strength (YS). These have included data for twelve new plates of the 12-5-3 (Ni-Cr-Mo) maraging steels and 9-4-.XXC (Ni-Co) quenched-and-tempered (Q&T) alloy steels that were recently procured. Fracture toughness evaluations were also conducted for new 160 and 180 ksi YS maraging steel TIG (tungsten-inert-gas) weldments fabricated with semiautomatic equipment by INCO research personnel and with manual equipment by NRL personnel. Considerable time was also expended during this reporting period in the procurement and installation of a new precision-built, fully-automatic MIG-TIG fusion welder and control package (600 amp direct current, three-phase,

full-wave rectifier type, constant current or constant potential output welding power source, main console and operator controls, and 10-ft.-long side-beam track and carriage). Data for weldments fabricated with this new welding facility are expected to be developed during the next reporting period.

#### FRACTURE TOUGHNESS INDEX DIAGRAM FOR STEELS

Fracture toughness characterization of the steels is primarily based upon drop-weight-tear-test (DWTT) assessments and the correlation of results with the large structural prototype element explosion tear test (ETT); these tests have been described in detail in Ref. 6. A simplified Fracture Toughness Index Diagram (FTID) evolved in these studies depicts the toughness characteristics of steels (indexed in terms of ETT performance of the material) as a function of YS data. The FTID data are separated by various "optimum material trend line" (OMTL) curves into characteristic groups of steels related to processing and/or rolling variables. The FTID relating specifically to all 1-in.-thick steel plates evaluated to date is presented in Fig. 33. The significance of toughness data developed with established engineering methods, such as the Charpy V ( $C_V$ ) test, has been presented previously for the steels in terms of the correlations with results for the primary test methods, described above. A FTID chart evolved in terms of  $C_V$ -YS data for all 1-in.-thick steel plates tested to date is presented in Fig. 34. The significance and interpretation of the FTID data given in Figs. 33 and 34 will not be repeated here since they have been covered in detail in several earlier reports (1,6,7,8,9). Wherever possible, new data (to be described) are reported in charts containing the basic curves and correlation features of the FTID charts to provide a ready comparison with data previously reported.

#### FRACTURE TOUGHNESS CHARACTERIZATION OF SPECIAL MELT PRACTICE 180-ksi YIELD STRENGTH STEELS

Previous studies of the recently developed, commercially available, high strength steels had shown the 12Ni-5Cr-3Mo maraging steels and the 9Ni-4Co-0.25C Q&T steels to be highly promising for welded applications involving materials

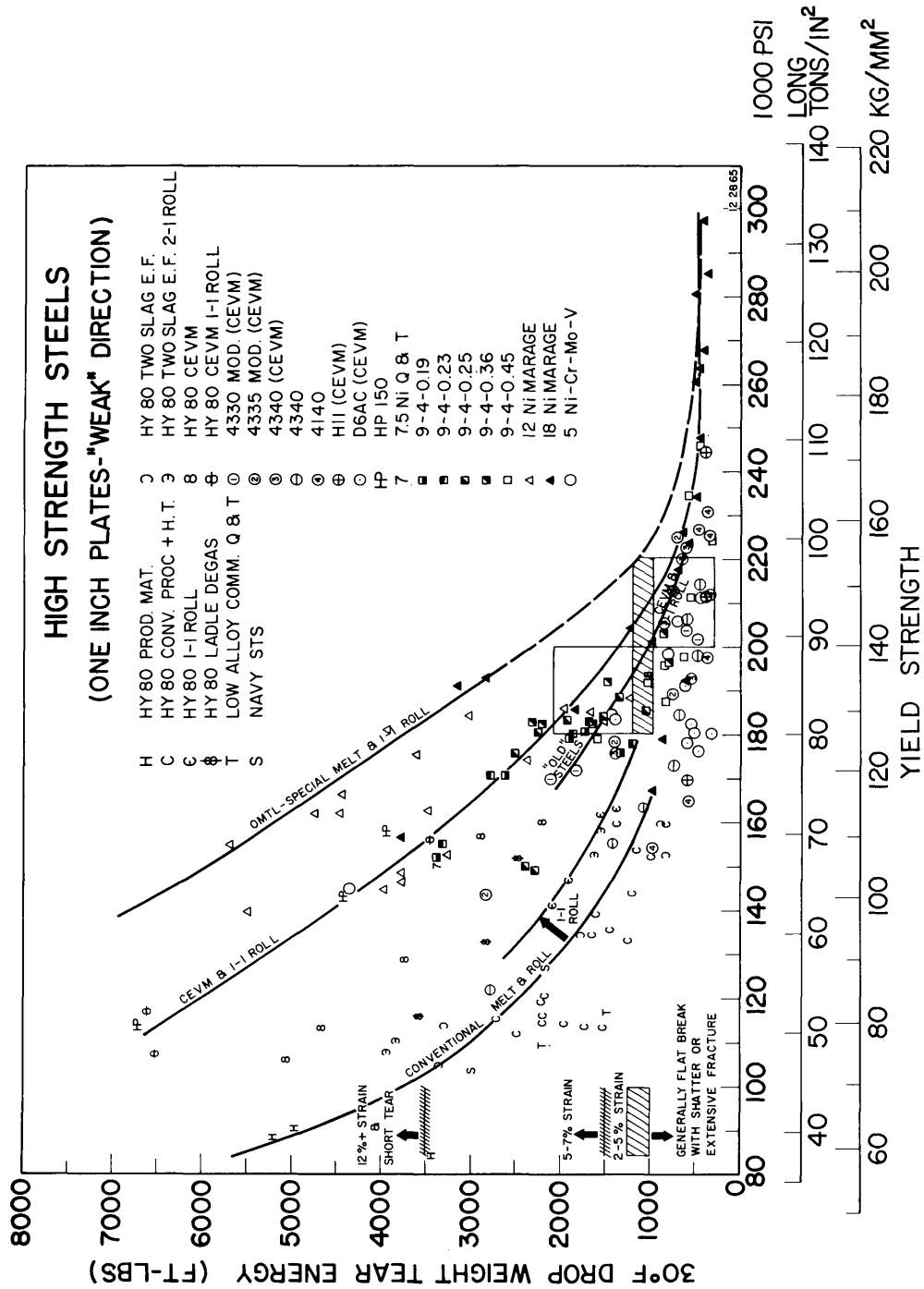


Fig. 33 - Spectrum of drop-weight tear test data for high strength steels as a function of yield strength and processing practices. By referencing the specific optimum materials trendline to the explosion tear test performance index data (percent strain for fracture propagation), the chart evolves to a Fracture Toughness Index Diagram (FTID) for all steel represented.

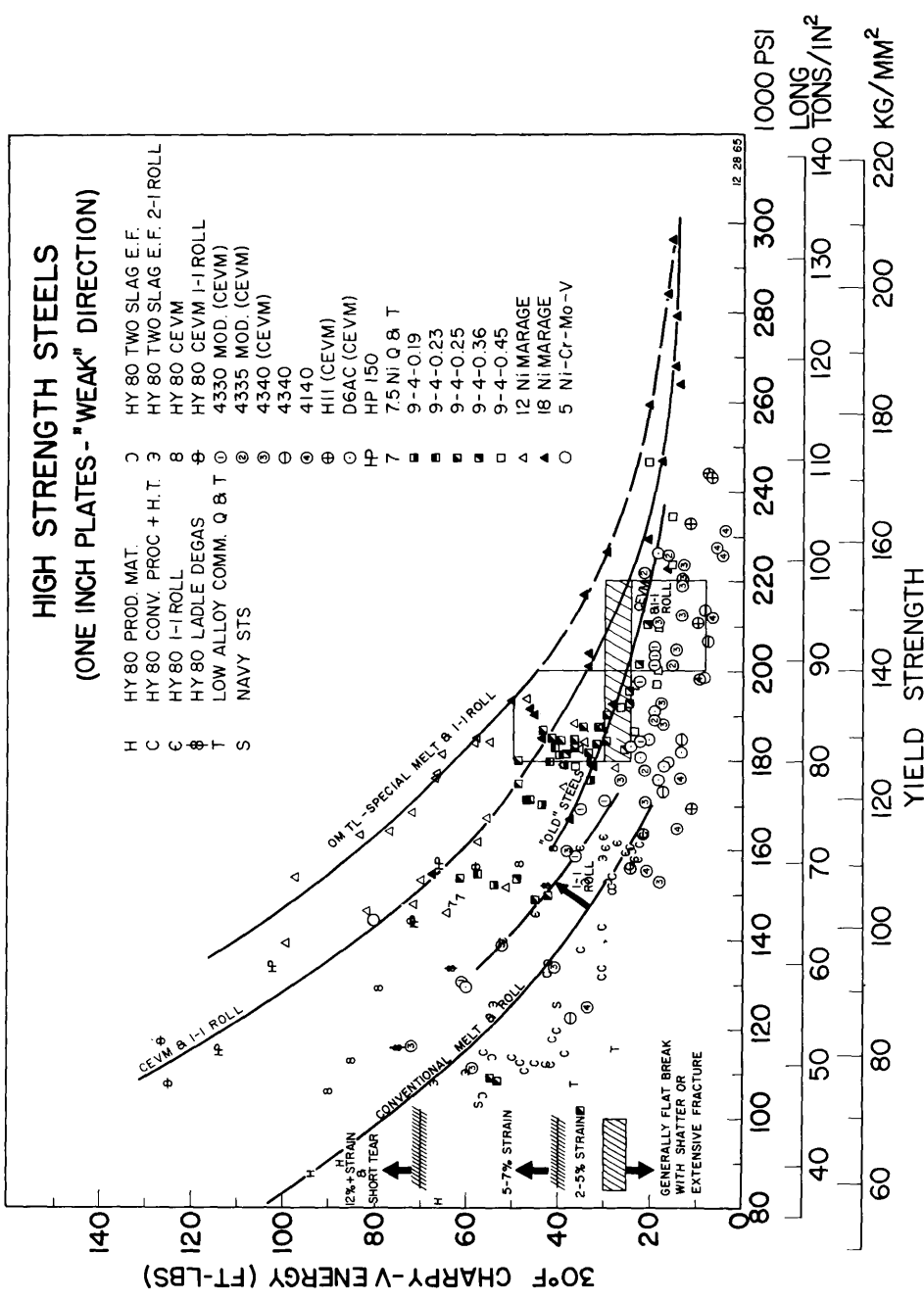


Fig. 34 - Spectrum of Charpy V test data for high strength steels as a function of yield strength and of processing practices (compare with Fig. 33).

with 180 ksi minimum YS. Extensive data for plate metals of "selected" origin and preliminary weldment data for both types of steels have been reported (8,9,10,11). For additional studies, new 1-in.- and 2-in.-thick plate materials of these alloys representative of expected "normal" production were purchased. In order to obtain "routine" production materials rather than "special project" steels, the specifications issued for procurement of the 9-4-0.25 and 12-5-3 alloy steel plates were deliberately void of any stringent requirements that might have imposed difficulties or hardships on the prospective producers. The general requirements of ASM 6546, stipulating a Q&T heat treatment to develop 180 ksi minimum YS and 30 ft-lb minimum  $C_V$  at 0°F, were specified for the 9-4-0.25 steel plates. Previously reported data indicated that the specified minimum YS and  $C_V$  values could readily be met by Q&T plates of the 9-4-0.25 alloy steel (9,10,11). The maraging steel plates were specified to be provided in the 1:1 cross-rolled, solution annealed (1500°F) and aged (900°F/3 hr) condition, with split-heat techniques to compare air melt, electric arc furnace material of optimum oxidizing plus reducing slag melt practice, with additional plates from consumable electrode vacuum remelt (CEVM) ingots of the air melt stock. Primary control of the maraging steel plates was exercised by specifying only the nominal 12-5-3 chemical composition expected to develop 180 ksi YS for the specified heat treatment. The nominal limits for the residual elements (percent C, percent S, percent P, percent Mn, and percent Si), given in ASTM A538-65 for the 18%-Ni maraging steels, were specified in order to obtain "routine" production 12-5-3 steels with a possible "maximum" amount of the critical residual elements that must be maintained at very low levels to obtain the optimum strength-toughness properties in the maraging steels (1). It was considered that minimum quality plates complying to the above specifications for 12-5-3 maraging steels would provide material for comparison of properties with those previously reported for the very low residual element "optimum-chemistry", vacuum-induction melt practice 12-5-3, 180 ksi YS maraging steels (9), and with those of another 2-in.-thick maraging steel plate (No. J78) of reasonably low residual element content developed by an electric furnace air melt, special multiple slag practice; this latter plate had been supplied to NRL by the International Nickel Company. The chemical compositions of the various 180 ksi YS Q&T and maraging steels under investigation herein are given in Table 7.

Table 7  
Chemical Composition of 180-ksi-Yield-Strength Steels

Specimen	Thick-ness (in.)	Composition (%)													
		C	Mn	Si	P	S	Ni	Cr	Mo	Ti	Al	V	Co		
<u>CEVM 9-5-.25C</u>															
Spec. range		0.24/0.30	0.10/0.35	0.10 Max	0.010 Max	0.35/0.60	0.35/0.60	0.10/0.20	0.06/0.12	3.50/4.50					
Mill check		0.26	0.33	0.01	0.008	0.008	0.008	0.008	0.008	8.41	0.40	0.48	0.18	0.07	3.90
J87	1	0.25	0.31	0.01	0.006	0.005	0.005	0.005	0.005	8.4	0.41	0.52	0.21	0.10	4.2
J88	1	0.25	0.30	0.01	0.006	0.007	0.007	0.007	0.007	8.4	0.40	0.52	0.21	0.12	4.2
J70	2	0.24	0.34	0.01	0.003	0.006	0.006	0.006	0.006	8.4	0.44	0.49	0.21	0.11	3.90
<u>Air Melt Marage</u>															
Spec. range		0.03 Max	0.10 Max	0.12 Max	0.010 Max	11.5/12.5	4.75/5.25	2.75/3.25	0.10/0.20	0.35/0.45					
Mill check		0.028	0.07	0.07	0.004	0.005	0.005	0.005	0.005	12.20	4.75	3.10	0.18	0.32	
J66	1	0.033	0.08	0.07	0.007	0.005	0.005	0.005	0.005	12.5	4.71	3.65	0.21	0.16	
J67	1	0.035	0.08	0.07	0.007	0.005	0.005	0.005	0.005	12.5	4.81	3.65	0.21	0.16	
J68	2	0.033	0.08	0.07	0.007	0.005	0.005	0.005	0.005	12.5	4.81	3.55	0.21	0.16	
J69	2	0.037	0.08	0.07	0.007	0.005	0.005	0.005	0.005	12.5	4.81	3.65	0.21	0.16	
<u>CEVM Marage</u>															
Spec. range		0.03 Max	0.10 Max	0.12 Max	0.010 Max	11.5/12.5	4.75/5.25	2.75/3.25	0.10/0.20	0.35/0.45					
Mill check		0.029	0.04	0.08	0.007	0.004	0.004	0.004	0.004	12.10	4.75	3.20	0.19	0.31	
J71	1	0.049	0.08	0.08	0.007	0.005	0.005	0.005	0.005	12.5	4.81	3.55	0.20	0.18	
J72	1	0.045	0.08	0.10	0.007	0.007	0.007	0.007	0.007	12.5	4.81	3.65	0.20	0.18	
J76	2	0.041	0.07	0.08	0.007	0.005	0.005	0.005	0.005	12.5	4.81	3.55	0.20	0.16	
J77	2	0.047	0.05	0.09	0.004	0.005	0.005	0.005	0.005	12.2	4.83	3.05	0.20	0.16	
<u>Electric Furnace Multiple-Slag Marage</u>															
J78	2	0.027	0.05	0.10	0.003	0.007	0.007	0.007	0.007	12.1	5.05	3.20	0.20	0.22	

The steels procured by NRL for these studies were specified to be provided in the fully heat-treated condition. Inadvertently, it had been agreed to permit mill retempering of the 2-in.-thick 9Ni-4Co steel plate (No. J70), which was then received in a YS condition lower than the specified 180-ksi-YS minimum. Full-cycle Q&T heat treatment of a 2 x 18 x 20-in. plate section was conducted by NRL to provide material for studies of this steel in the 180 ksi-YS level. The electric furnace special multiple slag, air melt practice plate of 12%-Ni maraging steel had been received in the mill annealed (1500°F) condition and full thickness plate sections (2 x 5 x 20 in.) were cut and aged (900°F/3 hr) by NRL prior to the preparation of various specimen blanks. The results for DWTT, tensile, and  $C_V$  tests for these 180-ksi-YS steels are given in Table 8. Figures 35 and 36 present a summary of the DWTT-YS and  $C_V$ -YS data, as referenced to the FTID for 1-in.-thick steels. It should be noted that the 2-in.-thick steels were heat treated in full thickness but DWTT were conducted in 1-in. thickness and the illustrated data are referenced to FTID for 1-in.-thick steels.

General analysis of the data summarized in Figs. 35 and 36 revealed highly unexpected results. The fracture toughness values of the 9Ni-4Co steel plates were noted to be considerably lower than those of any other previously tested 9-4-0.25 steel of similar (176 to 186 ksi) YS. Some of the maraging steels, on the other hand, exhibited toughness and strength values so far below those expected that considerable time and care were expended to determine whether major differences existed in chemical composition of the various maraging steel plates. Noting their similarity in chemical composition of major elements (Table 7) and the fact that all of the maraging steels were supposedly given identical heat treatments (anneal 1500°F/age 900°F/3 hr), the extreme differences exhibited by the various 12-5-3 maraging steels in strength (approximately 165 to 186 ksi YS) and toughness (approximately 800 to 3000 ft-lb DWTT or 20 to 50 ft-lb  $C_V$  energies) were considered inconceivable and difficult to rationalize. Early discussion of these "as-received" mill heat-treated data with the steel producer's representatives failed to develop any clues concerning reasons for the unexpectedly low toughness values in any of these steels.

From past heat-treatment experience and studies with other maraging steels, it was deduced that the observed differences in strength and toughness properties of the maraging steels

Table 8  
Mechanical Properties of Mill Heat Treated 180-ksi-Yield-Strength Steels

Specimen	Thickness (in.)	Fracture* Path	0.505-in.-Dia. Tension Test Data				Charpy V at 30°F (ft-lb)	Drop Weight Tear at 30°F (ft-lb)
			0.2% YS (ksi)	UTS (ksi)	El. in 2 in. (%)	R.A. (%)		
<u>Air Marage</u>								
J66	1	WR					29	1296
J66	1	RW	185.3	188.0	13.8	56.7	32	3228
J67	1	WR					31	1173
J67	1	RW	178.6	182.3	15.0	57.2	34	3068
J68	2	WR					21	681
J68	2	RW	171.2	177.2	14.0	49.1	25	750
J69	2	WR	165.6	171.7	11.8	38.0	28	750
J69	2	RW					31	1052
<u>CEVM Marage</u>								
J71	1	WR					42	3122
J71	1	RW	176.8	183.2	14.5	59.6	44	3775
J72	1	WR	177.3	183.3	14.5	59.2	47	2676
J72	1	RW					47	3866
J76	2	WR					40	2560
J76	2	RW	171.4	177.2	16.0	60.4	43	3060
J77	2	WR	169.6	171.2	14.5	57.0	34	1540
J77	2	RW					36	2146
<u>Electric Furnace Marage</u>								
J78	2	WR	185.5	188.7	14.0	59.7	40	2116
J78	2	RW					42	2146
<u>CEVM 9-4-.25C</u>								
J70	2	WR	176.3	186.6	16.0	55.2	40	1784
J70	2	RW	175.3	186.0	16.5	57.2	41	2325
J70 (Q&T,NRL J70 100 F Temp.)	2	WR	186.1	198.0	16.0	55.2	36	
	2	RW	186.1	197.4	17.0	58.4	39	1173
J87	1	WR	179.2	189.4	17.0	60.5	39	1966
J87	1	RW					46	2498
J88	1	WR	180.2	191.3	16.0	54.1		
J88	1	RW						

\*"The Slow Growth and Rapid Propagation of Cracks," ASTM Special Committee Report, Materials Research and Standards, Vol. 1, No. 5, May 1961, p. 389.

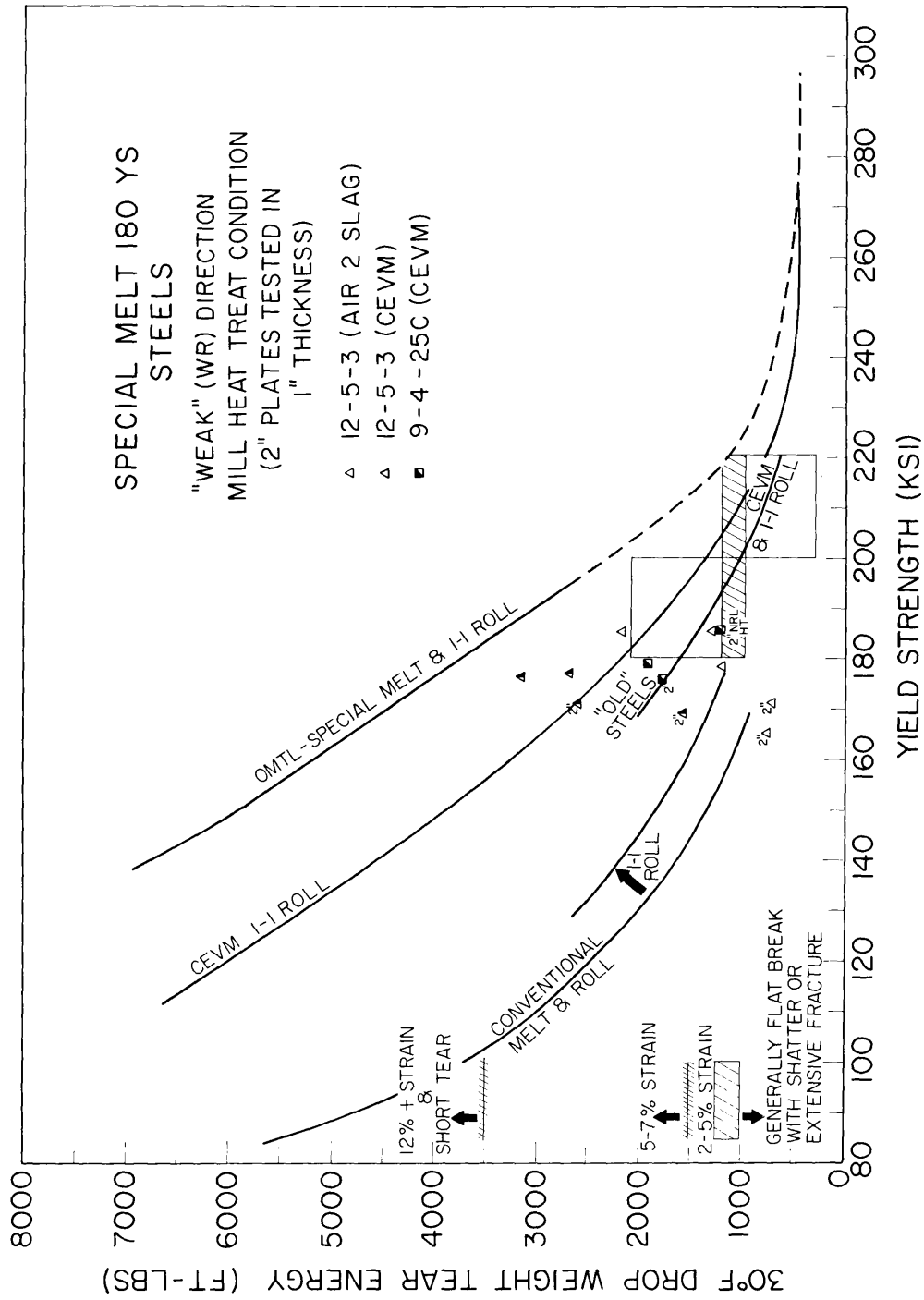


Fig. 35 - Summary of drop-weight tear test-yield strength relationships of mill heat-treated 1- and 2-inch-thick 180-ksi-yield-strength steel plates. FTID-OMTL curves for 1-inch plate are included for comparison.

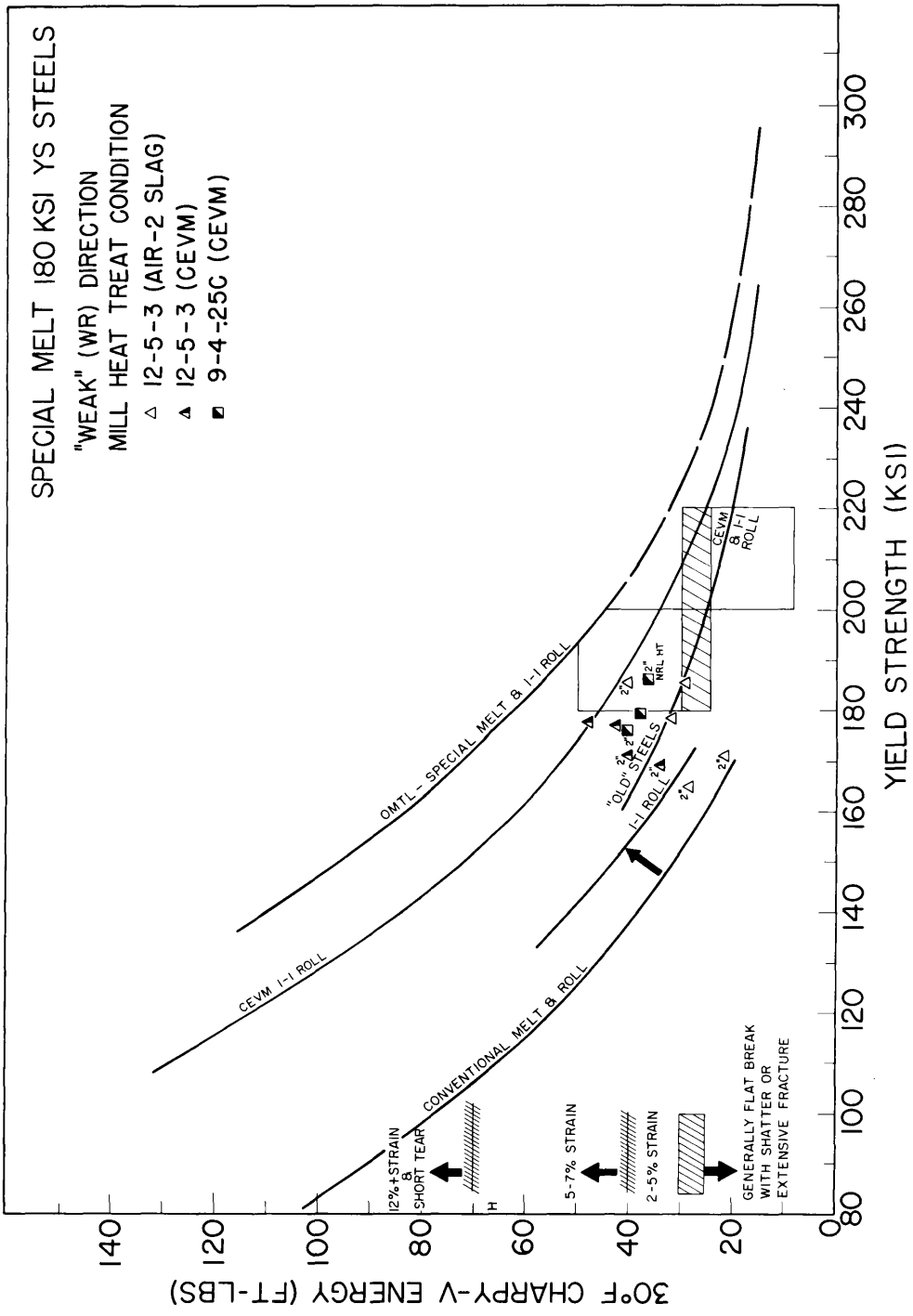


Fig. 36 - Summary of Charpy V-yield strength relationships for steels shown in Fig. 35

shown in Figs. 35 and 36 were probably attributable to heat-treatment deficiencies rather than to the minor differences in composition that were first suspected. An extensive program was established to investigate the response of these maraging steels to heat-treatment variables. The program of study of heat-treatment effects on the maraging steels under investigation herein was aimed at determining whether the mill deviated from the specified heat-treatment conditions, and at establishing specific heat-treatment conditions that would result in the development of considerably better toughness and strength properties than those (Table 8) obtained for the mill heat-treated plates. Small (1 x 5 x 6 1/2-in. or 2 x 2 x 10-in.) plate sections that had been cut with the intention of providing material for other studies of as-received properties were heat-treated and sectioned to provide material for tensile and  $C_V$  tests. In many cases, the use of this limited amount of material that had already been cut made it necessary to determine "strong" (RW) fracture direction  $C_V$  properties instead of the customary "weak" (WR) direction  $C_V$  properties. A total of seven heat-treatment conditions involving single anneal-plus-age and double anneal-plus-age treatments were investigated. Pertinent test results obtained to date in these studies are given in Table 9.

Detailed comparison of the data given for the maraging steels in Table 9 with those in Table 8 reveals that each of the seven laboratory reheat-treatment conditions studied resulted in the development of significantly higher toughness values (as measured by the  $C_V$  test) than that of the same steel plate in the mill heat-treated condition. In several of the heat-treatment conditions studied, the  $C_V$  energy value of 30°F for the laboratory reheat-treated plate is noted to be approximately double the value obtained for the mill heat-treated plate. A graphical summary of the data developed for one of the air melt maraging steel plates (No. J68) is presented in Fig. 37, as a typical illustration of results obtained for each of the eight maraging steel plates involving a questionable mill heat treatment. Similar data developed for the electric furnace, special multiple slag, air melt plate (No. J78) of maraging steel that had been received in the mill annealed (1500°F) condition are given in Fig. 38. For a given aging time at 900°F, a general decrease in YS and concomitantly slight increase in  $C_V$  toughness is noted for these maraging steels as the final solution-annealing temperature was raised within the range studied.

Table 9  
Response to Laboratory Heat Treatments of 180-ksi-Yield-Strength Maraging Steels

Code	Fracture Path†	Mill		A*		B*		C*		D*		E*		F*		G*	
		YS (ksi)	Charpy V at 30° F (ft-lb)	YS (ksi)	Charpy V at 30° F (ft-lb)	YS (ksi)	Charpy V at 30° F (ft-lb)	YS (ksi)	Charpy V at 30° F (ft-lb)	YS (ksi)	Charpy V at 30° F (ft-lb)	YS (ksi)	Charpy V at 30° F (ft-lb)	YS (ksi)	Charpy V at 30° F (ft-lb)	YS (ksi)	Charpy V at 30° F (ft-lb)
<u>Air Melt</u>																	
J66	WR	185.3	29	180.8	54	174.1	51	176.1	50	182.8	32	174.0	54	175.3	54	174.7	52
J67	RW	178.6	32	177.9	50	174.7	50	176.5	51	183.2	42	177.3	53	176.3	52	174.5	51
J68	WR	171.2	31	177.9	49	174.4	50	175.3	50	180.8	34	172.7	39	171.7	47	175.7	45
J69	RW	165.6	25	178.0	38	174.7	35	174.8	34	180.3	27	172.9	28	175.1	35	175.9	33
J69	RW		31								33						
<u>CEVM</u>																	
J71	WR	176.8	42	180.7	77	173.9	79	170.2	75	178.8	53	178.5	57	175.4	62	174.3	70
J72	RW	177.3	44	179.2	64	176.2	64	171.7	67	179.3	63	180.4	47	175.1	58	177.6	62
J76	WR	171.4	47	176.3	68	172.7	70	169.6	71	176.4	52	179.9	57	175.0	65	173.4	60
J77	RW	169.6	40	176.7	52	172.7	53	172.4	53	178.2	47	181.8	41	173.9	43	173.7	50
J77	RW		36								49						
<u>Electric Furnace</u>																	
J78	WR	185.5	40	181.8	58	176.8	54	174.6	52	174.5		174.5	46	173.3	51	178.0	46
J78	RW		42														

\*Condition A - 1700° F solution anneal, 1400° F solution anneal, age 900° F/3 hr  
 B - 1700° F solution anneal, 1500° F solution anneal, age 900° F/3 hr  
 C - 1700° F solution anneal, 1575° F solution anneal, age 900° F/3 hr  
 D - 1500° F solution anneal, 1575° F solution anneal, age 900° F/3 hr  
 E - 1575° F solution anneal, age 900° F/3 hr  
 F - 1650° F solution anneal, age 900° F/3 hr  
 G - 1700° F solution anneal, age 900° F/3 hr

† - The Slow Growth and Rapid Propagation of Cracks," ASTM Special Committee Report, Materials Research and Standards, Vol. 1, No. 5, May 1961, p. 389.

# J68 AIR MELT 12-5-3 MARAGE STEEL

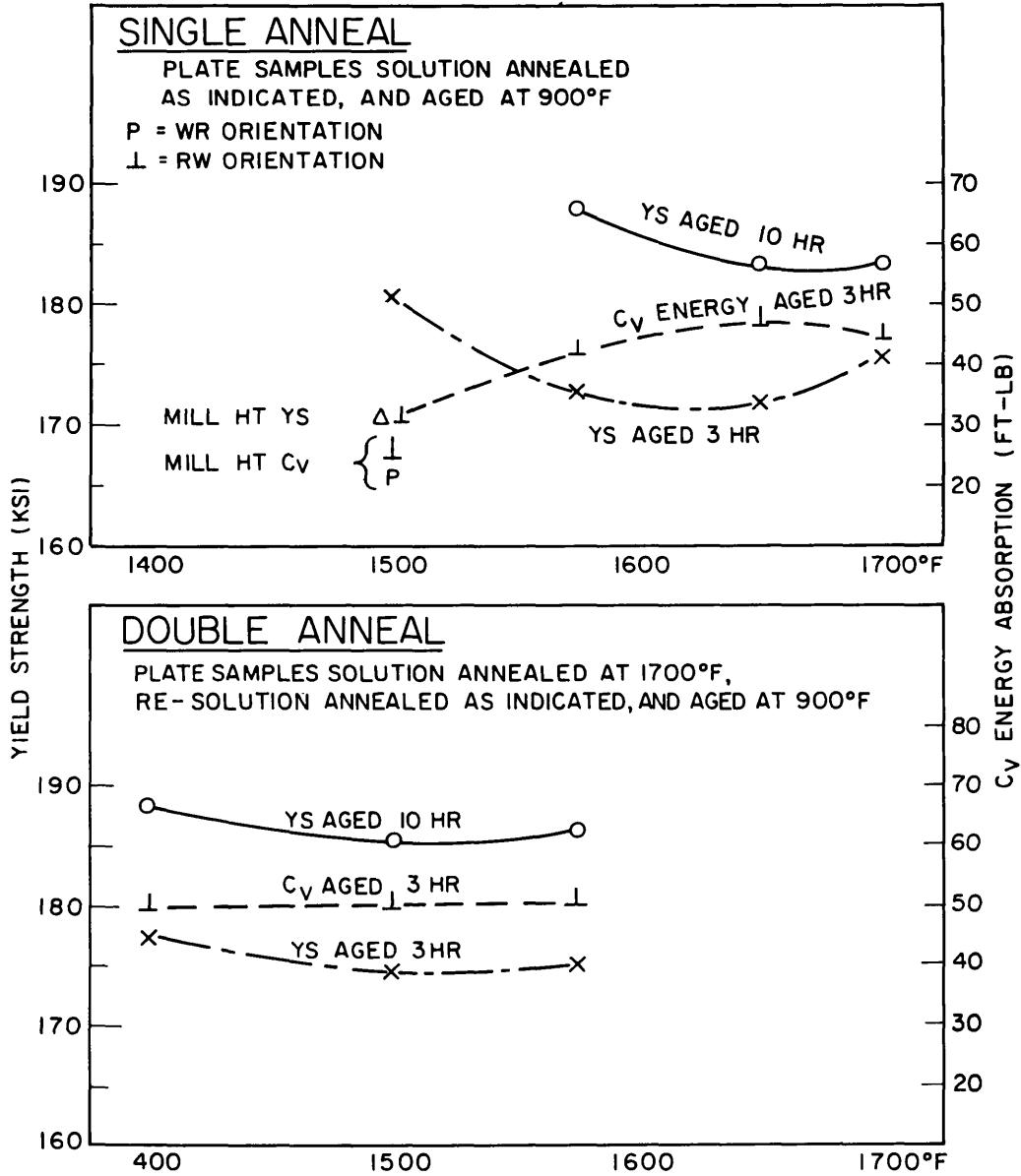


Fig. 37 - Summary of yield strength and Charpy V energy absorption data obtained for laboratory heat treatments of air melt marage steel plate (No. J68)

# J78 MULTI-SLAG EF 12-5-3 MARAGE STEEL

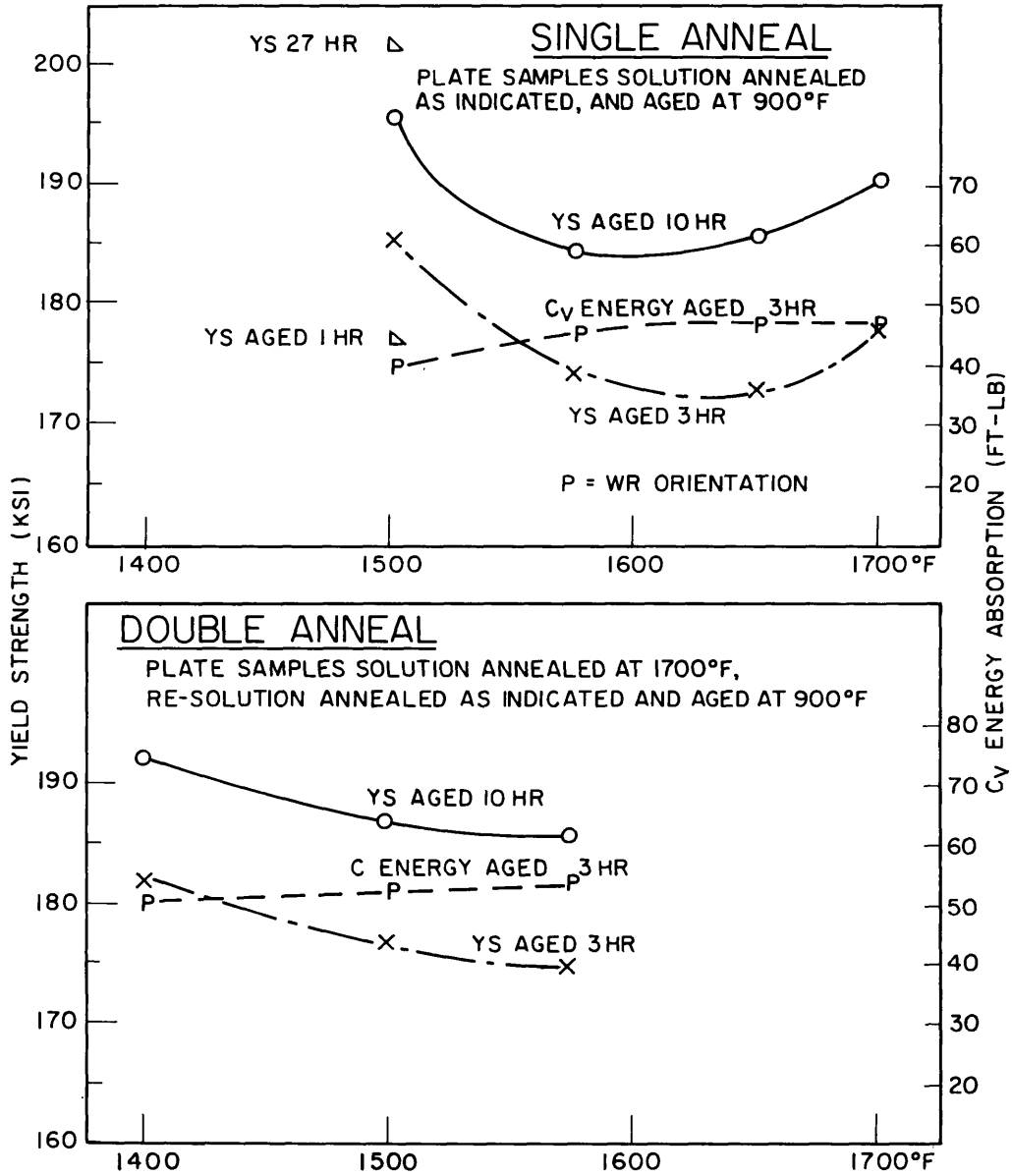
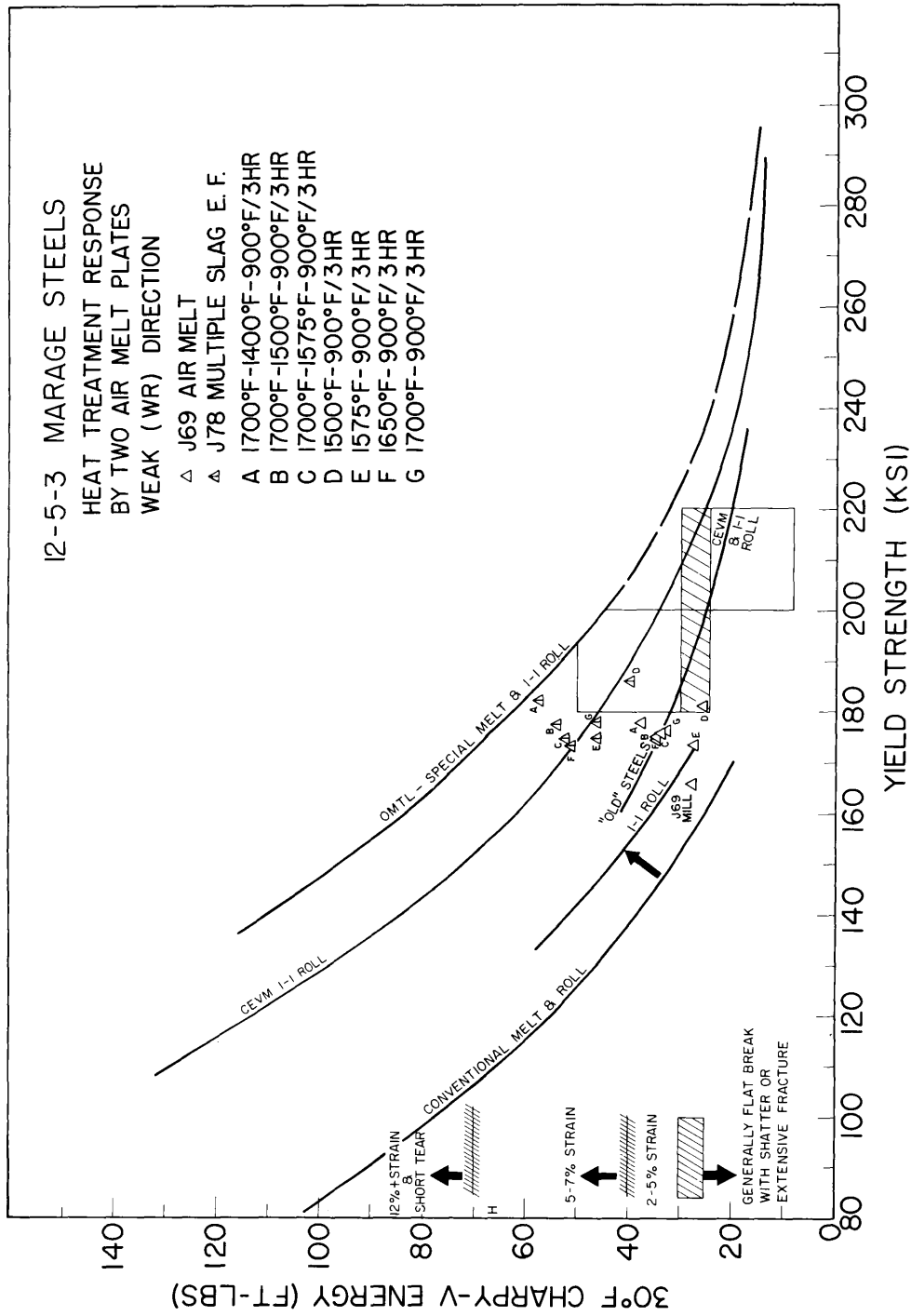


Fig. 38 - Summary of yield strength and Charpy V energy absorption data obtained for laboratory heat treatments of the multiple slag, electric furnace marage steel plate (No. J78) shown in Fig. 35

A summary of the  $C_v$ -YS data for two of the air melt 2-in. thick maraging steels (Nos. J69 and J78), as referenced to the FTID for 1-in.-thick steels, is presented in Fig. 39. The wide spread in YS values exhibited by both of these steels is attributable to the effects of different solution annealing temperatures, as described above. The apparently significant difference in levels of  $C_v$  toughness between these two steels for all the heat-treatment conditions studied is considered to be attributable to their differences in chemical composition (particularly percent C and percent S, see Table 7), as discussed in an earlier progress report (1). It should be noted that the illustrated range in YS developed by either of the two steels shown in Fig. 39 as a function of varying annealing temperatures is similar to the range in YS values for all of the mill heat-treated maraging steels shown previously in Fig. 36. For any given solution annealing temperature studied, essentially equivalent YS values were developed by the 900°F/3 hr aging treatment for each of the nine maraging steels under study herein, as shown by the data given in Table 9, and the summary of data for heat-treatment condition A (1700°-1400°-900°F/3 hr) given in Fig. 40.

The results obtained in these studies suggested that the spread in YS and toughness values given in Fig. 36 for the eight mill heat-treated maraging steel plates may have been caused by varying annealing temperatures or aging temperatures in the heat treatment of the different steel plates. Data developed early in this heat-treatment program were discussed with producer's representatives and it was agreed that the "mill heat-treated" properties of these maraging steels are not representative of those expected for these steels under conditions of optimum heat treatment. Generally, it was ascertained that the specified heat-treatment temperatures (1500°F anneal/900°F age) were probably exceeded in the annealing operation and never reached in the aging operation. A cooperative investigation is now underway to determine the actual annealing and aging temperatures used, as well as to determine the effects of the heat-treating process used in producing the inferior "mill heat-treatment" properties of these maraging steels.

The solution anneal treatment of maraging steel is accomplished by cooling (in air or liquid quenching) the plates from austenitizing temperatures (ranging from approximately 1400°F to 1900°F) to form a comparatively soft and ductile martensitic



**Fig. 39 - Yield strength-Charpy V energy absorption data for laboratory heat treatments of two air melt marage steel plates. FTID-OMTL curves included for reference.**

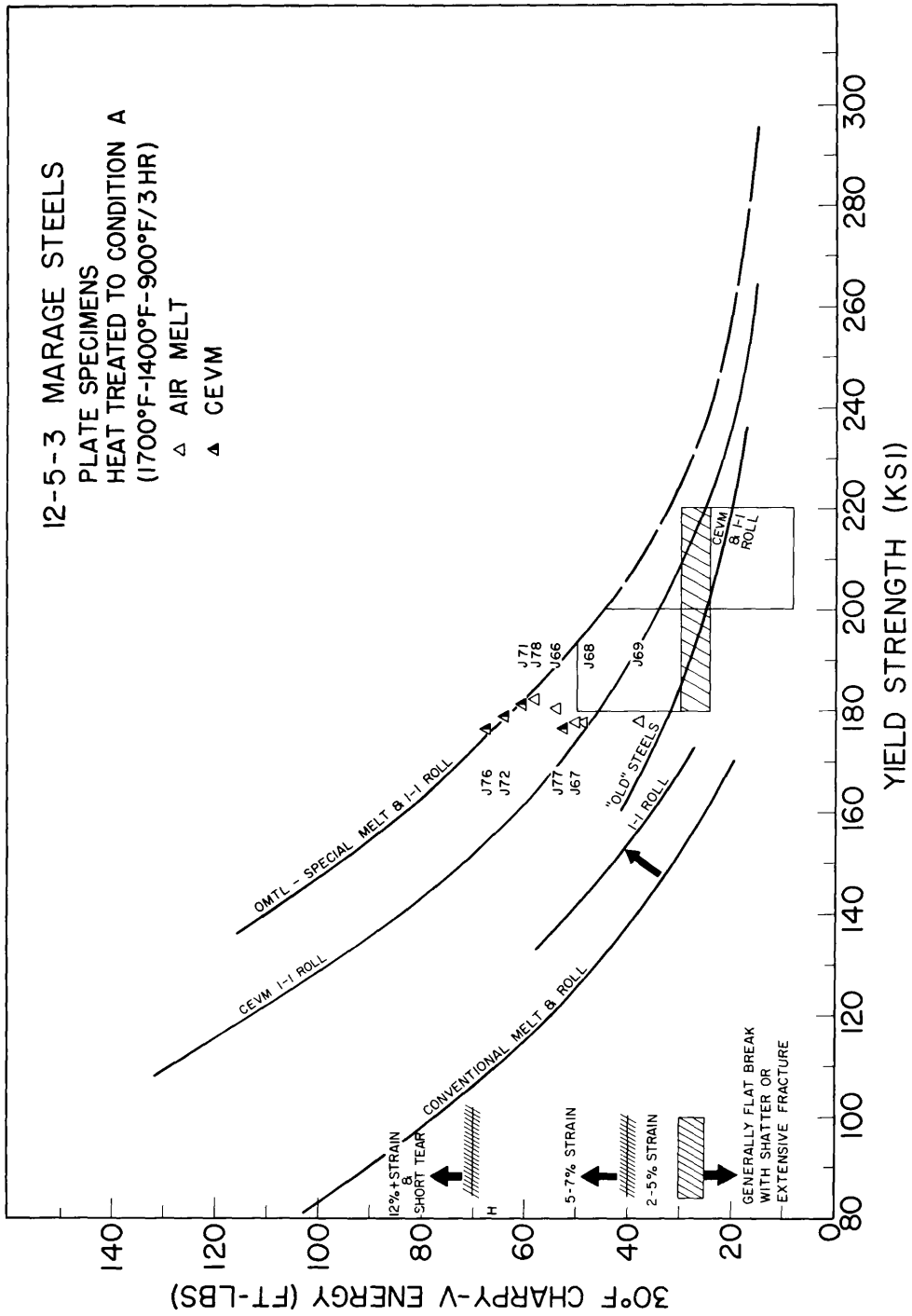


Fig. 40 - Yield strength-Charpy V energy absorption relationships for laboratory double-anneal heat treatment Condition A of nine marage steel plates. FTID-OMTL curves included for reference.

microstructure. Generally, the lowest annealing temperature which will effect recrystallization at midthickness of the product is preferred for the development of optimum properties. The soft martensite is strengthened (hardened) by complex precipitation reactions that occur in subsequent aging treatments at temperatures ranging up to approximately 1000°F. The strength and toughness levels developed by the aging heat treatment depend upon the specific steel composition, the aging time, and the aging temperature. The heat treatment generally expected to develop near-optimum strength and toughness properties in the maraging steels has normally been considered to be annealing at 1500°F and aging at 900°F for 3 hours. Detailed analysis of the heat-treatment studies data given in Table 9 indicates that the best combination of high strength and high toughness values were developed in all of the 12-5-3 maraging steels under investigation by the double anneal-plus-age treatment, Condition A, i.e., solution anneal 1700°F, re-solution anneal 1400°F, plus age 900°F/3 hr. Fracture toughness evaluations of these marage steels in heat-treatment condition A are now underway.

#### FRACTURE TOUGHNESS EVALUATION AND CONTROL OF HIGH STRENGTH STEEL WELD METALS

As emphasized early in this program (12), the controlling feature in the fracture-safe utilization of high strength steels for complex, welded fabrication has not been the fracture toughness of the base plate. On the basis of plate metal properties per se, the FTID reference charts of Figs. 33 and 34 suggest that a variety of plate alloys of 180 ksi minimum YS are available to provide materials that require plastic (overload) strains to sustain propagation of fracture. The controlling feature has been the weld and heat-affected-zone (HAZ) properties.

Reliable fracture toughness data for high strength steel welds are very limited at present because the weld wires have not been commercially available until very recently. The Bureau of Ships-U.S. Steel Corporation program for the development of a 130-150 ksi minimum YS hull steel weldment is presently limited to the 130-140 ksi YS range because of requirements for MIG (consumable electrode, metal arc, inert gas shielded) and STICK (manual, covered electrodes) welding capabilities. Such capabilities with steel welds exceeding approximately 150 ksi YS require the development of nonbrittle weld metals that would not require full-cycle (Q&T or solution anneal-plus-age) heat

treatments of the weldments. The 12-5-3 maraging steels and 9-4-0.25 Q&T steels have appeared promising for nominally 180 ksi minimum YS structural applications because of producers' claims of developing suitably tough, TIG process weld metals. Limited MIG process welds with both of these new weld wires are stated to have shown lower YS and considerably lower  $C_V$  toughness values than were obtained with the same wire composition used for TIG welds. Preliminary evaluations of producer-fabricated, TIG-process, 180-ksi-YS weldments, using "experimental" electrodes produced from small (150-lb) research quality heats, were reported to be highly encouraging for weldments in both of these alloy steels (8,9). For further studies required for the characterization of critical properties of such weldments, additional 12-5-3 maraging steel weldments were procured. Also, attempts were initiated to procure weld wires representative of semiproduction heats (1000 lb) of these alloy steels.

Short lengths (approximately 11 in.) of four producer-fabricated, TIG-process weldments of 1-in.-thick 12-5-3 maraging steels were supplied to NRL by the INCO Research Laboratory. Two of the weldments were made with a nominal 12Ni-3Cr-3Mo wire composition expected to develop a 160-ksi minimum YS upon aging and the other two were made with a nominal 17Ni-2Co-3Mo wire composition expected to develop a 180-ksi minimum YS upon aging. The welds were made in fully annealed and aged sections of 12-5-3 plate (Nos. J6 and J8) which comprised material remaining from two of the high purity, vacuum induction melt practice, maraging steels previously evaluated by NRL (9). After welding by INCO, the weldments were furnace-aged and tested by NRL. The specific aging temperatures and times used for the individual weldments were based on results of limited  $C_V$  and transverse weld tension tests of the welds conducted by INCO.

Each of the weldments described above was sectioned to provide material for DWTT,  $C_V$ , and transverse weld tensile tests. Table 10 presents a summary of the test results obtained. Figure 41 depicts a representative example of the appearance of DWTT specimens of these welds. A double V-joint preparation had been used and the relatively high DWTT values given depict an integrated energy absorption value for the fractures which involved weld, HAZ, and plate areas, as noted in Table 10. Figure 42 presents a summary of the  $C_V$ -YS relationships given

Table 10  
 Test Data For Maraging Steel Weldments  
 (12Ni-5Cr-3Mo Plate; Transverse weld tensile specimens)

Material	Condition	0.505-in.-Dia. Tension Test Data				Charpy V at 30° F (ft-lb)	Drop-weight Tear at 30° F (ft-lb)
		0.2% YS (ksi)	T.S. (ksi)	El. in 2 in. (%)	R.A. (%)		
J8 Plate	Mill (1500° F + 900° F/ 2 hr)	162.6	170.6	15.8	64.1	84	4478*
J8 Plate	Mill + 900° F/3 hr	172.2	178.5	14.8	62.7	73	4624
J63 Weld (12-3-3)	900° F/3 hr	164.0	165.6	13.0	64.1	54 (Top) 73 (Bottom)	3613*
J8 Plate	Mill + 900° F/19 hr	184.4	190.6	15.5	62.0	54	3360
J60 Weld (12-3-3)	900° F/19 hr	174.5	177.2	10.5	53.5	65	3486*
J6 Plate	Mill (1500° F + 900° F/ 20 hr)	184.4	190.0	13.5	55.7	58	3041
J6 Plate	Mill + 825° F/24 hr	192.6	198.0	13.0	56.8	50	2780
J65 Weld (17-2-3)	825° F/24 hr	180.6	183.0	†	†	43	1865
J6 Plate	Mill + 850° F/24 hr	193.3	198.4	13.5	57.9	49	2846
J64 Weld (17-2-3)	850° F/24 hr	184.4	187.7	13.0	58.0	40 (Top) 58 (Bottom)	3333*

\*DWT fracture involved weld, HAZ and plate.

†Not determined; weld defects in tensile specimens.

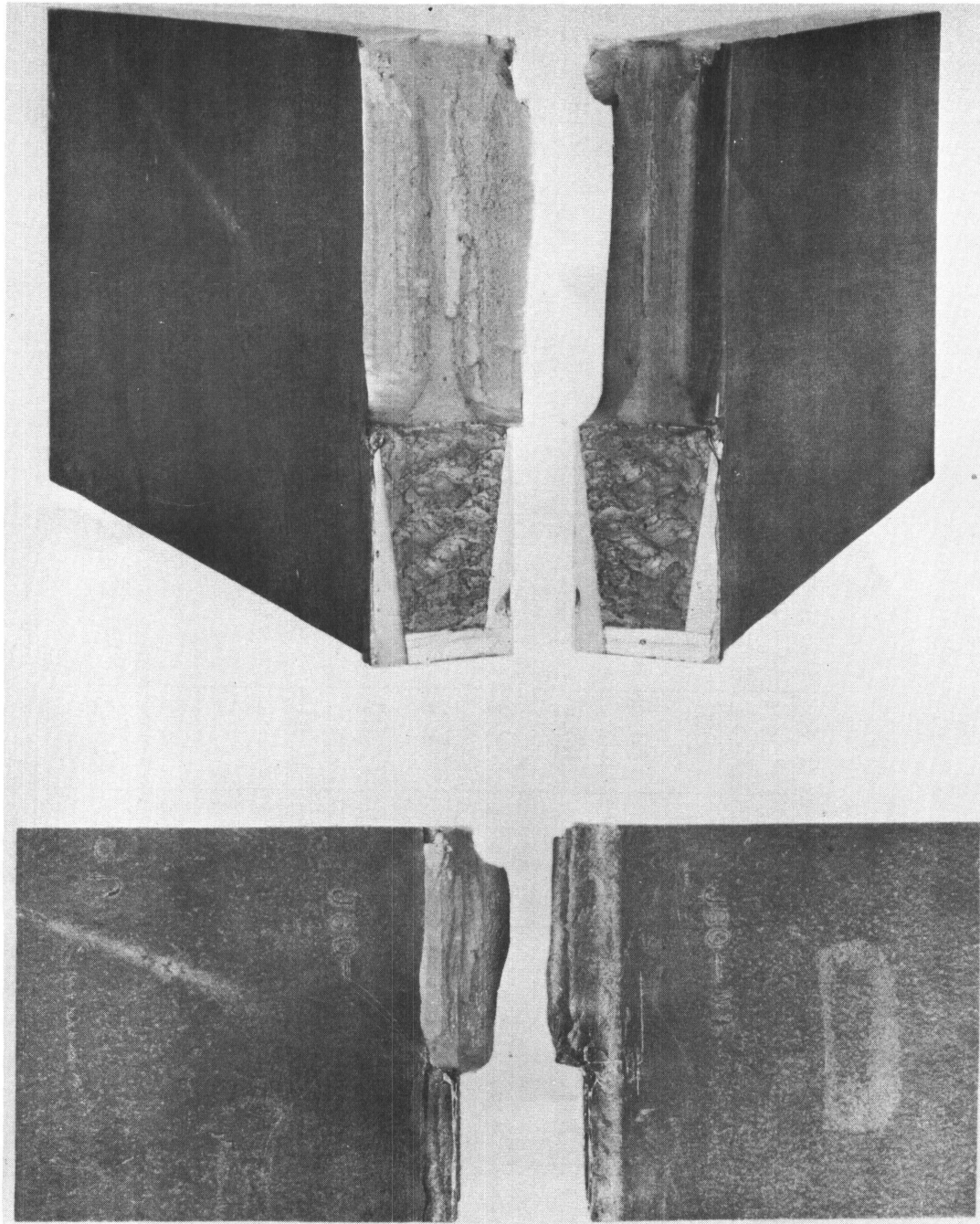


Fig. 41 - Fracture in drop-weight tear test specimen of double-V weld in 12-5-3 marage steel plate

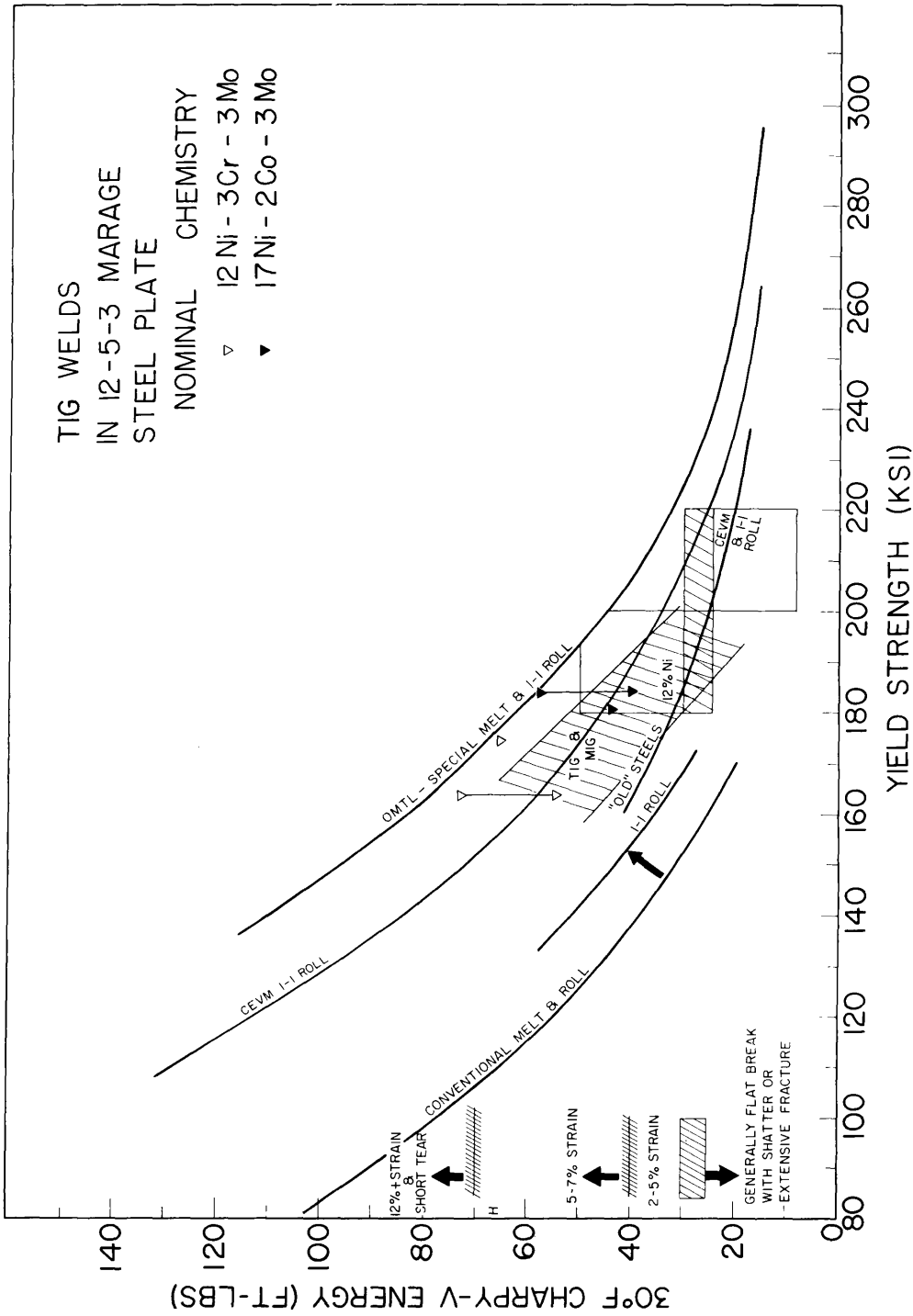


Fig. 42 - Summary of Charpy V-yield strength relationships of double-V welds in 12-5-3 marage steel plate. FTID-OMTL curves and data band for experimental welds in 1-inch plate included for reference.

in Table 10 for these maraging steel welds, as referenced to the FTID chart for 1-in.-thick steel plates. The shaded area in this figure encompasses the range of values previously reported for the best of the "experimental" TIG weld metal compositions produced in the 12%-Ni marage steel weld metal alloys. Significant differences were found between  $C_V$  tests for the top and bottom surfaces of two of the weldments and these are indicated in Fig. 42 by the vertical lines joining the data points for these welds. This spread in  $C_V$  values obtained from the top and bottom surfaces of these welds was noted for the two weldments which had been completed and then had required rewelding from one side only to replace material that had been machined to remove incompletely fused root passes.

Generally, Fig. 42 indicates that both of the maraging steel welds studied equaled or exceeded the  $C_V$  toughness levels of other "experimental" TIG weld metals of comparable strength. It is noted, however, that the expected 160-ksi YS level for the 12Ni-3Cr-3Mo weld is developed by relatively short (3-hr) aging times at 900°F. Longer times (19 hr) at 900°F increased the YS of this weld to approximately 175 ksi without significantly decreasing the  $C_V$  toughness level of the weld. Aging times of 24 hours at temperatures of 825°F and 850°F were required to develop the expected 180-ksi YS level in the 17Ni-2Co-3Mo weld. Extensive study of the effects of such aging treatments on plate and HAZ properties are considered necessary to establish fabrication confidence with weld metals which require unusually long aging treatments to develop weld properties.

The producer-fabricated TIG welds that were investigated had been made in plates that were supplied fully solution annealed and aged to YS levels of approximately 163 and 184 ksi, respectively. The  $C_V$ -YS relationships developed by these plates as the result of the additional aging treatments applied to the weldments are shown in Fig. 43. Significant increases in plate YS and concomitant decreases in  $C_V$  toughness are noted to result from the specific aging treatments applied to the weldments. For the resulting plate metal YS ranging from approximately 163 to 193 ksi, it is pertinent to note these high purity, special vacuum induction melt practice plates maintain optimum  $C_V$ -YS values as shown by the relative position of the data points to the limiting (ceiling) OMTL curve for special melt practice 1-in.-thick steel plates.

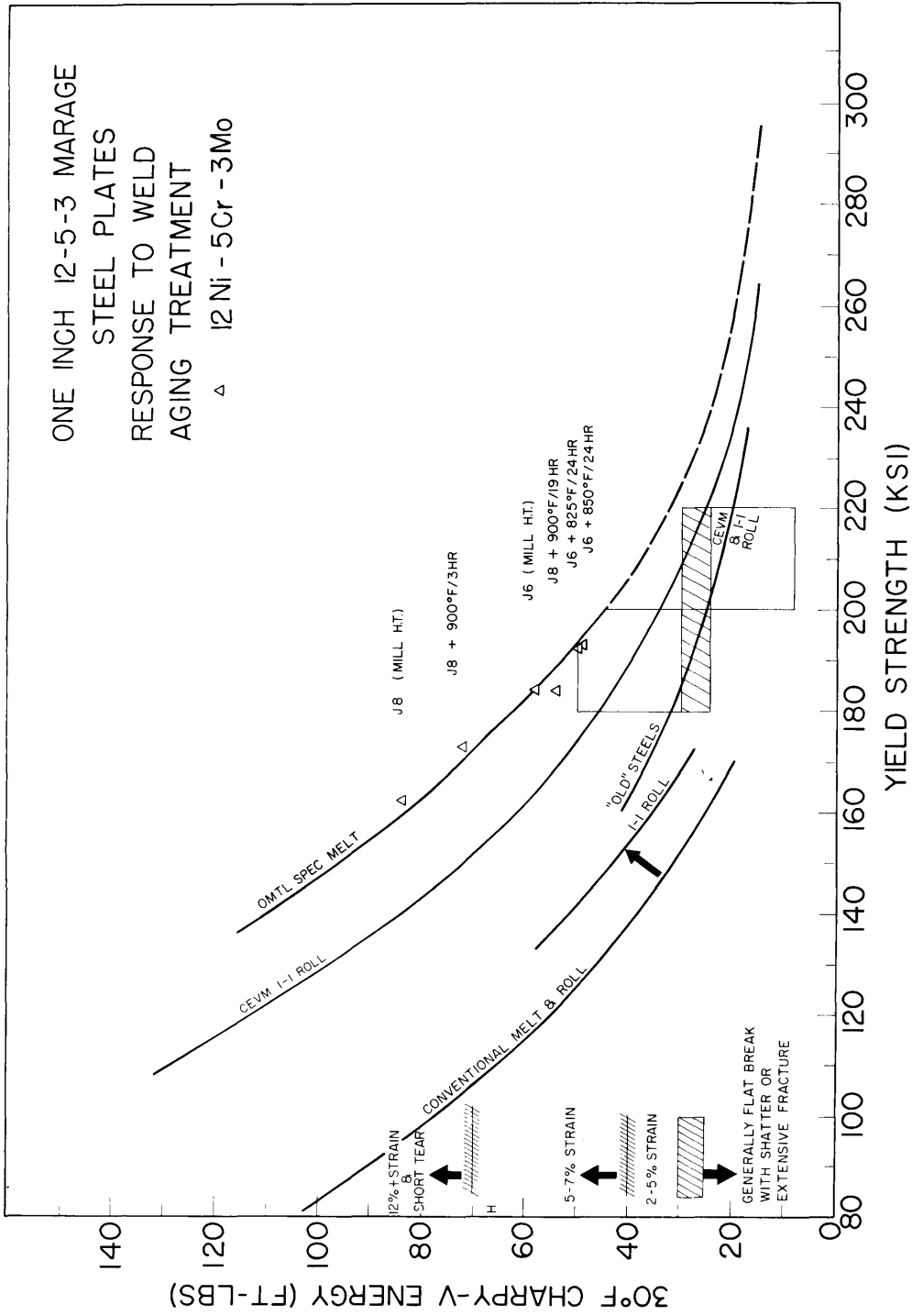


Fig. 43 - Charpy V-yield strength relationships of 1-inch marage plate as a function of weld heat treatments. FTID-OMTL curves included for comparison.

For NRL investigations of high strength welds, 1/16-in.-diam wire representative of the product from 1000-lb melts of the nominal 17-2-3 and 12-3-3 maraging steel weld compositions have been purchased. The chemical compositions of these weld wires are given in Table 11. Initial studies with these welds have been aimed at determining optimum aging treatment conditions necessary to develop the best combination of strength and toughness properties in welds deposited under a variety of conditions. Appropriately optimized weldments of these and other high strength materials are to be produced to meet the test and investigation requirements of plane strain fracture mechanics ( $K_{Ic}$ ) and engineering methods (DWTT,  $C_v$ , etc.) fracture toughness determinations, stress-corrosion-cracking, and fatigue (strain-range basis) crack propagation rate studies.

Prior to final installation of the new precision-built, fully-automatic MIG-TIG fusion welding facility, described earlier, exploratory weldments of these materials were made with manual TIG equipment. To facilitate operations, three strands of the 1/16-in.-diam wire were twisted to form a suitable filler wire for manual TIG welding. The welds were deposited in 60° double V-joint preparation plates comprising remnant sections of 1-1/2- and 2-in. maraging steels available from previous studies. Small blocks (thickness x 2-1/4 in. x 5 in.) of the weldments were cut and furnace-aged at various temperatures and times. These were then sectioned to provide material for one all-weld-metal 0.505-in. diam tensile test specimen and usually 10  $C_v$  test specimens per each heat-treatment condition.

The summary of results given in Table 12 comprise the data available to date for the nominal 17-2-3 weld composition for manual welds made with heat input energies of approximately 40,000 to 45,000 joules/inch. These conditions required that a relatively large number of small weld bead passes be used to complete the welds (approximately 85 to 90 passes for 2-in.-thick welds). A graphical summary of the  $C_v$ -YS relationships is given in Fig. 44, as referenced to the FTID for 1-in.-thick steel plates, and the data band (shaded band) established previously for experimental TIG welds in 12-5-3 marage steel plates. Generally, the YS and  $C_v$  toughness values of these manual TIG welds are noted to be lower than those depicted by the data band for experimental welds. Approximately 160-ksi YS levels are developed with short aging times (1-3 hr) and

Table 11  
 Chemical Compositions of Marage Weld Wire Vacuum Melter Heats  
 Drawn to 1/16-in. Diameter For TIG Welding

	Composition (%)											
	C	Mn	Si	P	S	Ni	Cr	Co	Mo	Ti	Al	
<u>17-2-3</u>												
Purchase specification	0.010 Max	0.10 Max	0.10 Max	0.005 Max	0.005 Max	16.0/17.5		2.0/2.5	2.8/3.1	0.53/0.63	0.05 Max	
Mill test	0.01	<0.01	0.01	0.003	0.006	16.65		2.34	2.98	0.59	0.04	
<u>12-3-3</u>												
Purchase specification	0.02 Max	0.10 Max	0.10 Max	0.005 Max	0.005 Max	11.9/12.7	3.4/4.5		2.6/2.9	0.4/0.5	0.05 Max	
Mill test	0.013	<0.10	<0.10	<0.005	0.004	12.3	4.00		2.75	0.40	<0.05	

Table 12  
Charpy-V and Yield Strength Data for  
Aged 17-2-3 Wire TIG Welds

Aging Temperature	1 Hour		3 Hours		10 Hours		24 Hours	
	YS	C <sub>v</sub>	YS	C <sub>v</sub>	YS	C <sub>v</sub>	YS	C <sub>v</sub>
800°F	147	68	162	42	178	30	178	25
850°F	157	44	171	31	177	30	178	35
900°F	170	31	173	34	175	39	174	40
950°F	171	38	172	40	170	36		

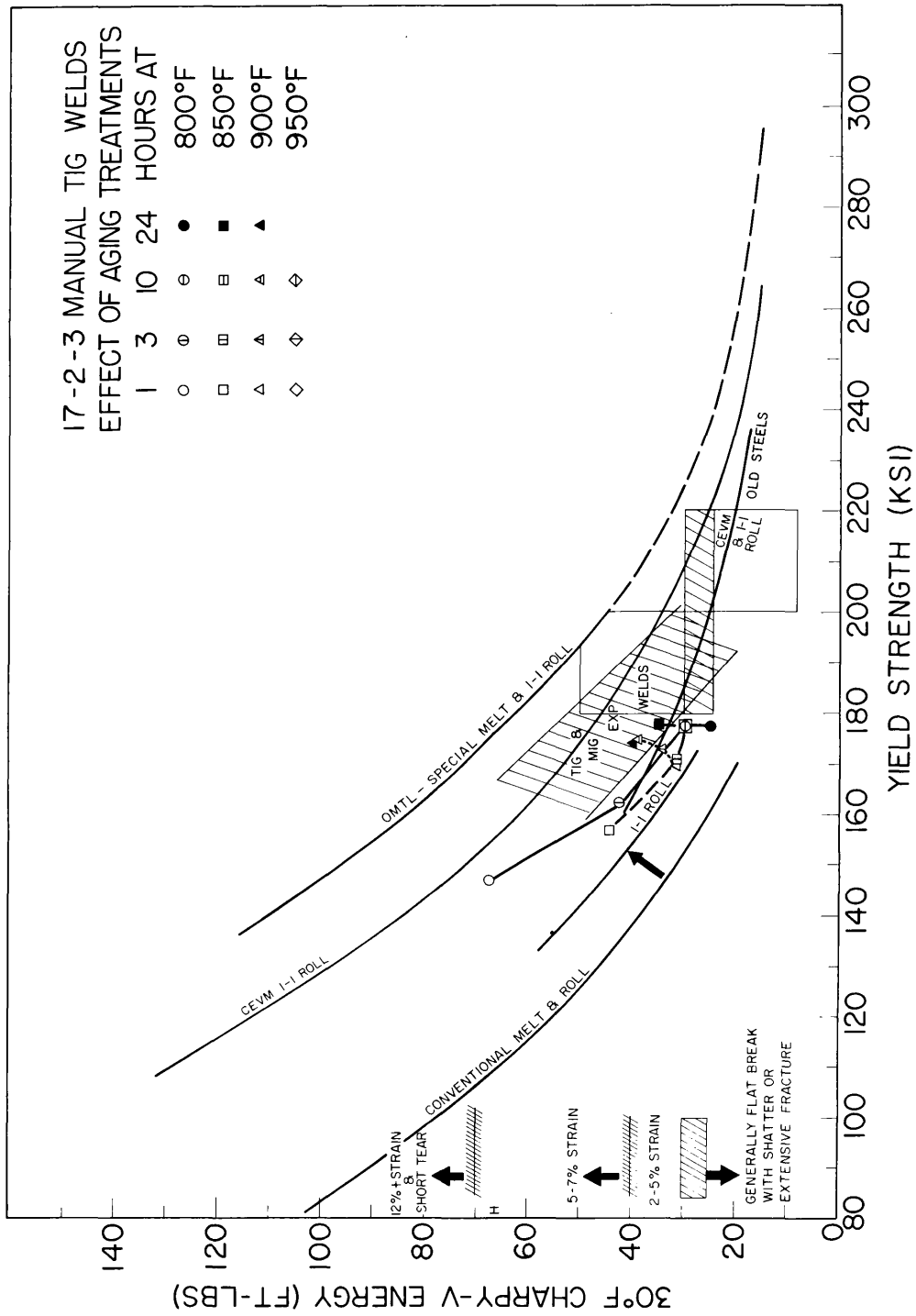


Fig. 44 - Effect of aging treatments of 17-2-3 MANUAL TIG welds on Charpy V-yield strength relationships. Data band for experimental welds and FTID-OMTL curves also shown for reference.

approximately 175 ksi YS with long aging times (10-24 hr) rather than the 180-ksi minimum YS expected for short-time aging treatments of this weld composition. Data for additional manual TIG and fully-automatic TIG weldments of the two weld metals described in Table 11 are expected to be developed during the next reporting period.

#### LOW CYCLE FATIGUE CRACK PROPAGATION IN 12%-Ni MARAGING STEELS

(T.W. Crooker, R.E. Morey, and E.A. Lange)

Current interest in materials for high performance structures has focused attention on metals from new alloy systems possessing high strength-to-density ratios, such as 12% Ni maraging steels. The suitability of such high strength metals for service applications in welded structures can be dependent upon the material's resistance to failure from the propagation of low cycle fatigue cracks, which are readily initiated from cracklike flaws. Such flaws are unavoidable in complex structures because of practical deficiencies in manufacturing and inspection techniques. Furthermore, high intensification of strains may be expected at critical points where flaws are most likely to occur. In many cases the structure must operate in a hostile environment, such as seawater, which can be expected to further aggravate flaw growth. Therefore, investigations were programmed to define and evaluate the factors which control the growth of low cycle fatigue cracks. Such knowledge is essential for reliable prediction of the life of fail-safe structures and for prevention of catastrophic failures by fast terminal fracture initiated from fatigue cracks which have grown to a critical size.

The low cycle fatigue crack propagation characteristics of a broad spectrum of metals, both ferrous and nonferrous, have been discussed in previous reports (1,7-11,13-16). This is a progress report on 12% Ni maraging steels at two yield strength (YS) levels--160 ksi (NRL Code J8) and 180 ksi (NRL Code J7). The testing procedures employed are the same as those described in the references so as to provide a common basis for comparisons with fatigue crack growth rates in other high strength materials.

#### TEST MATERIALS

Both samples of maraging steel were obtained from the same heat, and the two YS levels were obtained by variation in heat treatment.

The heat treatment consisted of a solution anneal at 1500°F and aging at 900°F. The 160-ksi-YS steel was aged for 2 hours and the 180-ksi-YS steel was aged for 20 hours.

The chemical composition (wt-%) of the steels was as follows:

C	Mn	P	S	Si	Ni	Cr	Mo	Ti	Al
0.007	0.04	0.005	0.007	0.07	11.8	5.12	3.30	0.24	0.11

Fatigue specimens were machined from 1-in. plate stock. Specimen orientation resulted in fatigue crack propagation parallel to the principal rolling direction--in the ASTM designated WR fracture direction.

## RESULTS AND DISCUSSION

Low cycle fatigue crack growth rate studies were conducted with center-notched, plate bend specimens loaded under full-reverse strain cycling in both air and 3.5-percent-salt-water environments. Figure 45 is a log-log plot of the fatigue crack growth rate data as a function of total strain range for both the 160-ksi- and the 180-ksi-YS 12%-Ni maraging steels. The open symbols denote air data and the solid symbols denote salt-water data. Based on previous subcritical crack growth characterizations of steels, several significant observations are evident from these data.

The results of the tests conducted in air make the 12% Ni maraging steel a very promising candidate as a high performance structural material. The characteristics of the fatigue crack growth rate curve for air (Fig. 45) on a total strain range basis are similar to those for lower YS, high fracture toughness steels, such as HY-80 (10,11,12) or 5Ni-Cr-Mo-V (9). A significant characteristic is the 4:1 slope of the crack growth rate curve exhibited in Fig. 45 which is a common slope for steels with high fracture toughness. It is important to note that at cyclic strain levels up to their respective proportional limits, no sharp increase in the slope resulting from crack instability occurs. This characteristic is in contrast to the fatigue crack propagation characteristics of some conventional high YS metals, such as D6AC and 4335 steels (8) or 7079-T6 aluminum alloy (15), which suffer from rapid fatigue crack propagation,  $dL/dN > 1000$  microinches/cycle, at nominally elastic cyclic load levels due to lower levels of fracture toughness.

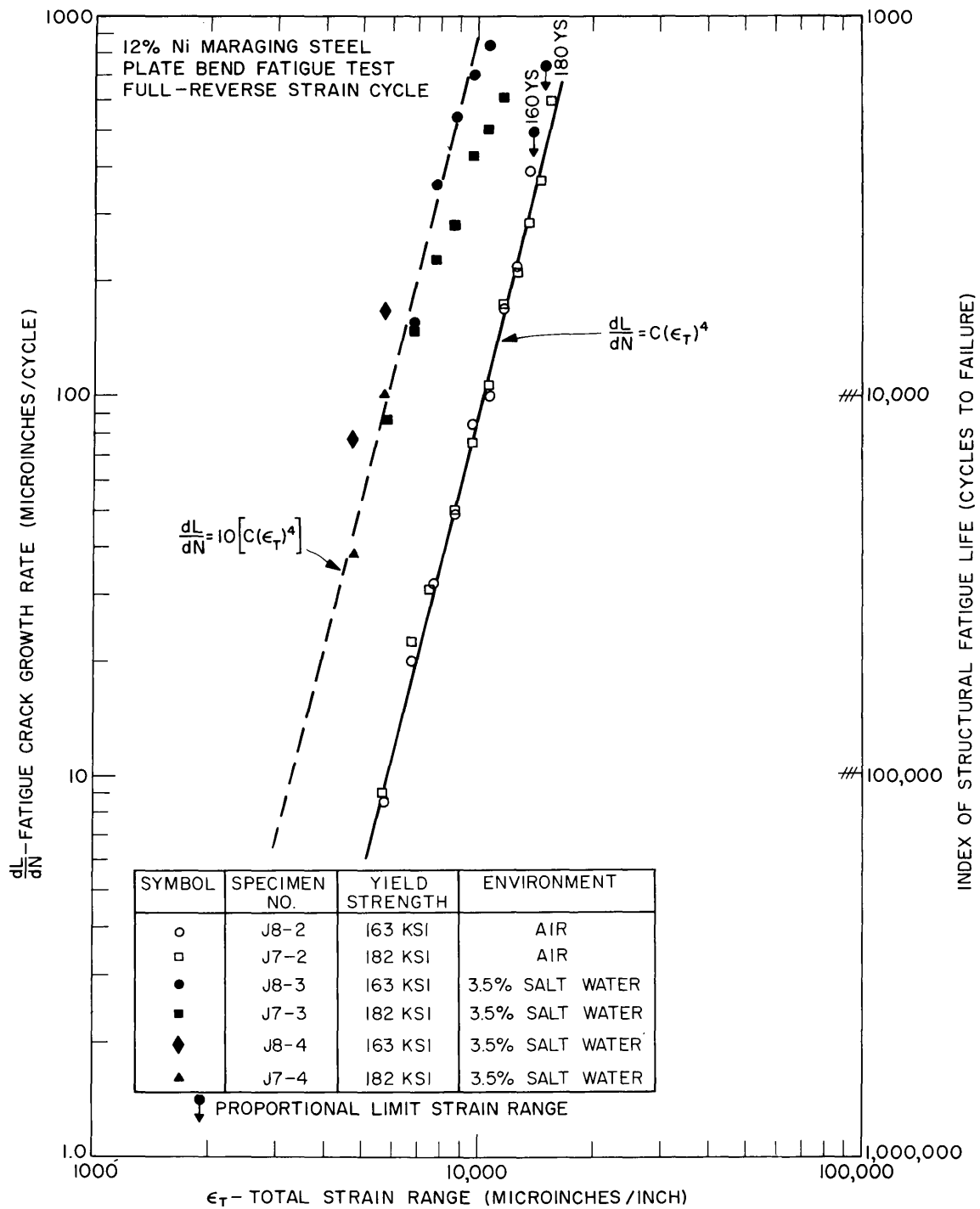


Fig. 45 - Log-log plot of fatigue crack growth rate as a function of total strain range for two 12% Ni maraging steels in air and 3.5% salt water environments

A salt water environment can normally be expected to significantly increase the growth rate of fatigue cracks in high strength steels, sometimes catastrophically. The effect of salt water on the fatigue crack growth rates for the two 12% Ni maraging steels under test was significant, but the effect was more comparable to that observed for HY-80 (13) and HY-140 (9) steels than for the older, high strength steels--D6AC and 4335 (8). Increases in fatigue crack growth rates due to a salt water environment ranged from five fold to more than an order of magnitude. The lower strength (160 ksi YS) material appeared to be more sensitive to salt water than the higher strength (180 ksi YS) material. Although the salt water environment caused an increase in fatigue crack growth rate, neither material showed a serious sensitivity to stress-corrosion cracking, as was seen in 4335 steel (8) or the Ti-7Al-2Cb-1Ta alloy (7). The environmental effect appeared to diminish at high strain levels for the 12% Ni steels, whereas the environmental effect increased with strain level for the 4335 steel and the Ti-7Al-2Cb-1Ta alloy. However, both maraging steels are sensitive to the salt water environment at low strain range levels. Fatigue crack growth rates are increased by an order of magnitude due to the salt water at strain ranges as low as one-third of the proportional limit in both steels; therefore, there does not appear to be a lower threshold strain value at a level which would have practical significance for high performance applications.

#### COMPARISON WITH OTHER STEELS

Figures 46 and 47 provide comparisons between the low cycle fatigue crack propagation characteristics of 12% Ni maraging steels and several other popular structural steels of both lower and higher YS. Figure 46 is a log-log plot of fatigue crack growth rate versus total strain range for 12% Ni maraging steels and seven other steels in air. It is of interest to note that, on a strain range basis, most of the medium-to-high-strength martensitic steels have very similar performance. Data from these materials, which include HY-80, T-1, 5Ni-Cr-Mo-V, and 12% Ni maraging steels, fall within a narrow band which follows a 4:1 slope. Exceptions to this behavior are the lower YS pearlitic steels A201B and A302B which possess a significantly different crack growth rate response to strain range, and the higher YS martensitic steels 4335 and D6AC which depart from this common fatigue behavior pattern because of low fracture toughness.

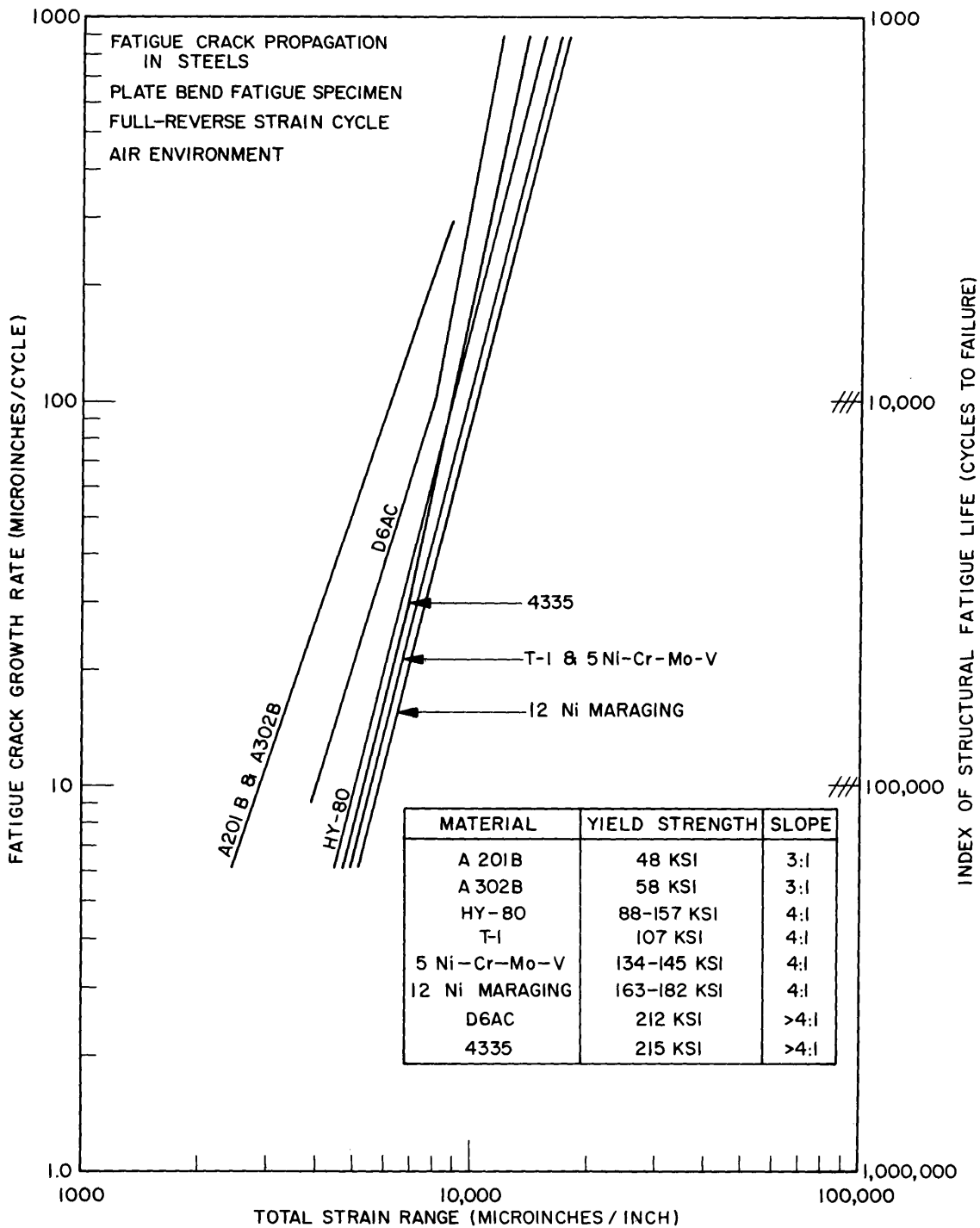


Fig. 46 - Log-log plot of fatigue crack growth rate as a function of total strain range for two 12% Ni maraging steels plus seven other popular structural steels. Curves are from plate bend fatigue tests in air environment.

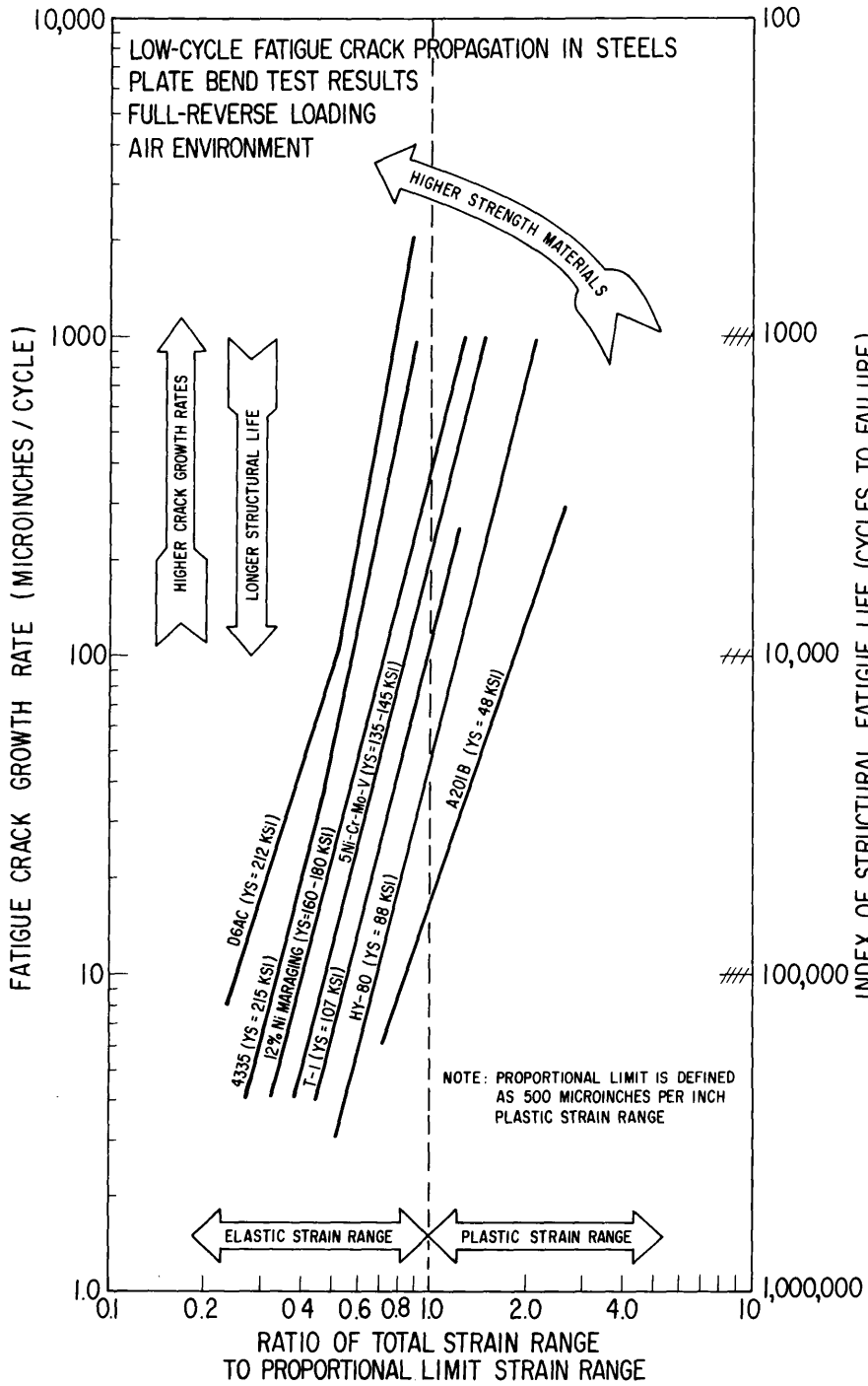


Fig. 47 - Data curves replotted from Fig. 46. Strain range has been normalized with respect to the plate bend proportional limit of each material.

This common fatigue crack propagation behavior among these several materials on a strain range basis also illustrates an important difference in their fatigue characteristics in structures. This is shown in Fig. 47 which is the data from Fig. 46 normalized on the basis of strength level. Here strain range is considered in relation to the proportional limit of each material as measured in the plate bend specimen. This index diagram portrays the relative ability of a spectrum of materials to tolerate plastic strains under cyclic loading in the presence of a growing flaw. It also demonstrates the potential decrease in fatigue life that designers must consider when higher strength materials are employed at higher cyclic strain levels, owing to design procedures based on a fixed percentage of YS. When compared on this basis, the 12% Ni maraging steels are seen to be bracketed as being slightly inferior to HY-140 but considerably superior to the "old" high strength steels 4335 and D6AC.

#### SUMMARY

Results from tests conducted in both air and salt water indicate that the 12%-Ni maraging steels, at 160 and 180-ksi YS levels, possess good low cycle fatigue crack propagation characteristics in both air and 3.5-percent salt water, and their performance compares favorably with lower YS, high fracture toughness steels such as HY-80 and HY-140.

However, it must be recognized that in high performance structures the higher elastic strength of these 12%-Ni maraging steels permits more rapid fatigue crack growth rates to develop under elastic strain conditions, in accordance with the fourth power response to cyclic total strain range observed in these materials.

#### ALUMINUM ALLOYS

(R.W. Judy, Jr. and R.J. Goode)

The fracture toughness properties of aluminum alloys are being investigated to determine the ability of small laboratory fracture toughness tests to provide engineering criteria for predicting service performance of these materials in large, complex structures. A large portion of this work has been directed to indexing drop-weight tear test (DWTT) data with the larger, structural prototype element test--the explosion tear test (ETT). A preliminary Fracture Toughness Index Diagram (FTID)

for 1-in.-thick commercially produced aluminum alloys has evolved. This diagram relates ETT performance to DWTT energy over a wide range of yield strength (YS), as has been done for steel and titanium alloys.

#### EXPLOSION TEAR TEST RESULTS

Previous ETT testing (1) had demonstrated that alloy 7005-T63 could withstand approximately 7-10 percent plastic strain in the presence of a flaw with limited fracture propagation, and that alloy 7106-T63 could withstand plastic strain in the range of 3-5 percent under similar conditions. Further testing in the ETT showed the limiting plastic strain level for fracture to be about 8 percent and 3.5 percent, respectively, on these two alloys. The 7005-T63 ETT specimen tested to nearly maximum strain conditions is shown in Fig. 48. A specimen of alloy 7106-T63 which exceeded the maximum plastic strain limit for fracture is shown in Fig. 49. Explosion tear test plates of the alloys 5083-0 (Fig. 50) and 5086-H112 (Fig. 51) were found to be able to withstand 17.7 percent and 15.5 percent plastic strain in the ETT without failure; however, as seen in Figs. 50 and 51, these levels of strain represent about the maximum capability for the two alloys.

#### FRACTURE TOUGHNESS INDEX DIAGRAM

The FTID for aluminum (Fig. 52) is a reference chart showing the correlation of YS, DWTT, and ETT performance for aluminum alloys. This diagram is very preliminary since it is based on a limited number of data points and, as such, is subject to changes as new information becomes available.

Some modifications of the FTID are evident; these are a result of more extensive DWTT and ETT of alloys 7005-T63 and 7106-T63. Additional DWTT data for these alloys showed slightly less energy required for fracture than had been previously reported (1). The 7005-T63 alloy changed from 1052 ft-lb to 870 ft-lb and the 7106-T63 alloy from 573 ft-lb to 519 ft-lb. These values, combined with the ETT results, permitted a more detailed breakdown of ETT capabilities in relation to DWTT energy. The hatched lines at the left of the diagram (Fig. 52) indicate minimum plastic strain levels expected at the DWTT energy levels indicated. For example, alloy 6061-T651 (38 ksi YS, 750 ft-lb DWTT) has the capability to withstand fracturing in the presence

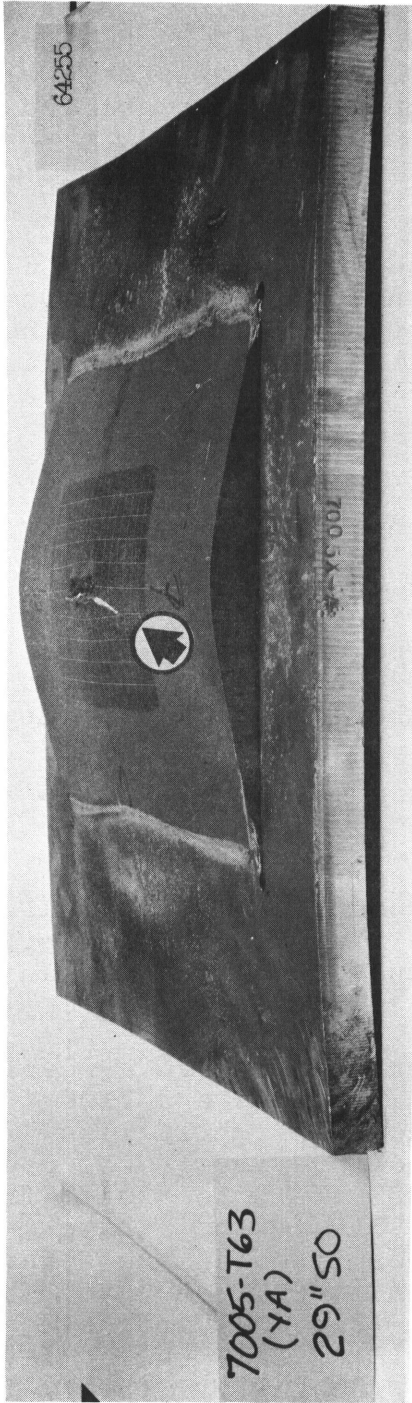


Fig. 48 - Explosion tear test specimen of aluminum alloy 7005-T63 tested to 7.5% plastic strain

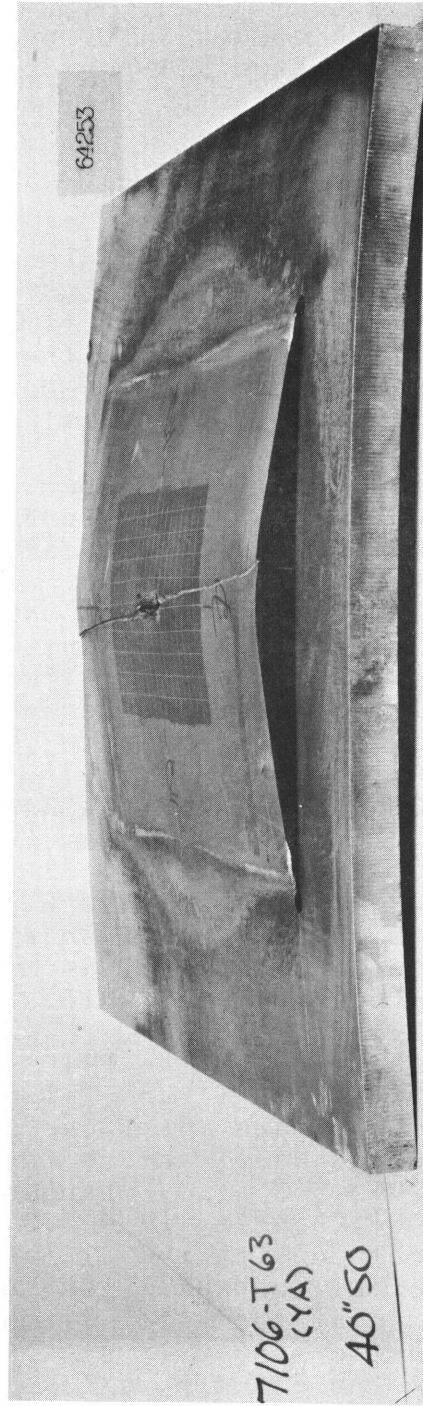


Fig. 49 - Explosion tear test specimen of aluminum alloy 7106-T63 tested to a plastic strain level in excess of 4%

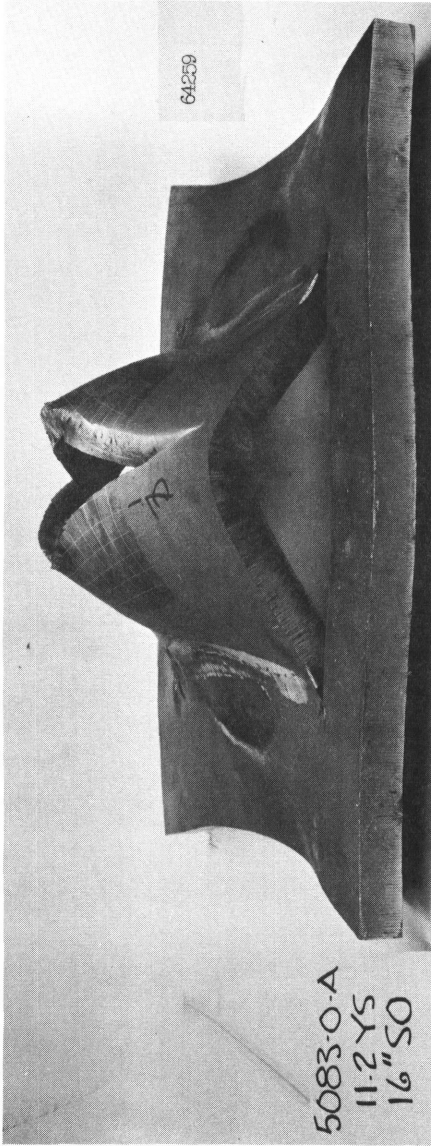


Fig. 50 - Explosion tear test specimen of aluminum alloy 5083-0 tested to 17.7% plastic strain

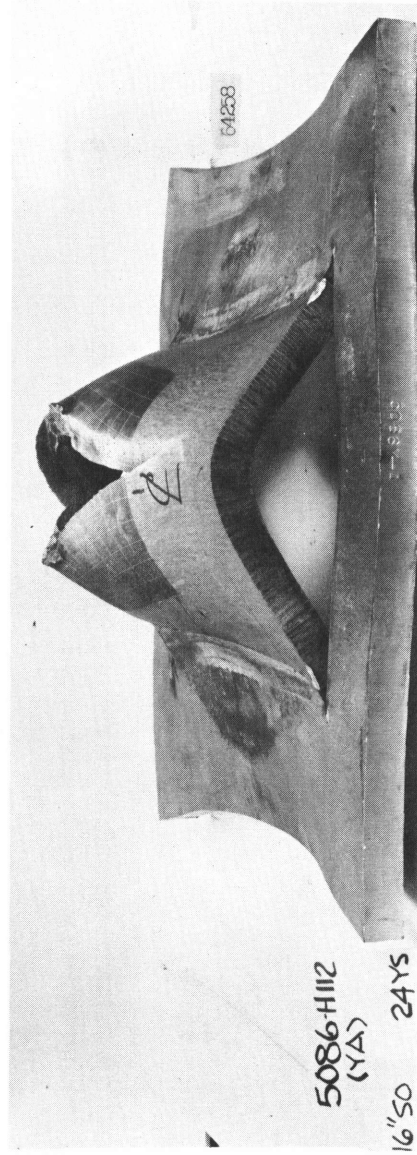
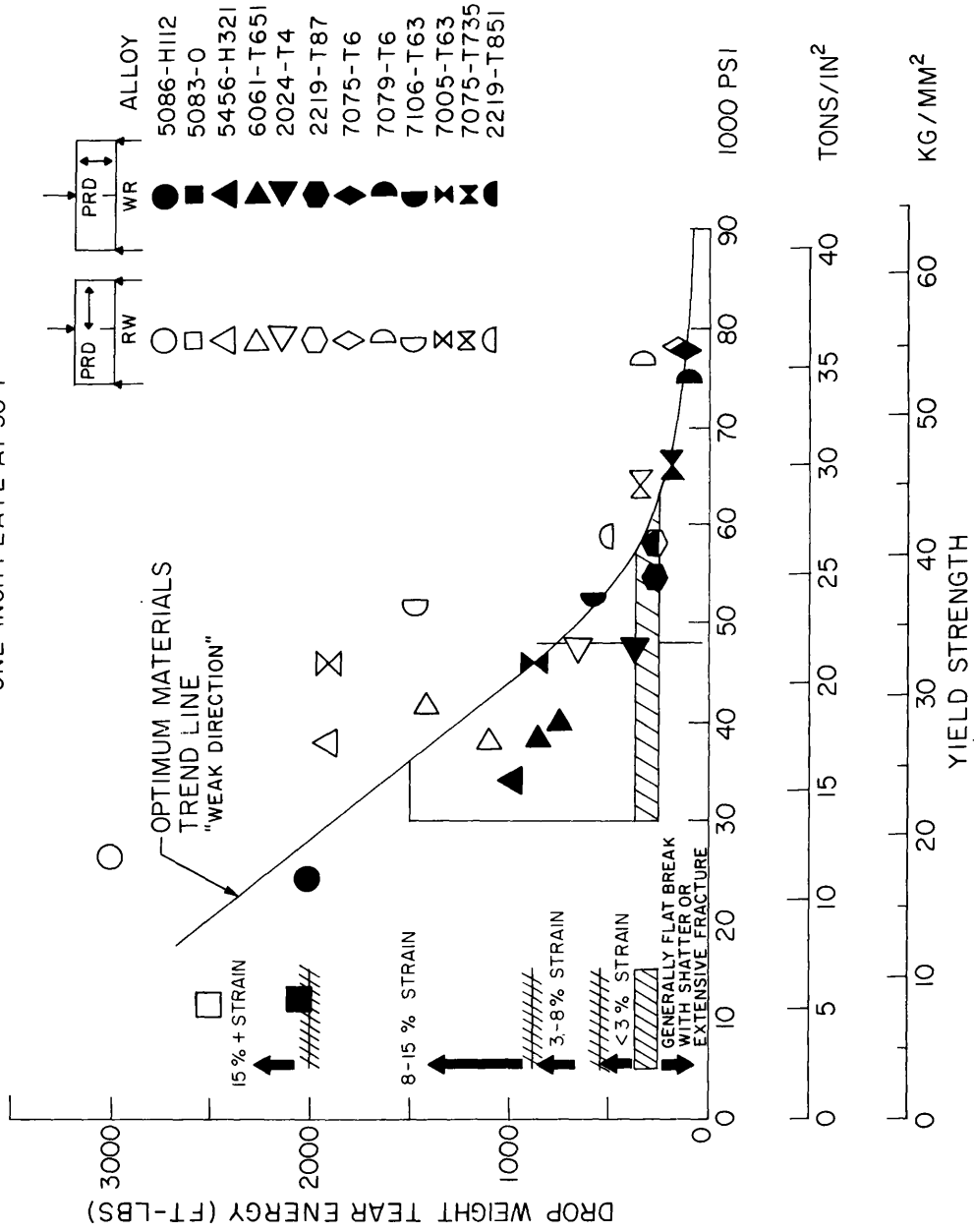


Fig. 51 - Explosion tear test specimen of aluminum 5086-H112 tested to 15.5% plastic strain

ALUMINUM ALLOYS  
ONE-INCH PLATE AT 30°F



of a 2T flaw when explosively loaded in the ETT up to 12 percent plastic strain (9); however, on the basis of the DWTT energy this alloy falls in the 3-8-percent plastic strain range on the FTID. On the other hand, the 7005-T63 alloy of the same DWTT energy level (760 ft-lb) and at 47 ksi YS is capable of only 8 percent plastic strain before failure occurs in the ETT. The precise level of fracture toughness (plastic strain in the ETT) which can be tolerated by any particular aluminum alloy is academic in considering its use in a large complex structure; most important is whether it can resist crack propagation for expected levels of plastic overloads in the presence of a flaw. As can be seen from the FTID, all the alloys below about 45 ksi YS are capable of much higher levels of plastic strain than any projected structures of aluminum alloys might require. Those above about 50 ksi YS would require the determination of critical flaw size-stress level for fracture with fracture mechanics techniques for failure-safe design.

#### TESTS OF SIX-INCH-THICK 7039-T6X31

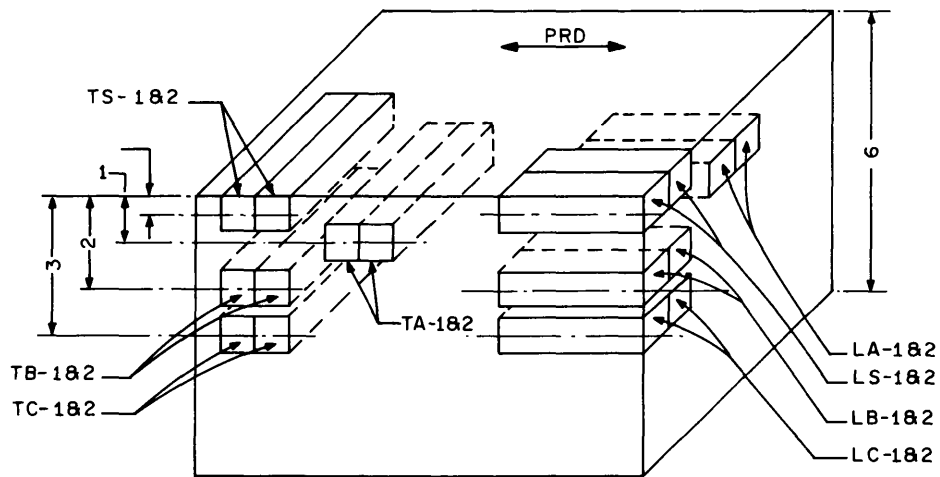
A study was conducted to determine whether a variation of mechanical properties would be present in a 6-in. thick section of alloy 7039-T6X31. Tensile and DWTT specimens (Fig. 53), taken at both surfaces, quarter thickness, and center of the plate in both the RW and WR orientations (4), and two specimens each in the RT and WT directions were tested. Table 13 contains the data obtained in this study.

No significant variation of mechanical properties due to specimen location were noted. Yield strength values ranged between 49.8 ksi and 54.7 ksi for all orientations and DWTT energy values ranged between 514 ft-lb and 931 ft-lb. No significant differences in YS or DWTT energy were observed that could be associated with thickness effects; however, the average of the DWTT energy values was slightly higher for the WR ("weak") fracture direction specimens (K, H, M, O, and N) in Fig. 53. This indicates that the principal rolling direction (PRD) may be 90° to that indicated in Fig. 53.

#### STRESS-CORROSION-CRACKING TESTS

Stress-corrosion-cracking (SCC) tests were conducted for the aluminum alloys in a manner described in the titanium section

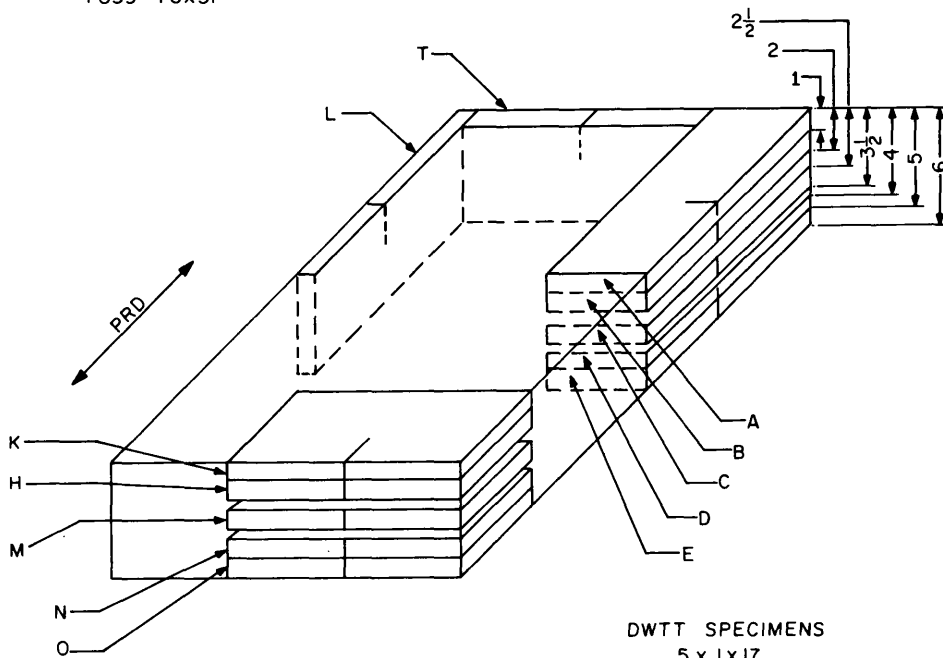
ALUMINUM ALLOY  
7039-T6X31



TENSILE SPECIMENS  
.505 DIA.

(a)

ALUMINUM ALLOY  
7039-T6X31



DWTT SPECIMENS  
5 x 1 x 17

(b)

Fig. 53 - Schematic illustration of tensile and drop-weight tear test specimen layout for six-inch-thick aluminum alloy 7039-T6X31

**Table 13**  
**Mechanical Properties of Aluminum Alloy**  
**7039-T6X31 in 6-inch Plate Section**

DWTT		Tensile Properties				
Spec. No.	DWTT Energy (ft-lb)	Spec. No.	YS (ksi)	UTS (ksi)	RA %	Elong. %
A	612	LS1	51.6	61.0	48.3	17.5
B	543	LS2	52.2	61.2	46.8	18.0
C	514	LA1	49.8	60.7	44.7	17
D	514	LA2	51.1	60.5	46.3	17
E	681	LB1	51.5	62.5	41.3	15
K	870	LB2	50.8	62.5	39.3	15
H	811	LC1	52.2	63.7	38.3	14
M	931	LC2	53.5	64.2	37.8	13.5
N	573	TS1	54.7	64.2	40.8	14.5
O	931	TS2	51.0	64.2	38.8	14.5
L		TA1	52.9	—	—	—
T	612	TA2	52.6	62.9	38.3	15
		TB1	50.2	60.7	35.8	15
		TB2	50.2	60.2	37.1	14
		TC1	52.6	62.2	37.3	14.5
		TC2	52.6	62.2	33.8	14.5

of this report. It is not known whether the laboratory test method, which uses a "stagnant" 3.5 percent salt water environment, is applicable to testing aluminum alloys. Thus, this study was of an exploratory nature.

Specimens of alloys 2219-T87, 7079-T6, 7075-T7351, and 7106-T63 were tested in the WR fracture orientation. These alloys were not expected to be particularly sensitive to SCC in this orientation; the greatest SCC sensitivity for aluminum alloys generally occurs on the planes parallel to the plane of rolling, i.e., the TR or TW fracture orientation. As was expected, the alloys showed no SCC tendency; however, alloys 7079-T6 and 7106-T63 did show a tendency to fracture along planes parallel to the rolling plane. This effect was particularly noticeable in the 7079-T6 specimens, where even the "dry" specimen broke on a 45° plane outside the side grooves (Fig. 54). The specimen step-loaded to the breaking point in salt water fractured for a considerable distance along an axial plane (Fig. 55). A specimen tested in salt water near the breaking point developed long cracks along an axial plane (Fig. 56), but did not fracture from this crack. The specimen was eventually broken with a large overload to reveal the fracture surfaces, and fracturing was primarily along the path of the side grooves. The tendency to fracture along axial planes was much less pronounced in alloy 7106-T63 (Fig. 57) but was present in a long-term specimen. The axial cracking in these two alloys tested in the WT fracture direction resulted in data of very questionable validity.

The 2219-T87 and 7075-T7351 alloys did not experience axial cracks in the test and also did not show any evidence of SCC when loaded slightly below the  $K_{IX}$  values of 50 and 61 ksi  $\sqrt{\text{in.}}$ , respectively, and held for over twenty days. Tests in the TR and TW fracture orientations are planned for all of these alloys in the future.

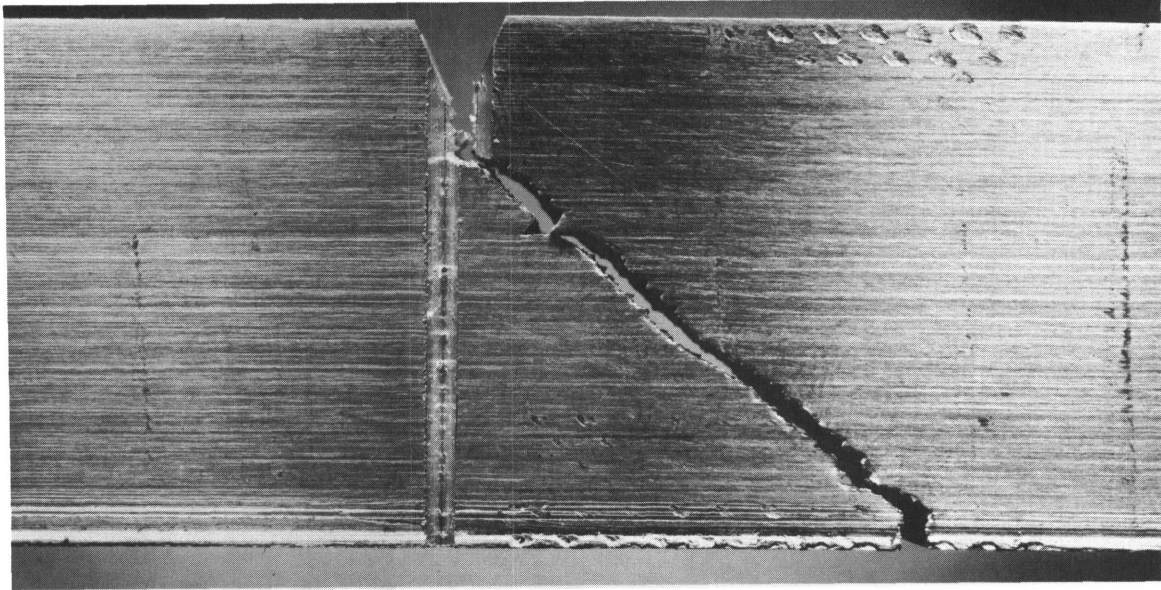


Fig. 54 - Stress-corrosion-cracking specimen of aluminum alloy 7079-T6 broken in "dry" environment at  $44 \text{ ksi}\sqrt{\text{in.}}$ . Note  $45^\circ$  plane of fracture despite side grooves.

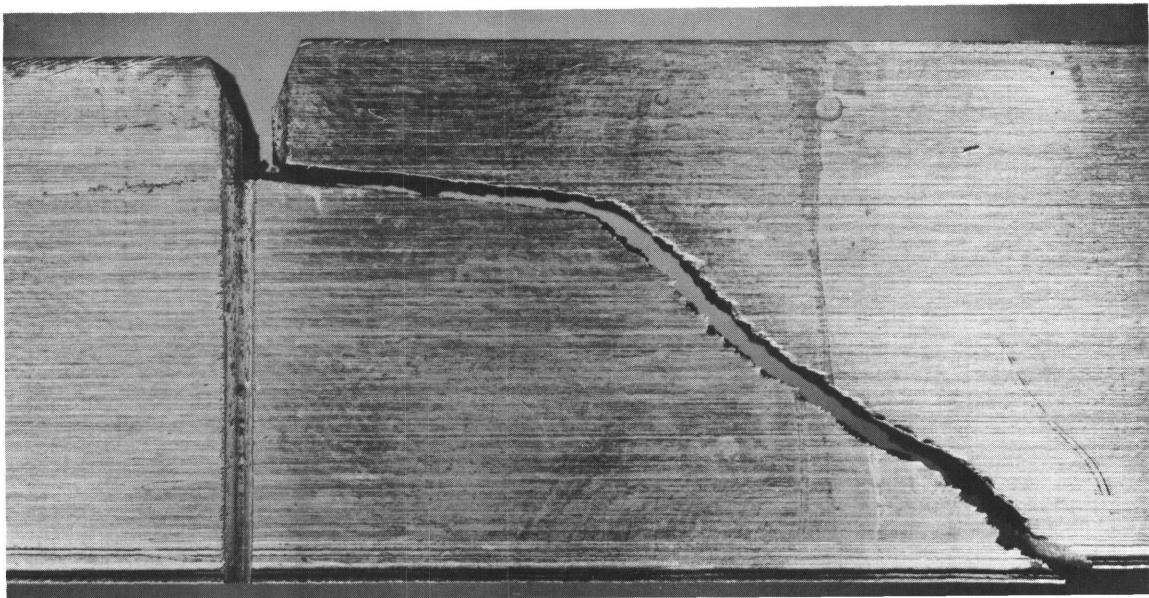


Fig. 55 - Stress-corrosion-cracking specimen of aluminum alloy 7079-T6 step-loaded in salt water to  $43.6 \text{ ksi}\sqrt{\text{in.}}$  before breaking. Note fracture path.

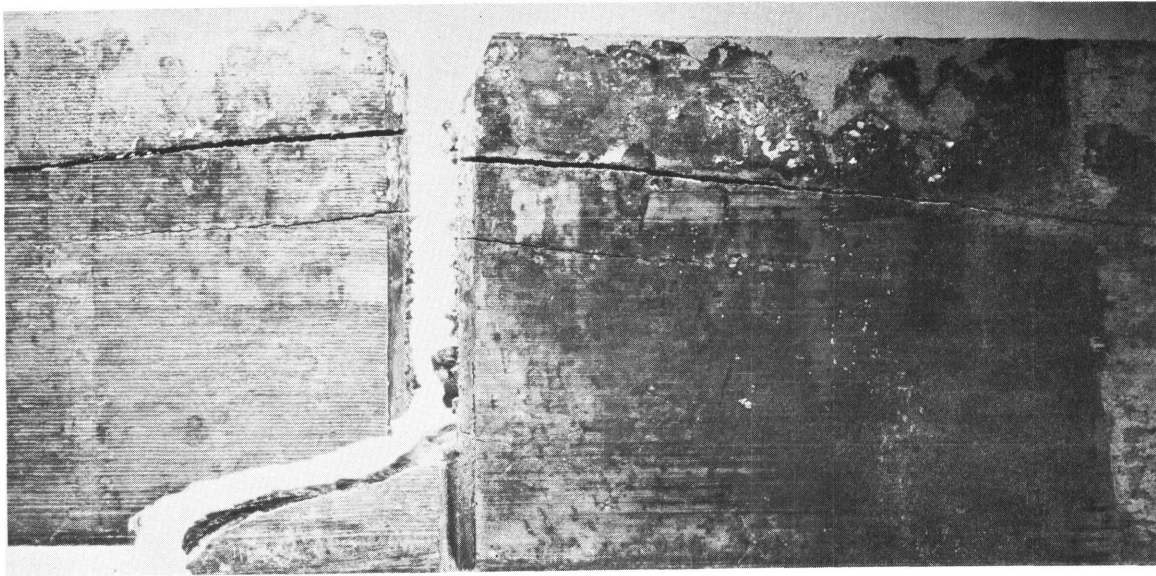


Fig. 56 - Stress-corrosion-cracking specimen of aluminum alloy 7079-T6 loaded near breaking point (not step-loaded) for several days. Note long cracks developed along axial plane.

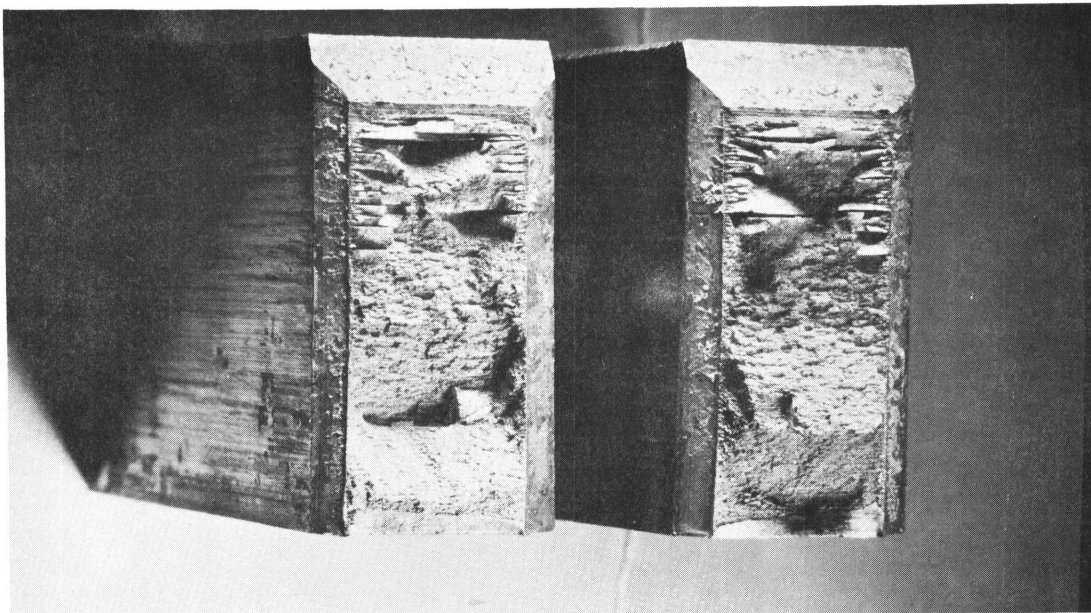


Fig. 57 - Stress-corrosion-cracking specimen of aluminum alloy 7106-T63 loaded near breaking point (not step-loaded) for several days. Note cracks and steps on fracture surface.

COMPARISON OF LOW CYCLE FATIGUE TEST RESULTS--  
INITIATION VERSUS PROPAGATION FAILURE CRITERIA

(T.W. Crooker and E.A. Lange)

The ultimate objective of the NRL low cycle fatigue crack propagation program is to establish fail-safe structural criteria for fatigue life. As a first step in this direction, fatigue crack growth rate data for high fracture toughness materials have been given an arbitrary relation to structural life in terms of the Index of Structural Fatigue Life (ISFL)(6).

INDEX OF STRUCTURAL FATIGUE LIFE

The ISFL is defined as the number of cycles of repeated load required to propagate a small subcritical flaw to 1-in. length at a given intensity of loading, as measured by the total (elastic plus plastic) strain range in the NRL plate bend fatigue test. Examples of the ISFL can be seen in Fig. 58 for 5Ni-Cr-Mo-V steel (9) or in Fig. 45 for 12%Ni maraging steel. In effect, the ISFL states that the structural fatigue life for these steels in an air environment is inversely proportional to the fourth power of total strain range for structural lives between approximately 1,000 and 100,000 cycles of repeated load.

The ISFL definition of fatigue failure is in contrast to other test procedures which either employ the initiation of a small fatigue crack of arbitrary size as the failure criterion, or inseparably combine crack initiation plus crack propagation to terminal fracture of the test specimen as the failure criterion. Gross has used the former method to investigate the fatigue crack initiation life of structural metals (17). His procedure defines initiation life as the number of cycles to produce a 3/16-in. fatigue crack, and is the basis for the initiation data cited in this report.

However, as a matter of philosophy of approach to the problem, the authors feel that the crack propagation phase of fatigue failure is a more suitable criterion for large, complex welded structures. Experience has shown that flaw-free fabrication and inspection of large welded structures cannot be ensured, consequently structural fatigue life will be dependent upon subcritical flaw growth. Well-known examples which substantiate this approach are to be found in the experiences of the

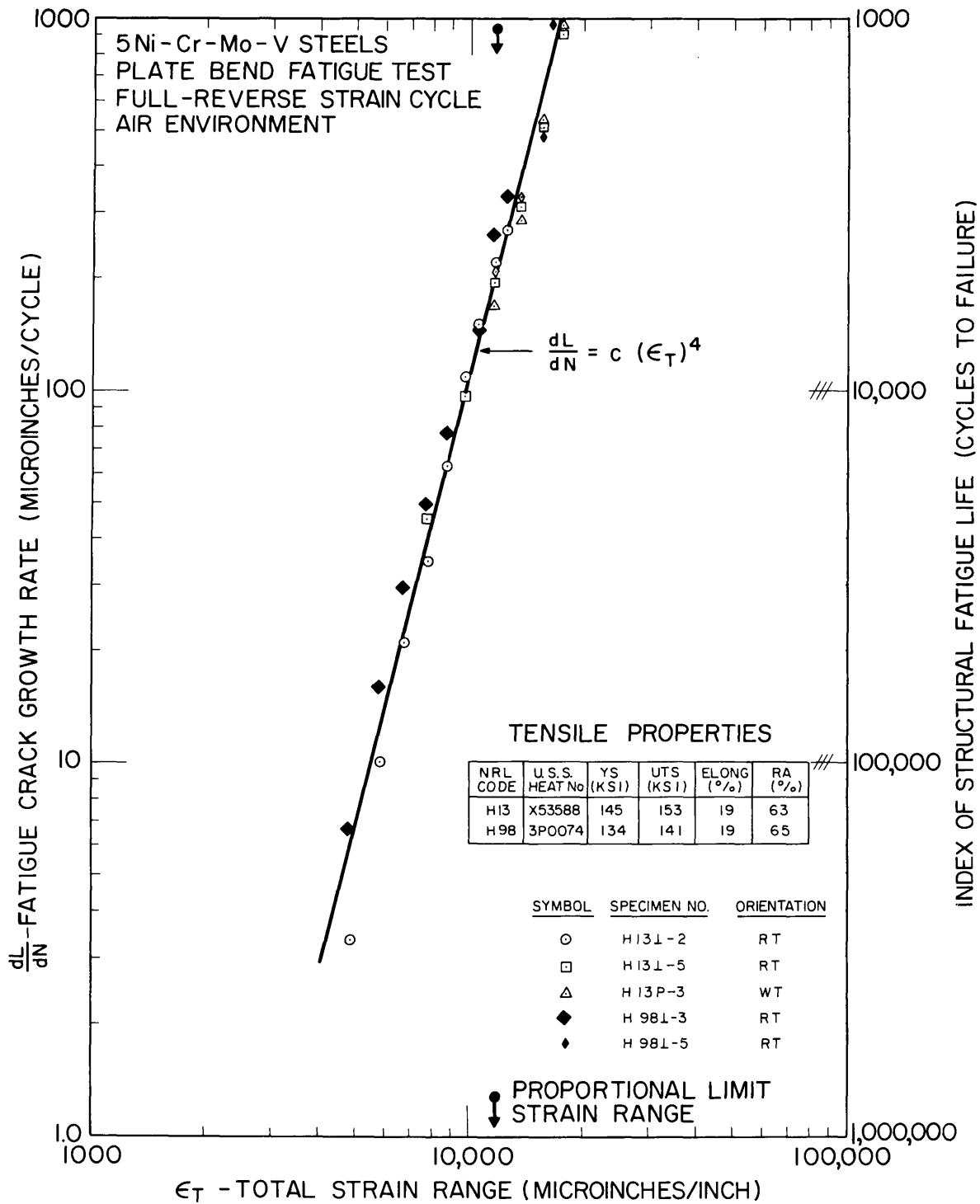


Fig. 58 - Log-log plot of fatigue crack growth rate versus total strain range showing the Index of Structural Fatigue Life for 5Ni-Cr-Mo-V steels at two yield strength levels

Pressure Vessel Research Committee's full-size pressure vessel tests (18) and the hydrotest failure of a 260-in.-diameter rocket motor case (19). It is important to point out that failures from undetected flaws occur in low strength as well as high strength materials, and even in cases where extreme efforts are made to achieve a very high quality of fabrication and inspection.

Catastrophic failures from the frequent occurrence of undetected fabrication flaws have stressed the requirement for a quantitative knowledge of subcritical flaw growth from low cycle fatigue. In order to ensure fail-safe design, a minimum criteria for fatigue strength must include a crack propagation factor at least equivalent to a crack initiation factor. Thus, a back-up is provided with sufficient fatigue crack propagation resistance to prevent failure from the growth of hidden flaws during the service life based upon the cyclic life required to initiate detectable surface fatigue cracks, as predicted by crack initiation test data.

## DISCUSSION

This report discusses plate bend fatigue test data for three steels: HY-80, 5Ni-Cr-Mo-V, and 12%-Ni maraging. The fatigue crack propagation data cited were taken from NRL studies conducted by the authors, which are reported in this and previous Quarterly Reports (9,10,13). The fatigue crack initiation data are taken from recent studies conducted at the U.S. Steel Applied Research Laboratory, using the same specimen configurations and cantilever loading system (20).

Log-log plots of total strain range versus the number of cycles to failure for the three steels are shown in Figs. 59, 60, and 61. Each figure contains four curves for a specific steel representing the two failure criteria--initiation and propagation--both in air and 3.5 percent salt-water environments.

The curves are composed of test results from several samples of each alloy. Other variables include differences in the orientation of test specimens with respect to rolling direction, degree of cross-rolling, yield strength (YS) level, chemical purity, and melting practice. However, experience indicates that variations in metal processing of alloys with a low level of nonmetallics do not significantly affect the conclusions

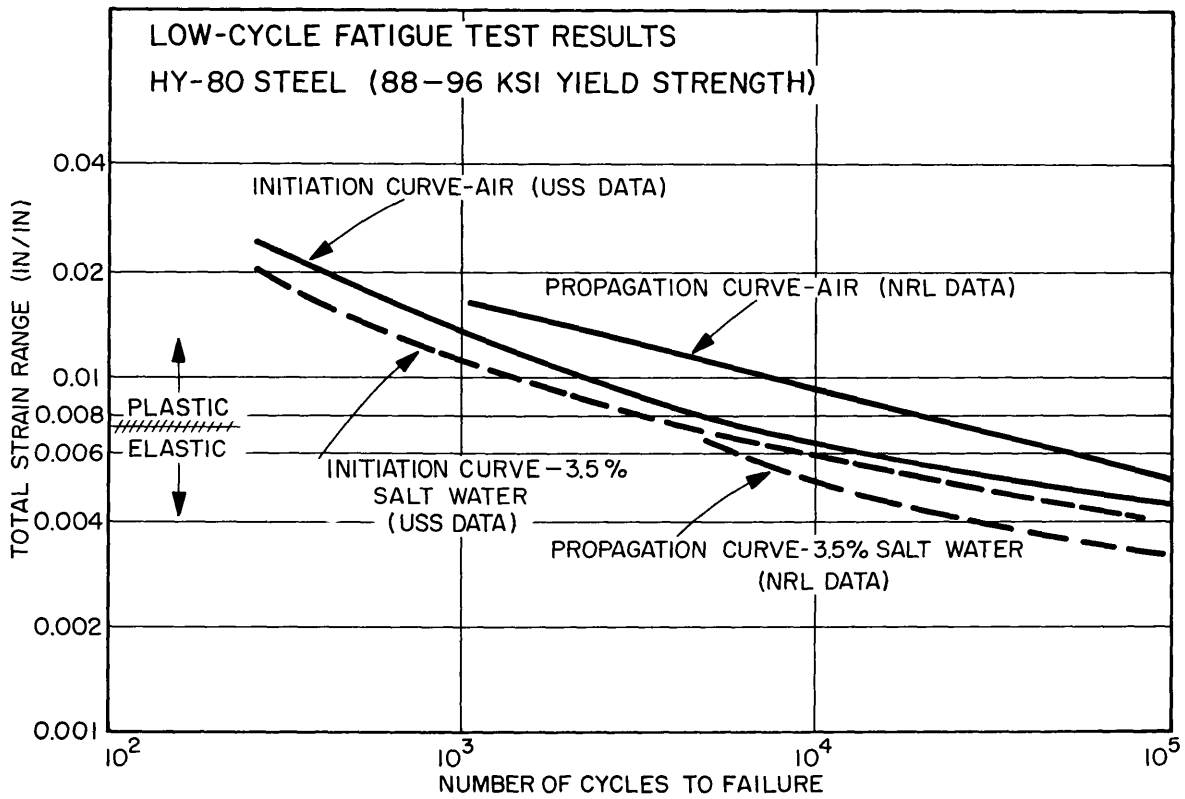


Fig. 59 - Log-log plot of total strain range versus cycles to failure for HY-80 steels. The curves indicate failure by initiation and failure by propagation (ISFL) in both air and 3.5 percent salt water environments.

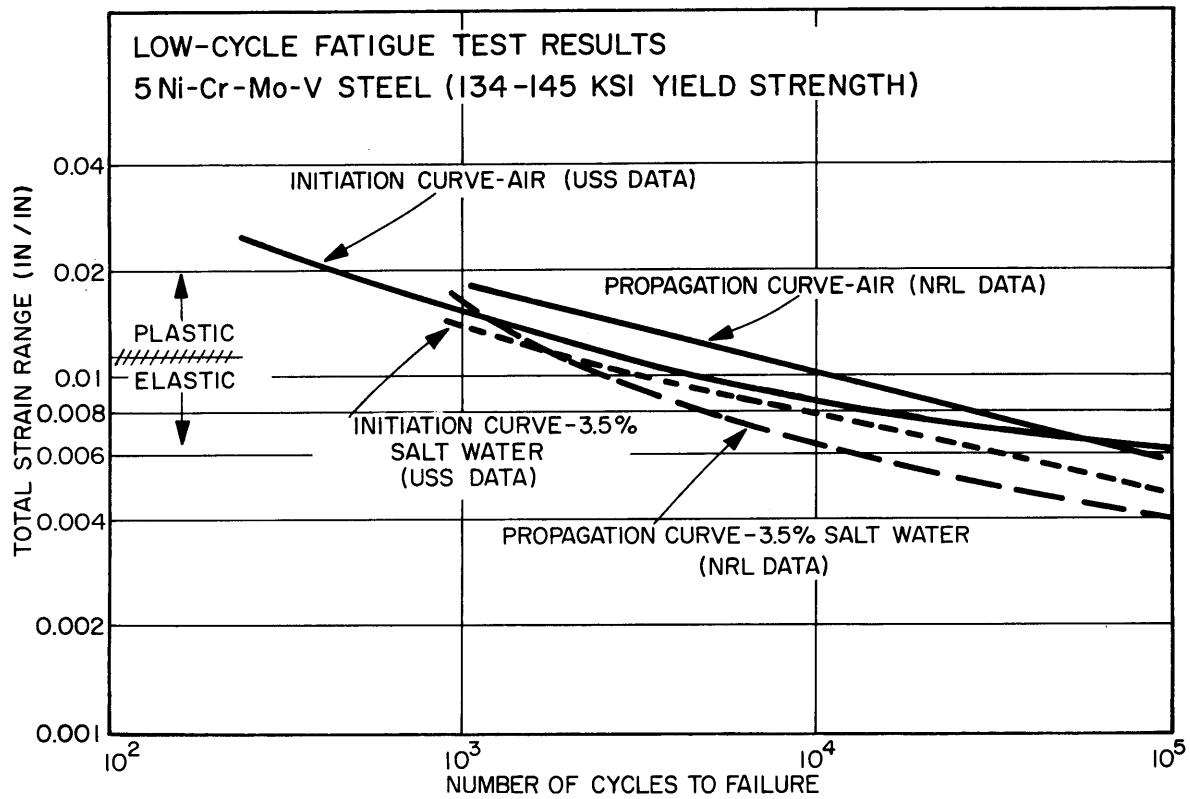


Fig. 60 - Log-log plot of total strain range versus cycles to failure for 5Ni-Cr-Mo-V steels. The curves indicate failure by initiation and failure by propagation (ISFL) in both air and 3.5 percent salt water environments.

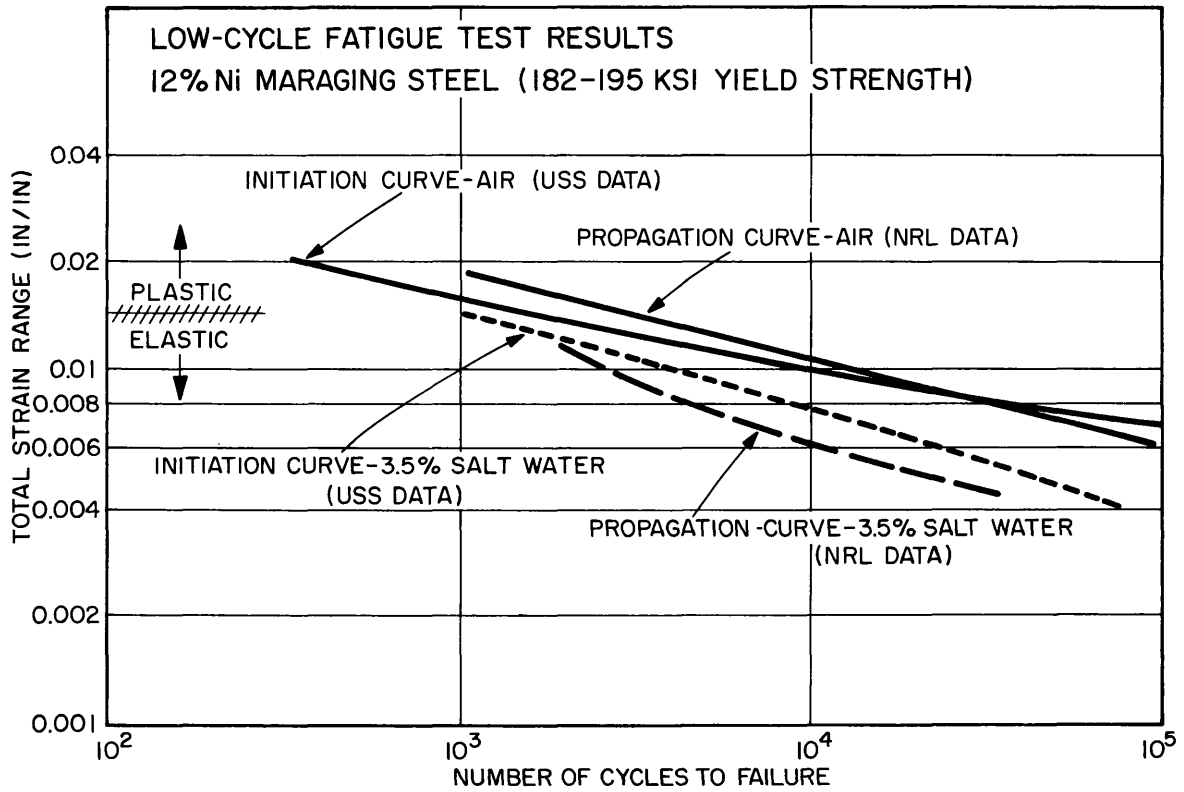


Fig. 61 - Log-log plot of total strain range versus cycles to failure for 12% Ni maraging steels. The curves indicate failure by initiation and failure by propagation (ISFL) in both a ir and 3.5 percent salt water environments.

drawn in this report. The authors have conducted low cycle fatigue crack propagation studies on specially melted and cross-rolled HY-80 steels, quenched-and-tempered heat-treated to several YS levels (10). These processing variables were not found to exert an appreciable influence on the fatigue performance of HY-80, as measured on a strain range basis. Similar processing variables have been introduced in other materials, including 5Ni-Cr-Mo-V steel (9) and 12% Ni maraging steel (see p.64), without altering this conclusion.

The life values for the crack initiation and the crack propagation failure criteria are significantly but not radically different, as indicated by the closely grouped curves in Figs. 59, 60, and 61. This is not surprising, since the initiation and growth of small fatigue cracks have been quite commonly observed during crack propagation tests. Such occurrences in 5Ni-Cr-Mo-V steel are described in Ref. 9.

The failure curves for the two criteria in air are close. Where differences do appear, the initiation criterion curve is generally a more conservative estimate of fatigue life. But it is important to note that the differences diminish with increasing YS level, indicating that failure from crack propagation becomes more critical in higher strength materials.

In salt water, however, the propagation curve consistently lies below the initiation curve, indicating that failure by fatigue crack propagation is the more critical of the two criteria for hostile environments even though the materials are not highly sensitive. At elastic strain range levels, the two salt water curves consistently differ by at least a factor of two, which is a sufficient margin to be of importance in critical applications.

The salt water propagation curves tend to deflect toward the air curves at higher strain levels above the respective elastic limits. This phenomena should be carefully examined where structural life is involved. These salt water fatigue crack propagation curves were derived from laboratory tests conducted at 5 cycles/minute with no hold period at peak load. The trend of the salt water propagation data towards air values may very well be altered by the introduction of slower rates of cycling and a hold duration at maximum load. In addition,

the effect of mean strain on fatigue crack propagation in salt water is likely to deleteriously alter the data shown. Finally, for materials that are sensitive to stress corrosion cracking, the salt water crack propagation curve can be expected to differ radically from the salt water initiation curve at the critical higher strain range levels. These aspects require and deserve further research.

## CONCLUSIONS

1. For HY-80, 5Ni-Cr-Mo-V, and 12%Ni maraging steels, fatigue life periods for crack initiation versus fatigue life periods for crack propagation in air are significantly but not radically different in the low cycle range of 1,000 to 100,000 cycles. The initiation criterion generally tends to be more conservative, but a back-up of equal life for the crack propagation stage is not always present.
2. In salt water, the two criteria differ significantly and fatigue crack propagation represents the more critical phase in all cases. The fatigue crack propagation lives of these materials in salt water at elastic strain levels is approximately half of the corresponding fatigue crack initiation lives.
3. In conclusion, it should be restated that this entire discussion is limited to high fracture toughness materials which lie beyond the present analytical capabilities of linear elastic fracture mechanics.

## PLANE STRAIN FRACTURE TOUGHNESS OF HIGH AND ULTRAHIGH STRENGTH MATERIALS

(C.N. Freed)

Plane strain fracture toughness,  $K_{Ic}$ , determinations are reported for a variety of low toughness materials which failed under conditions of elastic loading. The fracture mechanics values were determined by using both smooth and side-grooved single-edge-notched (SEN) specimens. A detailed description of specimen dimensions is presented in the Seventh Quarterly Report (8). Also included is a preliminary attempt at a correlation of drop-weight tear test (DWTT) and  $K_{Ic}$  results for titanium alloys which were heat treated to provide a range of toughness values from less than 250 to over 1500 ft-lb as measured by the DWTT.

A tabulation of the mechanical properties of six materials is reported in Table 14. The DWTT energy values for each alloy indicated that fracture would occur without macroscopic plastic deformation, and so fracture mechanics techniques were applied to measure toughness.

#### $K_{Ic}$ RESULTS FOR THREE ALUMINUM ALLOYS

Plane strain fracture toughness data has been determined for 7075-T7351, 2219-T851, and 2024-T4. These materials were tested in the as-received condition. As in all of the  $K_{Ic}$  tests reported, the edge notch was tipped with a fatigue crack; the length of this crack was at least 0.1 in. (except where noted), and the stress during fatiguing was usually less than one-half the yield stress. The detection of the load at which instability occurred was made with a beam displacement gage instrumented with a strain gage circuit (21). The plastic zone correction was not made.

The aluminum alloy 7075-T7351 was tested in both the RW and WR directions using smooth and side-grooved specimens. (A smooth specimen is one which has not been grooved.) The load-deflection curves are presented in Fig. 62. The smooth specimens (curves 1-4) did not break at maximum load; rather, departure from lineality was followed by slow growth. While the arrows indicate the load used to calculate  $K_{Ic}$ , the absence of a pop-in indication detracted from the accuracy of the  $K_{Ic}$  value. The load-deflection curves for the side-grooved specimens of the same material are represented by curves 5-10; the load at fracture was used to compute the plane strain fracture toughness.

Pertinent specimen data for this alloy is compiled in Table 15. The two smooth specimens broken in the RW direction produced estimated  $K_{Ic}$  numbers of 32,000 and 33,000 psi  $\sqrt{\text{in}}$ . Specimens which were side-grooved, so that the net thickness-to-total thickness ratio ( $B_N/B$ ) of the fracture plane was 0.9, had  $K_{Ic}$  values of 30,000 psi  $\sqrt{\text{in}}$ . The two specimens side-grooved to a slightly greater depth ( $B_N/B = 0.8$ ) also indicated an average  $K_{Ic}$  measurement of 30,000 psi  $\sqrt{\text{in}}$ . Curves 9 and 10 are traces of side-grooved specimens ( $B_N/B = 0.9$ ) broken in the WR direction. The  $K_{Ic}$  values from these curves (23,000 psi  $\sqrt{\text{in}}$ .) compare closely with the estimated results from the smooth WR specimens (27,000 psi  $\sqrt{\text{in}}$ .)

Table 14  
Mechanical Properties

Alloy	Fracture Direction	YS (0.2%) (ksi)	Tensile Strength (ksi)	Elong. (%)	RA (%)	Charpy V at 32° F (ft-lb)	Drop-Weight Tear Energy at 32° F (ft-lb)
D63A (18Ni-marage)	RW	229.5	240.3	9.0	45.9	24	<500*
D63B (18Ni-marage)	WR†	234.5	245.7	7.0	29.2	--	<500
7075-T7351	RW	63.9	75.4	--	--	6	339
7075-T7351	WR	65.6	75.5	--	--	4	240
2219-T851	WR	58.4	74.3	--	--	5	339
2024-T4	WR	47.8	71.9	--	--	7	281
T-55 (Ti-6Al-4Zr-2Mo)	WR	135.7	150.6	13.2	11.2	17	1022*
T-68 (Ti-6Al-4Zr-2Sn-0.5Mo-0.5V)	RW	119.2	130.2	9.7	22.4	30	1418*

\*Heat treatment noted in Table 18.

†RW data not available.

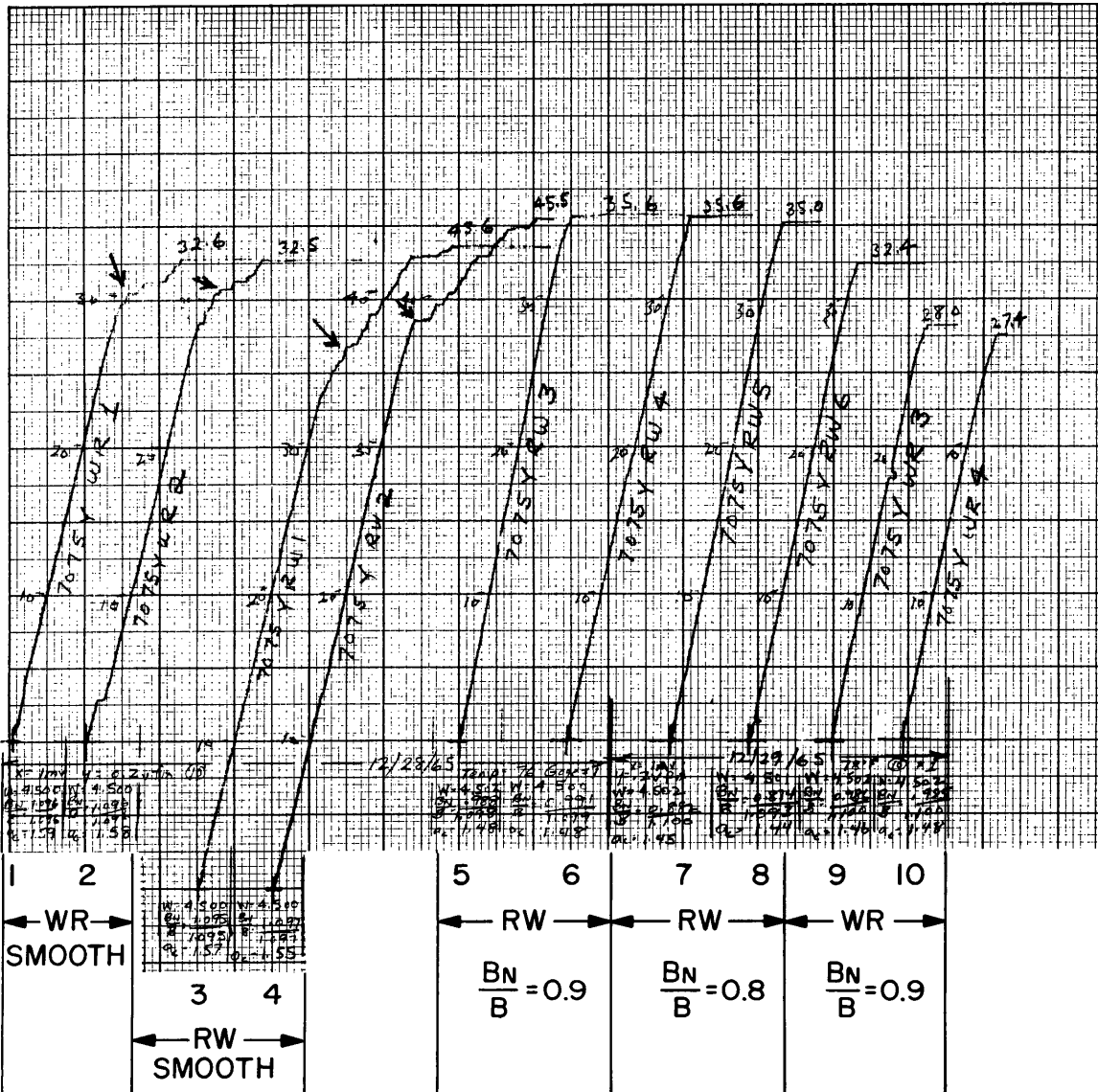


Fig. 62 - Load-displacement records for 7075-T7351 aluminum. Arrows indicate estimated load used to calculate  $K_{Ic}$ ; maximum load was used for Curves 5-10.

Table 15  
Plane-Strain Fracture Toughness Data for Smooth\* and Side-Grooved 7075-T7351 Aluminum

Fracture Direction	Thickness Between Side-Grooves $B_N$ (in.)	Total Thickness $B$ (in.)	$\frac{B_N}{B} \times 100\%$	Width $W$ (in.)	Crack Length $a_c$ (in.)	$\frac{a_c}{W}$	Load At $K_{Ic}$ $P$ (lb)	$K_{Ic}$ (psi/in.)	Nominal Stress To Yield Stress $\sigma_N / \sigma_y$	Percent Shear† (%)	Plastic Zone Size† $r_y$ (in.)
RW	No side-grooves	1.10	—	4.50	1.57	0.349	36,000	32,000	0.49	16	0.04
RW	No side-grooves	1.10	—	4.50	1.55	0.344	39,000	33,000	0.52	15	0.04
RW	0.99	1.10	90	4.50	1.48	0.329	35,600	30,000	0.47	—	0.04
RW	0.99	1.10	90	4.50	1.48	0.329	35,600	30,000	0.47	—	0.04
RW	0.88	1.10	80	4.50	1.45	0.322	35,000	31,000	0.52	—	0.04
RW	0.87	1.09	80	4.50	1.44	0.320	32,400	29,000	0.45	—	0.03
WR	No side-grooves	1.10	—	4.50	1.59	0.353	30,000	27,000	0.37	8	0.03
WR	No side-grooves	1.10	—	4.50	1.58	0.351	30,000	27,000	0.37	13	0.03
WR	0.99	1.10	90	4.50	1.46	0.324	28,000	23,000	0.36	—	0.02
WR	0.99	1.10	90	4.50	1.48	0.329	27,400	23,000	0.35	—	0.02

\*"Smooth" refers to a SEN specimen which is not side-grooved.

†Shear lips did not form on side-grooved specimens.

$$\dagger r_y = \left( \frac{K_{Ic}}{\sigma_{ys}} \right)^2 \frac{1}{2.77}$$

The aluminum alloy 2219-T851 was tested in the WR fracture direction with both smooth and side-grooved specimens, and the results are presented in Table 16. As the smooth curves indicated almost no slow growth prior to fracture, the maximum load was used to determine  $K_{Ic}$ . Three smooth specimens resulted in a  $K_{Ic}$  value of 37,000-38,000 psi  $\sqrt{\text{in}}$ . Three specimens with shallow side grooves ( $B_N/B = 0.9$ ) produced  $K_{Ic}$  numbers of 34,000 psi  $\sqrt{\text{in}}$ , while two specimens with slightly deeper grooves ( $B_N/B = 0.8$ ) recorded  $K_{Ic}$  data of 32,000 and 33,000 psi  $\sqrt{\text{in}}$ .

There is evidence to indicate that the side-groove depth should be kept shallow so that the  $K_{Ic}$  numbers obtained from these specimens will not be significantly different from smooth specimen values (1). In the 7075-T7351 aluminum alloy, both the 0.9 and 0.8 side-grooved ratios resulted in similar  $K_{Ic}$  numbers. Comparison of these values to those obtained from the smooth specimens is difficult since the latter were only estimated values. However, for 2219-T851 the smooth specimens produced valid  $K_{Ic}$  data, and these data were only slightly higher than those obtained from the grooved specimens. The shallow-grooved specimens ( $B_N/B = 0.9$ ) indicated  $K_{Ic}$  values which more closely approached those obtained with smooth specimens than did the specimens grooved to  $B_N/B = 0.8$ .

Plane strain fracture toughness values from 2024-T4 are also included in Table 16. Smooth specimen  $K_{Ic}$  data could not be obtained because of the excessive slow growth which occurred after the curve deviated from lineality. It is of interest to note that in spite of the slow growth indications the fracture surface was flat. As the nominal-to-yield stress ratio did not exceed 0.9, the specimen did not yield, but rather slow growth took place in the absence of shear lips. The side-grooved specimens broke at maximum load without indications of slow growth. This demonstrates the added constraint which is produced by the side grooves.

#### $K_{Ic}$ DATA FOR AN 18% Ni MARAGING STEEL

The  $K_{Ic}$  plane strain fracture toughness was determined for a 18Ni-7Co-0.05Mo maraging steel for two different heat treatments. All of the specimens were side-grooved so  $B_N/B = 0.7$ . (The specimens were machined before the advantage of shallow

Table 16  
Plane Strain Fracture Toughness Data For Smooth\* and Side-Grooved 2219-T851 and 2024-T4 Aluminum

Alloy	Fracture Direction	Thickness Between Side-Grooves $B_N$ (in.)	Total Thickness $B$ (in.)	$\frac{B_N}{B} \times 100\%$	Width $W$ (in.)	Crack Length $a_c$ (in.)	$\frac{a_c}{W}$	Load at $K_{Ic}$ $P$ (lbs)	$K_{Ic}$ (psi $\sqrt{in.}$ )	Nominal Stress to Yield Stress $\sigma_N/\sigma_y$	Percent Shear (%)	Plastic Zone Size $r_y$ (in.)
2219-T851	WR	No side-grooves	0.97	—	5.00	1.70	0.340	40,600	37,000	0.57	45	0.06
2219-T851	WR	No side-grooves	0.97	—	5.00	1.70	0.340	41,000	37,000	0.57	44	0.06
2219-T851	WR	No side-grooves	0.97	—	5.00	1.69	0.338	41,900	38,000	0.58	37	0.07
2219-T851	WR	0.87	0.97	90	5.00	1.65	0.330	37,000	34,000	0.57	—	0.05
2219-T851	WR	0.87	0.97	90	5.00	1.67	0.334	36,000	34,000	0.55	—	0.05
2219-T851	WR	0.88	0.97	91	5.00	1.64	0.328	36,700	34,000	0.51	—	0.05
2219-T851	WR	0.78	0.97	80	5.00	1.59	0.318	35,000	32,000	0.54	—	0.05
2219-T851	WR	0.77	0.97	79	5.00	1.63	0.326	34,200	33,000	0.53	—	0.05
2024-T4	WR	0.92	1.02	90	5.00	1.64	0.328	35,000	31,000	0.56	—	0.07
2024-T4	WR	0.92	1.02	90	5.00	1.64	0.328	35,200	31,000	0.56	—	0.07
2024-T4	WR	0.92	1.02	90	5.00	1.65	0.330	34,700	30,000	0.63	—	0.06
2024-T4	WR	0.92	1.02	90	5.00	1.65	0.330	34,500	30,000	0.62	—	0.06
2024-T4	WR	0.82	1.02	80	5.00	1.51	0.302	39,500	33,000	0.67	—	0.08
2024-T4	WR	0.82	1.02	80	5.00	1.55	0.310	37,000	32,000	0.67	—	0.07
2024-T4	WR	0.82	1.02	80	5.00	1.51	0.302	42,000	35,000	0.71	—	0.09

\*"Smooth" refers to a SEN specimen which is not side-grooved.

†Shear lips did not form on side-grooved specimens.

side grooves was ascertained.) As Table 17 shows, an additional variable was introduced in these specimens; the length of the fatigue crack was varied from an extremely short crack (0.01 in.) to a crack of recommended length (0.10 in.). The indications are that the short fatigue cracks resulted in higher  $K_{Ic}$  values (78-81 ksi  $\sqrt{\text{in.}}$ ) than did the longer cracks (74-78 ksi  $\sqrt{\text{in.}}$ ) for the RW fracture direction. Referring again to the 2024-T4 data of Table 16, the fatigue crack length of specimens side-grooved to 80% ( $B_N/B \times 100\%$ ) are 0.01-0.05 in., while the specimens grooved to 90% are 0.11-0.13 in. The specimens with the short fatigue cracks produced higher  $K_{Ic}$  values than specimens with longer cracks. These results are consistent with the findings of other experimenters which emphasize the importance of a minimum fatigue crack length of 0.10 in.

#### $K_{Ic}$ DATA FOR TWO TITANIUM ALLOYS

Two titanium alloys--Ti-6Al-4Zr-2Sn-0.5Mo-0.5V (T-68) and Ti-6Al-4Zr-2Mo (T-55)--were given the same heat treatment and both smooth and side-grooved specimens were tested (Table 18). It is thought that the results are valid although the exact yield strengths have not yet been determined. The spread in  $K_{Ic}$  values for T-55 is considerably greater between smooth and side-grooved specimens than that observed for the aluminum alloys. The spread in the data for T-68 appears about the same for each type of specimen; the cause of this spread in values is not known at this time, but may be the result of inhomogeneity of the material or slight variations in heat treatment.

#### CORRELATION OF $K_{Ic}$ WITH DWTT

The DWTT measures the resistance of a material to propagation of a moving crack. Although the energy measured in this test also includes that energy needed to initiate the crack in the brittle weld, initiation energy is thought to generally represent a small fraction of the total fracture energy in tough materials such that it may be ignored. Brittle metals, however, have a low crack propagation energy, and the crack initiation energy of the brittle weld can be a significant portion of the total energy for fracture; in fact, in some cases it represents practically all of the total energy. Since these two components of the total energy are not separately measured in the DWTT, the test loses its effectiveness in the evaluation of highly

Table 17  
Plane Strain Fracture Toughness Data For a 18%-Ni Maraging Steel

CODE*	Fracture Direction	Thickness Between Side-Grooves $B_N$ (in.)	Total Thickness B (in.)	$\frac{B_N}{B} \times 100$ (%)	Width W (in.)	Load At $K_{Ic}$ P (lb)	Total Crack Length $a_c$ (in.)	Fatigue Crack Length (in.)	$K_{Ic}$ (psi $\sqrt{in.}$ )	Nominal Stress To Yield Stress $\frac{\sigma_N}{\sigma_y}$	Plastic Zone Size† $r_y$ (in.)
D63 A1A	RW	0.73	1.04	70	4.50	84,200	1.41	0.01	81,000	0.38	0.02
D63 A1D	RW	0.73	1.04	70	4.50	81,200	1.40	0.01	78,000	0.37	0.02
D63 A1C	RW	0.72	1.03	70	4.50	66,500	1.48	0.08	69,000	0.34	0.01
D63 B1E	RW	0.73	1.04	70	4.50	82,900	1.43	0.03	81,000	0.37	0.02
D63 B1D	RW	0.73	1.04	70	4.51	81,500	1.50	0.05	85,000	0.40	0.02
D63 B1C	RW	0.72	1.03	70	4.50	75,900	1.48	0.08	78,000	0.38	0.02
D63 B1B	RW	0.72	1.03	70	4.50	69,500	1.50	0.10	74,000	0.35	0.02

\*Heat Treatment:

D63 A - Mill anneal at 1500°F; aged at 900°F/3 hours/air cooled.

D63 B - Mill anneal at 1750°F; aged at 900°F/3 hours/air cooled.

$$\dagger r_y = \left( \frac{K_{Ic}}{\sigma_{ys}} \right)^2 \frac{1}{2\pi}$$

Table 18  
 Plane Strain Fracture Toughness Data For Smooth\* and Side-Grooved  
 Ti-6Al-4Zr-2Mo (T-55) and Ti-6Al-4Zr-2Sn-0.5Mo-0.5V (T-68) Titanium

Alloy	Fracture Direction	Thickness Between Side Grooves $B_N$ (in.)	Total Thickness $B$ (in.)	$\frac{B_N}{B} \times 100$ (%)	Width $W$ (in.)	Crack Length $a_c$ (in.)	$\frac{a_c}{W}$	Load at $K_{Ic}$ $p$ (lbs)	$K_{Ic}$ (psi $\sqrt{in.}$ )	Heat treatment
T-55	WR	No side grooves	1.11	--	5.00	1.67	0.334	155,500	121,000	1750° F/1 hr/WQ
T-55	WR	No side grooves	1.08	--	5.01	1.66	0.332	151,000	119,000	then 1100° F/2 hr/AC
T-55	WR	0.98	1.09	90	5.00	1.69	0.338	115,000	98,000	(same for all 3 specimens)
T-68	RW	No side grooves	1.00	--	5.04	1.66	0.332	123,000	104,000	1750° F/1 hr/WQ
T-68	RW	No side grooves	1.03	--	5.00	1.62	0.324	145,100	116,000	then 1100° F/2 hr/AC
T-68	RW	0.90	1.01	89	5.00	1.63	0.326	129,400	113,000	(same for all 4 specimens)
T-68	RW	0.86	0.95	91	4.99	1.60	0.321	116,000	106,000	

\*"Smooth" refers to a SEN specimen which is not side-grooved.

brittle materials for failure-safe use in structures where flaw size and stress intensity become important parameters in characterizing fracture toughness.

Plane strain fracture mechanics,  $K_{Ic}$ , allows measurement of the energy required to initiate a crack in a material from a sharp notch or a fatigue crack. This procedure is well-suited to measure the toughness in brittle materials, and the critical flaw size at a given stress level can be calculated from the  $K_{Ic}$  value. However, as the toughness of a material is increased, a point is reached at which plane strain conditions can no longer be obtained for a given specimen size and the DWTT becomes a more meaningful measure of toughness.

In the DWTT (described in Ref. 6), a brittle weld was produced by using an electron beam to diffuse iron from an iron wire through the thickness of the titanium specimen. The specimen was broken in the 5,000 ft-lb impact machine and the total energy for fracture was measured. The material tested measured 5x5x1 in. (length x width x thickness); tabs were welded to the length direction in order to provide the required 17-in. beam length for the DWTT specimen. The brittle weld measured 1.5 in. along the width dimension, leaving 3.5 in.<sup>2</sup> of material to be tested.

The fracture mechanics values were determined by single-edge-notched specimens of 1-in. thickness. A fatigue crack of approximately 0.1 in. length tipped each edge notch. When side-grooved specimens were used, the groove depth was shallow ( $B_N/B = 0.9$ ). In this preliminary correlation, a correction for the plastic zone has not been made.

It is evident in Fig. 63 that as the DWTT energy increases there is a corresponding rise in  $K_{Ic}$  values. Inaccuracies are likely to occur at low DWTT energies for reasons previously discussed. Data scatter at the 70-80 ksi  $\sqrt{\text{in.}}$  level requires that several points be rechecked. Future work on titanium alloys will attempt to define the correlation limits in the direction of both lower and higher toughness for 1-in. thick material.

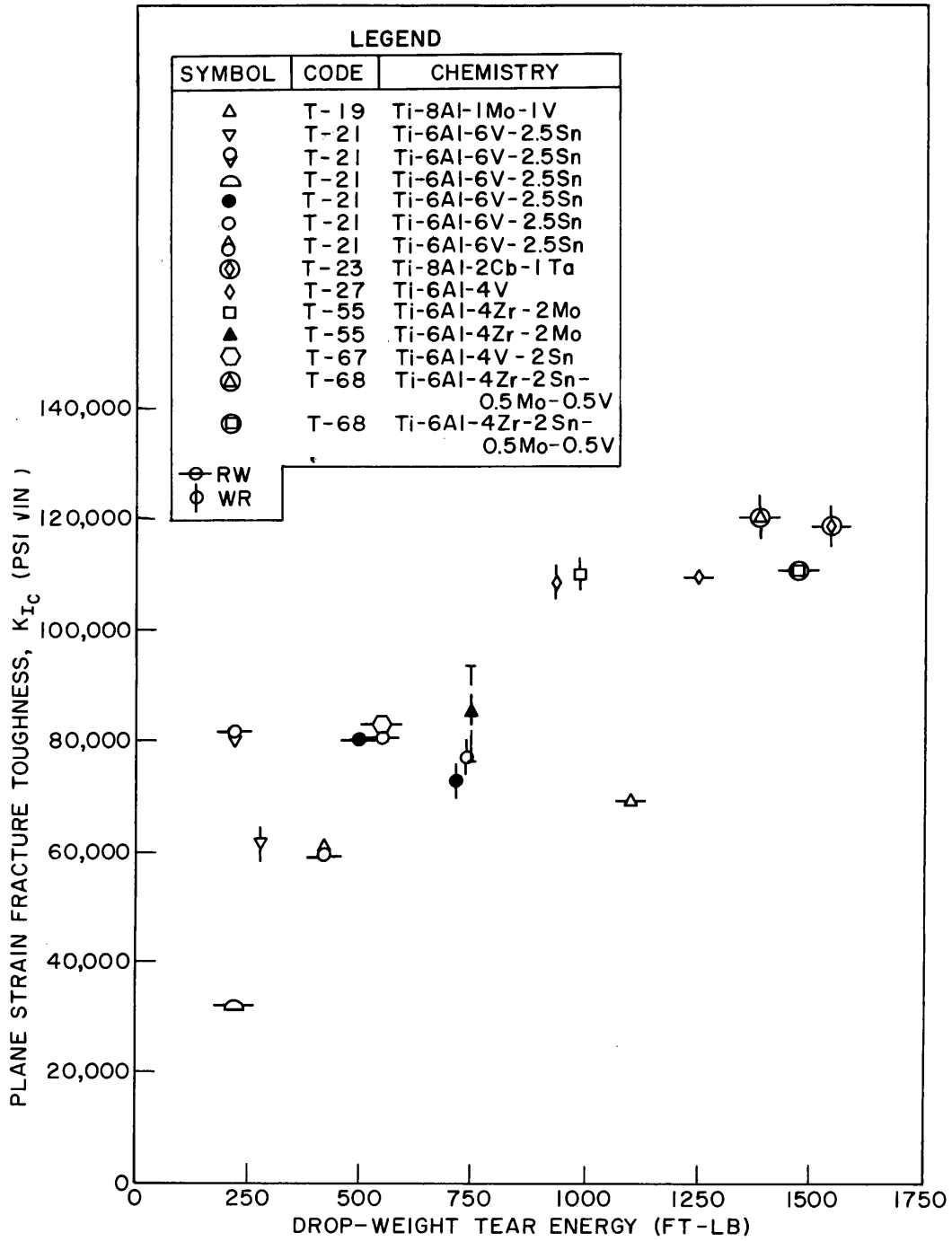


Fig. 63 - Spectrum of plane-strain fracture toughness ( $K_{Ic}$ ) data as a function of drop-weight tear energy for a variety of titanium alloys

## REFERENCES

1. Goode, R.J., et al., "Metallurgical Characteristics of High Strength Structural Materials (Ninth Quarterly Report)," NRL Report 6405, November 1965
2. Brown, B.F., "A New Stress-Corrosion Cracking Test Procedure for High-Strength Alloys," Materials Research and Standards, Vol. 66, No. 3, March 1966
3. Brown, B.F., et al., "Marine Corrosion Studies (Third Interim Report of Progress)," NRL Memorandum Report 1634, July 1965
4. ASTM Materials Research & Standards, Vol. 1, No. 5, May 1961
5. Brown, B.F., and Beachem, C.D., "A Study of the Stress Factor in Corrosion Cracking by Use of the Pre-Cracked Cantilever Beam Specimen," Corrosion Science, Vol. 5, No. 11, November 1965, pp. 745-750
6. Pellini, W.S., Goode, R.J., Puzak, P.P., Lange, E.A., and Huber, R.W., "Review of Concepts and Status of Procedures for Fracture-Safe Design of Complex Welded Structures Involving Metals of Low to Ultra-High Strength Levels," NRL Report 6300, June 1965
7. Pellini, W.S., et al., "Metallurgical Characteristics of High Strength Structural Materials (Sixth Quarterly Report)," NRL Report 6258, December 1964
8. Goode, R.J., et al., "Metallurgical Characteristics of High Strength Structural Materials (Seventh Quarterly Report)," NRL Report 6327, May 1965
9. Puzak, P.P., et al., "Metallurgical Characteristics of High Strength Structural Materials (Eighth Quarterly Report)," NRL Report 6364, August 1965
10. Puzak, P.P., et al., "Metallurgical Characteristics of High Strength Structural Materials (Third Quarterly Report)," NRL Report 6086, January 1964

11. Goode, R.J., et al., "Metallurgical Characteristics of High Strength Structural Materials (Fourth Quarterly Report)," NRL Report 6137, June 1964
12. Pellini, W.S., and Puzak, P.P., "Factors that Determine the Applicability of High Strength Quenched and Tempered Steels to Submarine Hull Construction," NRL Report 5892, December 5, 1962
13. Crooker, T.W., et al., "Metallurgical Characteristics of High Strength Structural Materials (Fifth Quarterly Report)," NRL Report 6196, September 1964
14. Crooker, T.W., Morey, R.E., and Lange, E.A., "Low Cycle Fatigue Crack Propagation," Report of NRL Progress, June 1964, pp. 30-33
15. Crooker, T.W., Morey, R.E., and Lange, E.A., "Low Cycle Fatigue Crack Propagation," Report of NRL Progress, June 1965, pp. 37-40
16. Crooker, T.W., Morey, R.E., and Lange, E.A., "Low Cycle Fatigue Crack Propagation Characteristics of Monel 400 and Monel K-500 Alloys," NRL Report 6218, March 10, 1965
17. Gross, M.R., "Low-Cycle Fatigue of Materials for Submarine Construction," Naval Engineers Journal, Vol. 75, No. 4, October 1963
18. Kooistra, L.F., Lange, E.A., and Pickett, A.G., "Full-Size, Pressure-Vessel Testing and Its Application to Design," TRANS of the ASME Journal of Engineering for Power, Vol. 86, Series A, No. 4, October 1964
19. Srawley, J.E., and Esgar, J.B., "Investigation of Hydrotest Failure of Thiokol Chemical Corporation 260-Inch-Diameter SL-1 Motor Case," NASA TM X-1194, January 1966
20. Boblenz, T.L., and Rolfe, S.T., "Corrosion-Fatigue Characteristics of HY-80, 5Ni-Cr-Mo-V, 12Ni-5Cr-3Mo, and 18Ni-8Co-3Mo Steels," Technical Report, U.S. Steel Applied Research Laboratory, 1 January 1966
21. Krafft, J.M., "Fracture Toughness of Metals," Report of NRL Progress, November 1963, pp. 4-16

**This page intentionally left blank.**

UNCLASSIFIED

Security Classification

DOCUMENT CONTROL DATA - R&D		
<i>(Security classification of title, body of abstract and indexing annotation must be entered when the overall report is classified)</i>		
1. ORIGINATING ACTIVITY (Corporate author) Naval Research Laboratory Washington, D.C. 20390		2 a. REPORT SECURITY CLASSIFICATION Unclassified
		2 b. GROUP
3. REPORT TITLE METALLURGICAL CHARACTERISTICS OF HIGH STRENGTH STRUCTURAL MATERIALS (Tenth Quarterly Report)		
4. DESCRIPTIVE NOTES (Type of report and inclusive dates) A progress report on various problems		
5. AUTHOR(S) (Last name, first name, initial) Goode, R.J., Huber, R.W., Judy, R.W., Jr., Howe, D.G., Puzak, P.P., Lloyd, K.B., Crooker, T.W., Morey, R.E., Lange, E.A., and Freed, C.N;		
6. REPORT DATE April 1966	7 a. TOTAL NO. OF PAGES 104	7 b. NO. OF REFS 21
8 a. CONTRACT OR GRANT NO. NRL Problems F01-17, M01-05, M01-18, & M03-01 b. PROJECT NO. SP-01426; SF 020-01-01 0724,0731,0850; SF 020-01-05-0731; RR 007-01-46-5405,5420,5414; and MIPR-ENG-NAV-66-2		9 a. ORIGINATOR'S REPORT NUMBER(S) NRL Report 6454
		9 b. OTHER REPORT NO(S) (Any other numbers that may be assigned this report) None
10. AVAILABILITY/LIMITATION NOTICES Distribution of this document is unlimited		
11. SUPPLEMENTARY NOTES None		12. SPONSORING MILITARY ACTIVITY Dept. of the Navy (Office of Naval Research and Naval Ship Systems Command), Dept. of the Army (Office of Chief of Engineers), and Special Projects Office
13. ABSTRACT  A progress report covering the research studies in high strength structural metals conducted in the period December 1965 through March 1966 is presented. The report includes fracture toughness studies on expected normal production 12%-Ni maraging and 9Ni-4Co-0.25C steels, a variety of circular rolled and conventionally rolled titanium alloys, and aluminum alloys using a standard engineering, <del>ten</del> developed, and linear elastic fracture mechanics type fracture toughness tests. Preliminary correlations of $K_{Ic}$ with drop weight tear test energy for a variety of titanium alloys are presented. Low cycle fatigue crack propagation in 12%-Ni maraging steels in air and salt water is described and compared to the behavior of other steels. Also, crack initiation versus propagation failure criteria for low cycle fatigue in air and in aqueous environments is presented for HY-80 and 5Ni-Cr-Mo-V steels and 12%-Ni maraging steels. The stress-corrosion-cracking resistance of a variety of titanium alloys and several aluminum alloys has been determined using a cantilever-bend test; comparison of results obtained in the laboratory and in natural seawater at Key West are presented for a Ti-7Al-2Cb-1Ta alloy.		

DD FORM 1473  
1 JAN 64

103

Security Classification

Security Classification

14. KEY WORDS	LINK A		LINK B		LINK C	
	ROLE	WT	ROLE	WT	ROLE	WT
Titanium alloys Aluminum alloys High strength steels Fracture toughness Low cycle fatigue Stress-corrosion-cracking Corrosion fatigue Mechanical properties Welding Heat treatment Drop-weight tear test Explosion tear tests						

INSTRUCTIONS

1. **ORIGINATING ACTIVITY:** Enter the name and address of the contractor, subcontractor, grantee, Department of Defense activity or other organization (*corporate author*) issuing the report.

2a. **REPORT SECURITY CLASSIFICATION:** Enter the overall security classification of the report. Indicate whether "Restricted Data" is included. Marking is to be in accordance with appropriate security regulations.

2b. **GROUP:** Automatic downgrading is specified in DoD Directive 5200.10 and Armed Forces Industrial Manual. Enter the group number. Also, when applicable, show that optional markings have been used for Group 3 and Group 4 as authorized.

3. **REPORT TITLE:** Enter the complete report title in all capital letters. Titles in all cases should be unclassified. If a meaningful title cannot be selected without classification, show title classification in all capitals in parenthesis immediately following the title.

4. **DESCRIPTIVE NOTES:** If appropriate, enter the type of report, e.g., interim, progress, summary, annual, or final. Give the inclusive dates when a specific reporting period is covered.

5. **AUTHOR(S):** Enter the name(s) of author(s) as shown on or in the report. Enter last name, first name, middle initial. If military, show rank and branch of service. The name of the principal author is an absolute minimum requirement.

6. **REPORT DATE:** Enter the date of the report as day, month, year, or month, year. If more than one date appears on the report, use date of publication.

7a. **TOTAL NUMBER OF PAGES:** The total page count should follow normal pagination procedures, i.e., enter the number of pages containing information.

7b. **NUMBER OF REFERENCES:** Enter the total number of references cited in the report.

8a. **CONTRACT OR GRANT NUMBER:** If appropriate, enter the applicable number of the contract or grant under which the report was written.

8b, 8c, & 8d. **PROJECT NUMBER:** Enter the appropriate military department identification, such as project number, subproject number, system numbers, task number, etc.

9a. **ORIGINATOR'S REPORT NUMBER(S):** Enter the official report number by which the document will be identified and controlled by the originating activity. This number must be unique to this report.

9b. **OTHER REPORT NUMBER(S):** If the report has been assigned any other report numbers (*either by the originator or by the sponsor*), also enter this number(s).

10. **AVAILABILITY/LIMITATION NOTICES:** Enter any limitations on further dissemination of the report, other than those

imposed by security classification, using standard statements such as:

- (1) "Qualified requesters may obtain copies of this report from DDC."
- (2) "Foreign announcement and dissemination of this report by DDC is not authorized."
- (3) "U. S. Government agencies may obtain copies of this report directly from DDC. Other qualified DDC users shall request through \_\_\_\_\_."
- (4) "U. S. military agencies may obtain copies of this report directly from DDC. Other qualified users shall request through \_\_\_\_\_."
- (5) "All distribution of this report is controlled. Qualified DDC users shall request through \_\_\_\_\_."

If the report has been furnished to the Office of Technical Services, Department of Commerce, for sale to the public, indicate this fact and enter the price, if known.

11. **SUPPLEMENTARY NOTES:** Use for additional explanatory notes.

12. **SPONSORING MILITARY ACTIVITY:** Enter the name of the departmental project office or laboratory sponsoring (*paying for*) the research and development. Include address.

13. **ABSTRACT:** Enter an abstract giving a brief and factual summary of the document indicative of the report, even though it may also appear elsewhere in the body of the technical report. If additional space is required, a continuation sheet shall be attached.

It is highly desirable that the abstract of classified reports be unclassified. Each paragraph of the abstract shall end with an indication of the military security classification of the information in the paragraph, represented as (TS), (S), (C), or (U).

There is no limitation on the length of the abstract. However, the suggested length is from 150 to 225 words.

14. **KEY WORDS:** Key words are technically meaningful terms or short phrases that characterize a report and may be used as index entries for cataloging the report. Key words must be selected so that no security classification is required. Identifiers, such as equipment model designation, trade name, military project code name, geographic location, may be used as key words but will be followed by an indication of technical context. The assignment of links, roles, and weights is optional.